Application of Plasma Arc (PAV) Vitrification to Improve Stability of Weak Soil and Weathered Rock

By

Mohammed A. Gabr

Andrew Nash

Department of Civil Engineering

North Carolina State University

Paul W. Mayne

Amr Elhakim

Kathryn Wehrle

School of Civil and Environmental Engineering

Georgia Institute of Technology

In Cooperation with

The North Carolina Department of Transportation

and

The Institute for Transportation Research and Education

North Carolina State University

Raleigh, North Carolina

August, 2001

Technical Report Documentation Page

1. Report No. **FHWA/NC/2002-014**	2. Government Accession No.	3. Recipient's Catalog No.
4. Title and Subtitle **Application of Plasma Arc Vitrification (PAV) to Improve Stability of Weak Soil and Weathered Rock**		5. Report Date **August 2001** 6. Performing Organization Code
7. Author(s) **M. Gabr, A. Nash, and P. Mayne, A. Elhakim, and K. Wehrle**		8. Performing Organization Report No.
9. Performing Organization Name and Address **North Carolina State University** **Department of Civil Engineering** **Campus Box 7908** **Raleigh NC 27695-7908**		10. Work Unit No. (TRAIS) 11. Contract or Grant No.
12. Sponsoring Agency Name and Address **NC Department of Transportation** **Research and Analysis Group** **1 South Wilmington Street** **Raleigh NC 27601**		13. Type of Report and Period Covered **Final Report** **April 2000 – June 2001** 14. Sponsoring Agency Code **HWY-0860**
15. Supplementary Notes		

16. Abstract

A slope failure along US-1, South, near Apex, North Carolina is utilized as a case study for the application of Plasma Arc Vitrification (PAV) as a soil improvement technique. The project work encompassed in situ and laboratory characterization of the site soils, laboratory burn of site soils, as well as slope stability computer analysis. Field exploration of the slope material was performed by conducting traditional standard penetration testing (SPT) and extensive geophysical testing. Samples were collected during the drilling for laboratory classification of the material as well as measurement of site soils' strength properties. Furthermore, inclinometers were installed at the site to assess the location of the possible slip plane and the possibility of further movement. From this information, an idealized model of the slope is developed and utilized in the slope stability software "XSTABL" which performs Rotational Equilibrium Analysis of Multilayered Embankments (REAME). Due to the inability to perform PAV field testing, soil was excavated from the slope site and vitrified in the plasma laboratory at Georgia Institute of Technology. Once completed, additional lab tests were performed on the vitrified sample to determine the strength parameters for vitrified column model. The unit weight of the vitrified material increased by 46% from approximately 17 to 25 kN/m^3. The igneous Mass created (in kg) was equal to 0.78 $E^{(0.76)}$, where E is the energy consumed in kWh. The Slope stability analyses included many trials by varying the diameter of the PAV columns, the length of the embedment, and the spacing between columns. The analysis indicated the possibility of increasing the factor of safety of the slope from less than one to approximately 1.3 by including the PAV columns with length of 20 feet and a diameter of 4 foot, spaced at 3D, and placed 20 feet up the slope. Based upon the results of laboratory work and PAV modeling, further research is proposed to focus on alternative fuel sources. In addition, studying burn rates (time burn vs. amount of improvement) is needed to optimize the process.

17. Key Words in situ, rock, plasma arc, properties, soil improvement, slope, stability, vitrification	18. Distribution Statement		
19. Security Classif. (of this report) Unclassified	20. Security Classif. (of this page) Unclassified	21. No. of Pages 137	22. Price

Form DOT F 1700.7 (8-72) **Reproduction of completed page authorized**

ABSTRACT

A limited study is conducted to investigate the applicability of Plasma Arc Vitrification (PAV) to improve the strength of weak soils and weathered rock. Destructive and non-destructive characterization tests are conducted in the field along with laboratory testing to estimate the physical and strength parameters of potentially weak materials before the application of PAV. Data analyses are performed to estimate the properties of the in-situ materials and level of improvement related to PAV application. Since a planned field-scale test using PAV did not materialize, a limited scale laboratory application of PAV to site soils is conducted and improvements in strength properties are characterized. In addition, slope stability analyses are performed to determine the optimum placement of the vitrified zone and the corresponding improvement in the factor of safety of the slope. Placement of the PAV columns within a slope will improve its resistance to movement. For the US-1 site, a vitrified column with length of 20 feet and a diameter of 4 foot, spaced at 3D, and placed 20 feet up the slope was determined to be the ideal configuration. Based upon the results of laboratory work and PAV modeling, further research is proposed to focus on alternative fuel sources. In addition, studying burn rates (time burn vs. amount of improvement) is needed to optimize the process. Finding improvement within these areas would reduce the expense of conducting PAV burns. At present, constructibility and high operation costs prove this method of slope stabilization to be prohibitive in practical application.

Table of Contents

List of Figures

Page No.

List of Tables

Page No.

1.0 INTRODUCTION

Nontransferred arc plasma technology represents a novel and powerful means for melting soil solids in an efficient and expedient manner. Plasma is the fourth state of matter and produces very high temperatures in the range over 4000°C. With a nontransferred arc plasma torch (see Figure 1 below), high temperatures can be controlled and directed at any desired target. This technology is capable of melting soils and rocks, as well as contaminated ground, thus creating a molten pool of surficial lava or subsurface magma. Tungsten has the highest melting point on earth, melting at 2450°C. The molten region eventually cools to form an inert glassy igneous rock, often similar to obsidian and in some instances similar to crystalline granite and/or basalt (Mayne, et al. 1994, 1996, 2000).

Figure 1. Nontransferred Arc Plasma Torch (Mayne, 2000)

Past work on nontransferred arc plasma has been largely conducted in the laboratory setting with a limited pilot scale demonstration in the field. The research described herein is related to demonstration of plasma arc in an application on stabilization of a slope along US-1 south, near Raleigh, North Carolina. Geologically, the site is located in the Triassic Basins of North Carolina. The area is characterized by irregular rock bedding and thickness, with abrupt elevation changes both laterally and vertically. The soil and rock at the proposed site are mainly defined as residual plastic clay derived from

underlying weathered mudstones. The mudstone (claystone) is known for potential short-term physical disintegration or slaking.

The applicability of the Plasma Arc Vitrification (PAV) to improve the strength of weak soils and weathered rock is investigated. Destructive and non-destructive tests are conducted in the field along with laboratory testing to estimate the physical and strength parameters of potentially weak materials before and after the application of PAV. Data analyses are performed to estimate the properties of the in situ materials and level of improvement related to PAV application. Since a planned field-scale test using PAV did not materialize, a limited scale laboratory application of PAV to site soils is conducted and improvements in strength properties are characterized. In addition, slope stability analyses are performed to determine the optimum placement of the vitrified zone and the corresponding improvement in the factor of safety of the slope.

1.1 Scope of Research

The work presented in this thesis serves to evaluate the suitability of PAV to improve the strength of weak in-situ materials with specific emphasis on slope stabilization. Slope failures in Piedmont residual soil profiles have been reported by Ledbetter (1968), Moore (1986), Riad and Lambe (1990), Tice (1974), and Borden and Putrich (1986).

The use of PAV is a relatively new technology that has not been well verified in the field. One of the potential applications is in the realm of soil improvement whereby relatively high strength columns can be created within the soil mass using PAV. Accordingly, for unstable slopes, the risk of slope failures can be reduced due to the inclusion of PAV columns for soil reinforcement. For slopes that have already failed, PAV columns can potentially be used as a remedial measure as vitrified columns may be able to provide a great deal of improvement in a constrained area using the in-situ material. The advantage of such a remediation measure is a reduced need for excavation of the slope, and the ability to maintain the original slope angle. In addition, PAV could be used in an array of stability issues including the construction of steeper slopes and improvement of soft foundation material under embankments. Accordingly, PAV may be added as one

alternate method to conventional measures used for special embankments and slope stabilizing applications.

A slope failure along US-1, South near Apex, North Carolina will be utilized as a case study. The project work encompasses in situ and laboratory characterization of the site soils as well as slope stability computer modeling. Preliminary field exploration of the slope material was performed by conducting traditional standard penetration testing (SPT) and extensive geophysical testing. Samples were collected during the drilling for laboratory classification of the material. Furthermore, inclinometers were installed at the site to determine the location of the possible slip plane and the possibility of further movement. From this information, it was possible to develop an idealized model of the slope in stability software "XSTABL" and Rotational Equilibrium Analysis of Multilayered Embankments (REAME). Lateral loads applied to the PAV columns are considered.

Due to the inability to perform PAV field-testing, soil was excavated from the slope site and vitrified in the plasma laboratory at Georgia Institute of Technology. Once completed, additional lab tests were performed on the vitrified sample to determine the strength parameters for the vitrified column model. Slope stability analyses included many trials by varying the diameter of the PAV columns, the length of the embedment, and the spacing between columns. Such analyses provided a notion of how these parameters affected the resulting factor of safety and the optimum location of the vitrified columns along the slope.

1.2 Research Objectives

The main objective of this research is to develop and validate a procedure for using PAV columns for slope failure prevention and repair. Specifically, the following objectives are investigated:

i. In situ characterization of the soils at US-1 site,

ii. Investigation of site soil properties pre- and post- vitrification process,

iii. Performance of a parametric study of the US-1 slope and PAV columns (location, size, column spacing, depth vs. factor of safety) for optimum location based on the strength properties of the vitrified columns, and,

iv. Propose a methodology for the design and analysis of PAV columns as a means of slope stability based on the analyses results.

2.0 LITERATURE REVIEW

Landslides in the United States are on the rise in most regions, in spite of an improved understanding of landslide processes and a rapidly developing technical capability for slide prediction and mitigation. This can be attributed to increased urbanization and development. Slope failures in Piedmont residual soil profiles have been reported by Ledbetter (1968), Moore (1986), Riad and Lambe (1990), Tice (1974), and Borden and Putrich (1986).

Each slope possesses unique soil characteristics and geometric features. Slope failures can occur slowly, due to creep along slick and weak planes, or suddenly due to rise in pore pressure and malfunctioning of drains. Slope failures have caused unquantified amounts of economic and life losses over time. Slope movements account for 25 – 50% of all natural disaster deaths worldwide. Within the United States alone, between 25 and 50 lives are lost each year (Walkinshaw, 1992). Future slides will undoubtedly occur for several reasons, including poor existing site conditions (i.e. development in a slide-prone area), removal of vegetation (deforestation), and increased regional precipitation caused by changing climate patterns.

It is difficult to estimate the total cost of such failures due to the fact that not all slope failures are reported. Walkinshaw (1992) conducted a study on federally funded highways that examined the cost related to slope failures between the years of 1986 and 1990. Annual slope maintenance and repair costs during the study period, of slope failures by highway agencies, averaged over $100 million. A state by state breakdown of Walkinshaw's results can be seen in Figure 2. As seen, North Carolina exceeded $3 million in slide-related repairs over the study period. It is important to note, however, that Walkinshaw's study only represented about 20% of the public highway / road system (state / federal). It did not include smaller slides that are commonly corrected by maintenance or indirect costs related to traffic interruptions, delays, or inconveniences. Further, slope maintenance and repair costs could have been even more elevated if Walkinshaw's study had taken into account the additional private transportation systems (i.e. railroads) and non-roadway related issues.

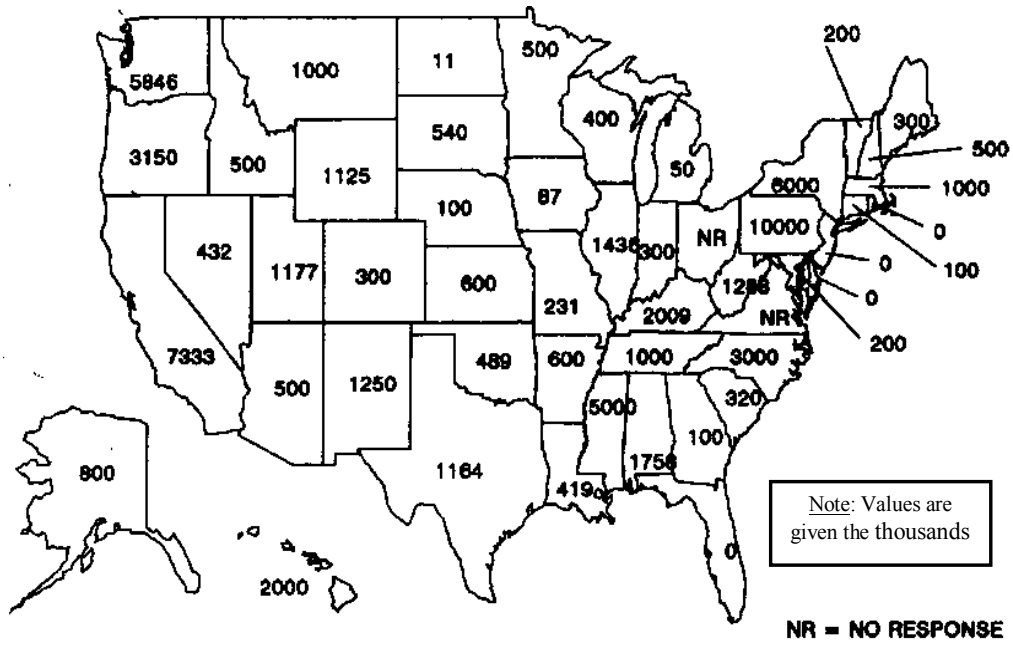

Figure 2. Average Annual Costs for Construction Highway Repairs 1986 – 1990 (TRB Special Report 247, 1996)

2.1 Slope Failures

Depending on the in-situ geological and geometric conditions as well as weather conditions, slopes can fail in different modes. Slope failures occur due to loss in shear strength (s) or an increase in the applied shear stress (τ). Most slope stability analyses are based on the comparison of these two values, in terms of a ratio called a factor of safety (FS) as shown in Equation 2.1, and for which the resisting forces are estimated based on limit equilibrium analyses. The limit equilibrium method uses principles of static equilibrium to evaluate the balance of driving and resisting forces on the postulated mechanism of failure (slip surface), as shown in Figure 3. A factor of safety greater than one indicates a stable slope; values less than one indicate possible failures. While commonly used in practice, it is well known that the factor of safety does not quantify the probability of failure since it does not take into account spatial variability of soil physical and strength properties within slope site.

$$FS = \frac{s}{\tau} \qquad \text{(Equation 2.1)}$$

where: FS = factor of safety, s = average shear strength of the soil, and τ = average shear stress developed along the potential failure surface.

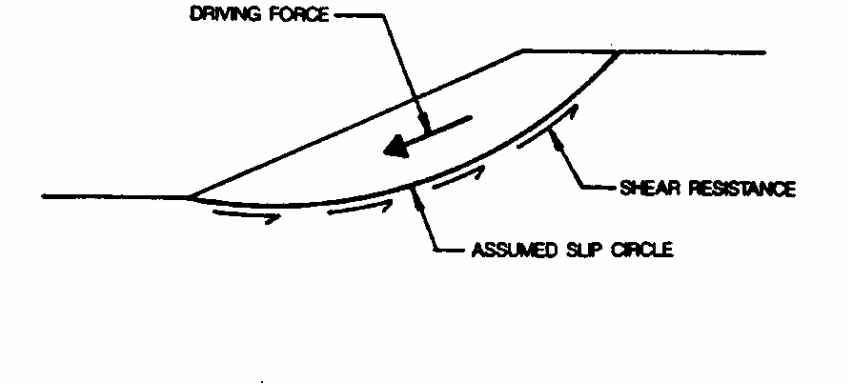

Figure 3. Slope Failure (FHWA, 1994)

In general, soil slopes have the tendency to slide under the influence of shear stresses created by gravitational, water flow, or seismic forces. These forces are resisted by shear strength of the material commonly expressed by Mohr-Coulomb Theory in terms of total stresses (Equation 2.2) or effective stresses (Equation 2.3).

$$s = \sigma_n \tan \phi + c \qquad \text{(Equation 2.2)}$$

where: s = shear strength of the soil, c = cohesion of soil, σ_n = normal stress, and ϕ = angle of internal friction.

$$s' = (\sigma_n - u) \tan \phi' + c' \qquad \text{(Equation 2.3)}$$

where: s' = effective shear strength of the soil, c' = effective cohesion of soil, ϕ' = effective angle of internal friction, u = pore water pressure.

Primary factors causing failures (changes in shear strength or stresses) can be man-made or naturally occurring. Man-made causes include ground water drawdown, the introduction of water, excavation, the removal of vegetation, and loading placed atop the slope. Natural causes include intense weather conditions and geological events (such as earthquakes), and weak materials and structures, which are less evident. However, increases or decrease in pore pressure, seepage forces, and runoff are often cited as causes of slope failures.

2.2 Highway Slopes

In highway construction, steep slopes are often necessary due to right-of-way constraints. Such slopes can take the form of either fill construction, or cuts in natural materials. Although fill slopes are often used, the research herein is focused on cut slopes since this was the variety encountered at the US-1 site. While embankments or fill slope failures are usually due to poor construction or design, cut slope failures are more a response to changes in geometry and site conditions (i.e. unloading or drainage). The stability of cut slopes can be time-dependent and while such slopes can be stable in the short-term, they may fail many years later, instantaneously. In Figure 4, Bishop and Bjerrum (1960) showed generally how the factor of safety, shear strength, excess pore pressure, load, and shear stresses relate and vary over time for a clay cut slope.

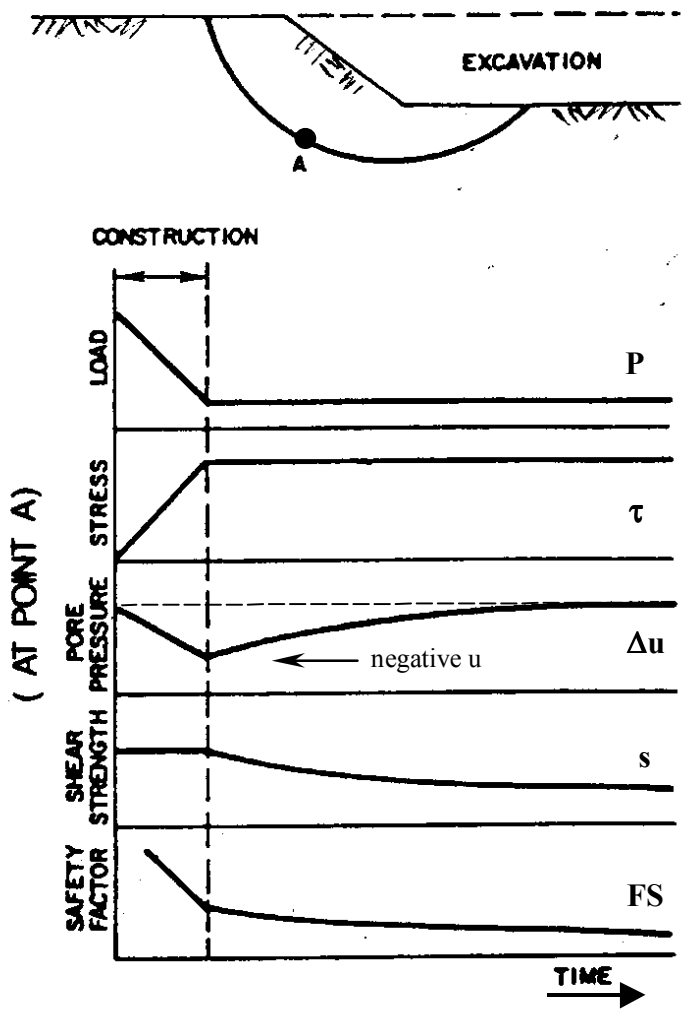

Figure 4. Stability Conditions of a Cut Slope (Bishop and Bjerrum, 1960)

As material is excavated over a short period of time, no drainage occurs, and the initial shear strength is equal to the undrained shear strength (s_u). The effective overburden pressure is reduced, thus inducing a reduction in pore pressure. The negative pore pressure dissipates (decreases) within the slope over time. The shear strength of the soil decreases over time and the slope may reach an unstable condition. An estimation of the time of anticipated failure can be calculated. This loss in strength, as previously stated, is a time-dependent function related to the rate of dissipation of negative pore pressure.

Permanent cut slope stability also is dependent on the final ground water level in the soil profile. After excavation, the ground water table will usually drop slowly to a stable zone at a variable depth below the new cut surface. This drawdown occurs slowly for clayey material. Since long-term stability is a function of pore pressure, slope stability analysis should be performed in terms of effective stress. Such analysis requires both the effective strength parameters of the soil as well as the distribution of pore pressure in the slope (location of phreatic surface).

2.3 Slope Failure Modes

Skempton and Hutchinson (1969) indicated that slides in clays generally take one of three forms as shown in Figure 5 (or sometimes a combination of these forms):

i. rotational,

ii. translational, or

iii. flows (lateral spreads).

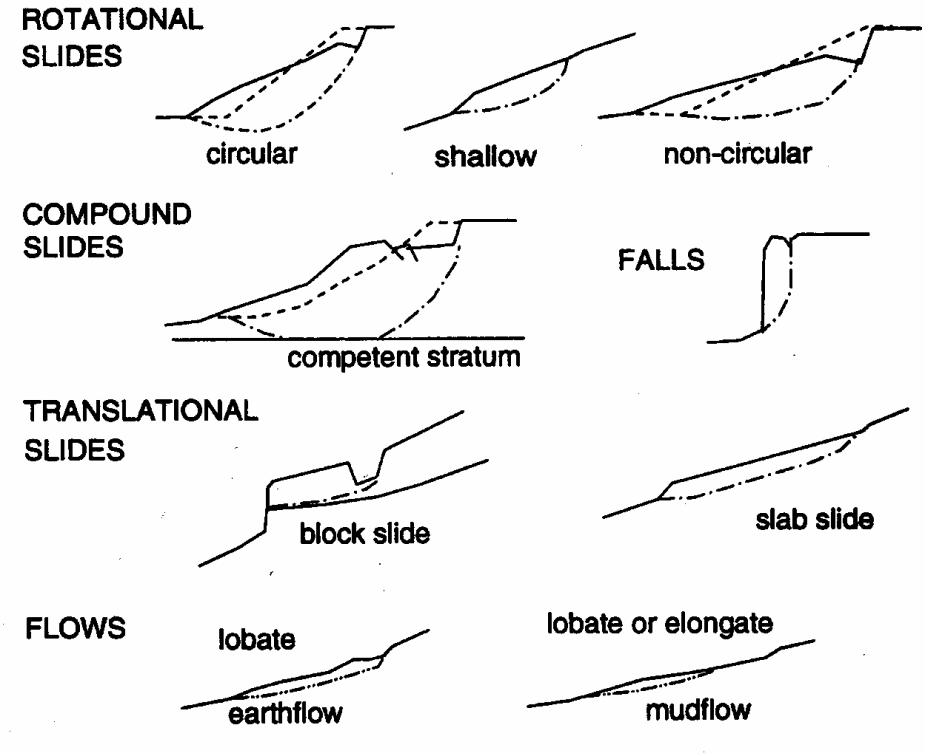

Figure 5. Clay Slope Failure Modes (Skempton and Hutchinson, 1969)

2.4 Stabilization Measures

Stabilization or mitigation methods are selected to address the most probable mechanism of failure, but ultimately site conditions, funding, and constructibility issues determine the final solution. A wide array of technologies and techniques are employed in stabilization projects as follows (FHWA, 1994):

Unloading: reducing the weight driving (i.e. excavation / light weight fill)

Toe Loading: additional force resisting (i.e. buttressing, berms)

Drainage: reduction in seepage force (i.e. surface / subsurface)

Reinforcement: mechanisms that intersect the surface plane and transfer the forces down or outward toward stable stratum (i.e. columns, geosynthetics)

Retaining: holding back earth (i.e. walls)

Vegetation: help with erosion; water, and roots provide reinforcement

Slope Protection: helps water infiltration (i.e. shotcrete, riprap)

Soil Improvement: increasing in-situ soil properties by chemical, thermal, or mechanical means (compaction, grouting, lime, thermal treatment)

The plasma arc vitrification (PAV) technique can be viewed as a means of soil improvement by thermally creating improved strength soil columns. The in-situ material is transferred from soil into circular columns of igneous rock . The columns form reinforcement elements that resist soil movements and transfers loads to more stable underlying layers, as depicted in Figure 6.

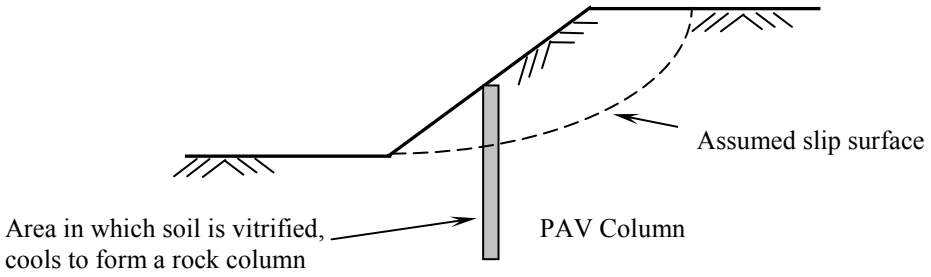

Figure 6. Basis of Plasma Arc Stabilization

2.5 Thermal Treatment of Soils

Thermal treatment of soils has been used in the past and proven to increase soil properties (i.e. brick manufacturing). Heating clayey soil at temperatures exceeding 400°C leads to pronounced (irreversible) permanent changes of its engineering properties. Clayey soils with prolonged exposure to increased temperatures have reduced sensitivity to water, show notable increases in shear strength, and decreased compressibility. These results can be varied by heat application type, time of exposure, and temperature. In addition, the mineralogical composition of the clay dictates the final properties. As seen in Figure 7, from studies conducted by Kezdi, the clay's lattice gradual loss of water happens at different temperatures; in particular, all free water has evaporated at 105 - 110°C. About 500^{o} C typically is the temperature where all water has been burned off (Hausmann, 1990).

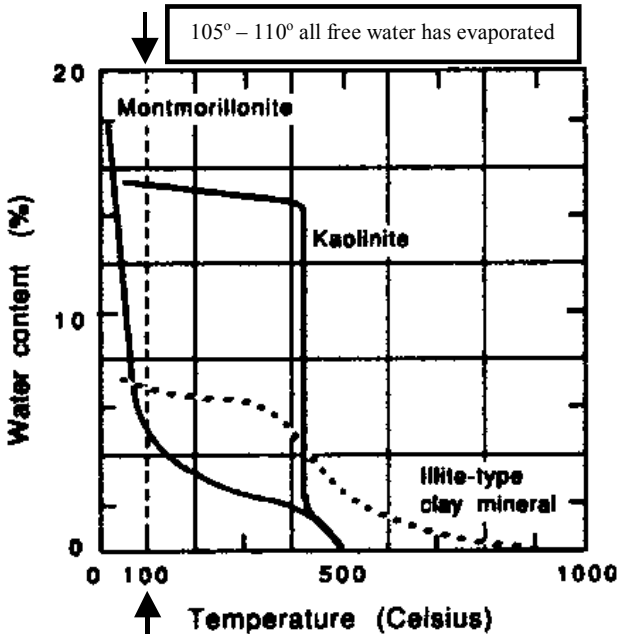

Figure 7. Characteristic Water Losses in Clay Minerals (Hausmann, 1990)

Laboratory investigations by Beles and Stanculescu (Figure 8) show decreases in plasticity after longer durations of thermal exposure. Further, the compressibility of clay soils can be reduced due to exposure of high temperature, as seen in Figure 9.

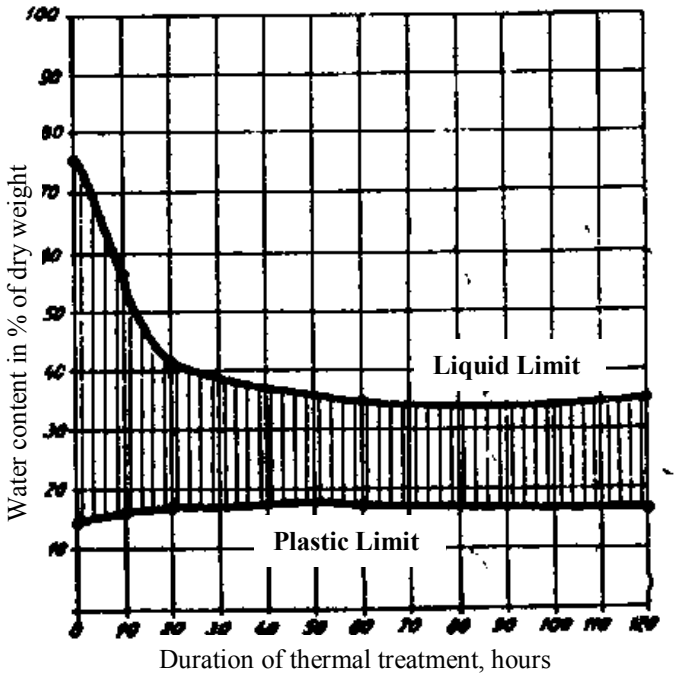

Figure 8.: Plasticity Index (Beles and Stanculescu, 1958)

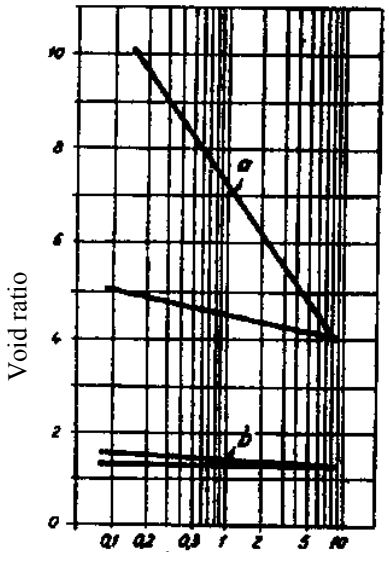

a = dried at 60° C b = dried at 300° C

Figure 9. Compressibility (Beles and Stanculescu, 1958)

2.6 In-Situ Thermal Measures

As seen in the previous section, heating of soil results in decreased compressibility and increased strength. Thermal improvement of soils has been utilized for over one hundred years. Thermal treatment has been used as a means for soil improvement of weak foundation material and stabilization of slopes. In-situ thermal treatment generally is achieved by the burning of liquid, gaseous, or solid fuels at the ground surface or in a borehole, and some times more advanced burning devises have been employed.

2.6.1 Ground Surface Heating

Ground surface treatment has typically involved the burning of coal or wood on the surface or in ventilated containers over an extended period. This proved to be difficult to control as the amount of heat being applied was not regulated. In the Untied States, in the late 1880s, clays were burned (wood) to create aggregate for highways and railroad ballast (Janiewicz, 1972).

In Australia in the 1930s, surface treatment took on a mobile form. Irvine designed and built a wood furnace, which traveled at a maximum rate of about 30 ft/hr. The device depicted in Figure 10 baked a 2- to 8-inch thick layer of soil, producing a non-plastic stiff layer of a previously very plastic clay. The devise required 25 pounds of wood per one ft^3 of soil treated. In areas where ordinary aggregates were not readily available, road surfaces were constructed with the heat-treated soils, termed “burnt clay” (Hausmann, 1990).

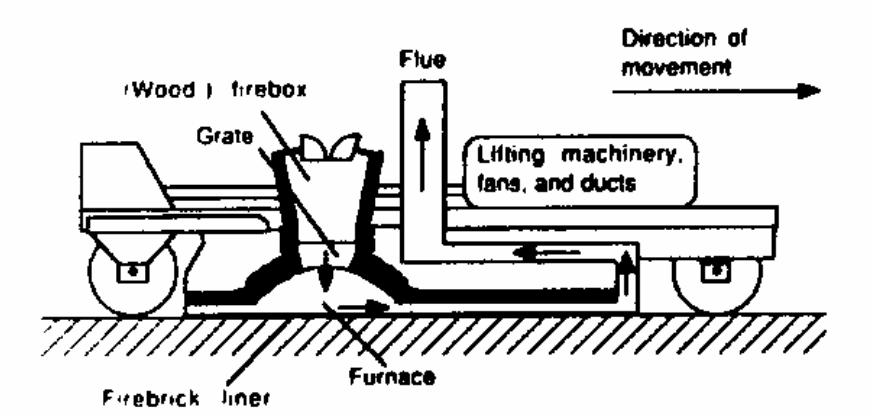

Figure 10. Diagram of Irvine Heat Treatment Machine (Hausmann, 1990)

A similar device was used later in constructing roads in Argentina using a mobile oil furnace.

2.6.2 Borehole Treatment

Borehole heat treatment has been used in the Untied States, Japan, Rumania, and Russia to stabilize plastic clay in-situ. Both super heated air and fossil fuel sources have been used. Borehole treatments usually are categorized as closed or open-hole systems.

Closed-hole Systems

In Russia (USSR), methods for thermal treatment of soil by burning fuel in a closed system were investigated. The first applications involved introducing heated air under pressure into a boring, as seen in Figure 11 (Beles and Stanculescu, 1958).

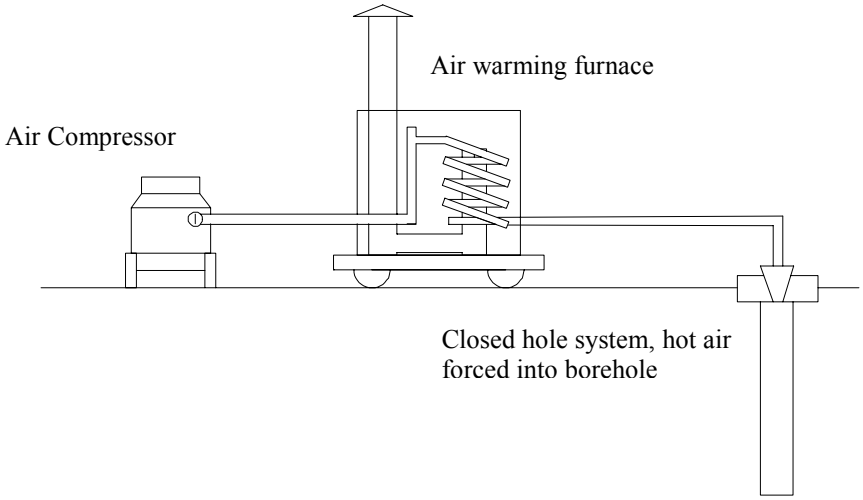

Figure 11. Compressed Air Burner (After Litvinov, 1955)

A later design by Litvinov used compressed air burners injected with gaseous/liquid fuels (see Figure 12). The method involved burning the fossil fuel under pressure (25 to 50 percent above atmospheric pressure) in a burner fixed at the top of a sealed borehole. Infiltration of the combustion heat into the soil's pores stabilized the mass. Treatment after ten days resulted in thermally treated zones of 6 foot in diameter and 30 foot in depth.

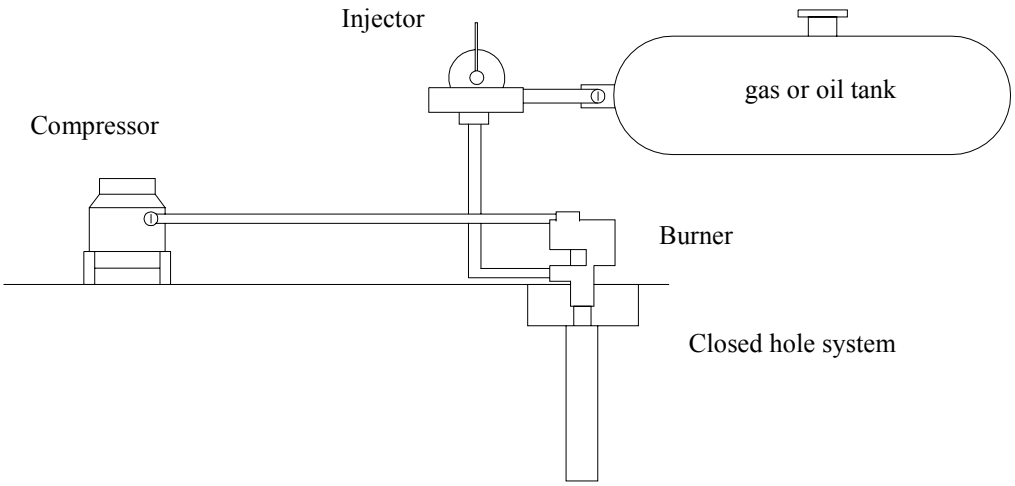

Figure 12. Compressed Air Burner with Fuel Injector (After Litvinov, 1957)

Improvements in soil properties were observed as manifested by an increase in cohesion, doubling of the friction angle, and about a five times decrease in compressibility. This method yielded better results than the heated air only system, but at a high cost. Litvinov utilized heat treatment for reduction of settlement and stabilization of slides. Litvinov later developed a down-hole burner system.

Similar closed-hole systems were employed in Fukuoka, Japan, in the late 1970s by Fujii on a waste disposal project. Two hundred twenty-seven boreholes were drilled at a depth of 6.5- to 20-feet and spaced at 16-feet apart. Each borehole was heated for 7 to 15 days and averaged about 200 gallons of fuel oil. About a 3-ft radius was affected around the holes' walls, resulting in a 12 gal/yd^3 consumption (Hausmann, 1990).

Hill (1934) used a furnace system, which forced air through tunnels and drill holes to remedy landslides, which had occurred near Santa Monica, California. Slip surface developed within underlying clay layers. Large volumes of air were heated and then

forced into the tunnels continuously. The blower handled air at a rate of 6500 ft^3/min with a fuel consumption rate of 400 ft^3/hr. Clays along the tunnels were transformed into a brick-like material. Hill stopped the outward movement of the slope by the increased frictional resistance between the clay layers.

Open-Hole Systems

In Romania, borehole burns were tried to achieve both an economical and an efficient method for open-hole methods. Experiments with draught boring to increase ventilation were conducted. Special devices to connect the draught boring and the test boring being fired were developed. Initial tests used compressor and injector setups at the ground surface, similar to the Litvinov system. In later tests, the burner source was actually lowered into the borehole and raised incrementally during the process, as depicted in Figure 13.

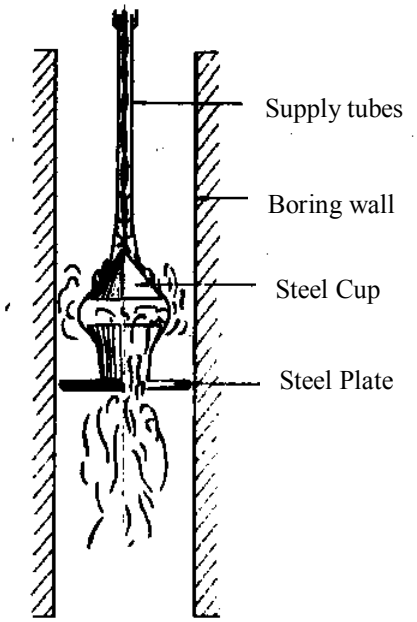

Figure 13. Down-Hole Burner Design (Beles and Stanculescu, 1958)

The burner consisted of a steel plate with a diameter equal to that of the boring. The burner was suspended by a cable from the surface. Heat was transferred down a metal tube and thought the plate. The device was used to successfully strengthen soils under existing structures, reducing settlement under embankments, and stabilize landslides.

The Romanians mainly dealt with soaked-loess and sensitive clays (Beles and Stanculescu, 1958).

An open-type fire system was used by Fujii (1971) in Kanazawa, Japan, to stabilize an embankment for a railroad. A diagram of the system can be seen below in Figure 14.

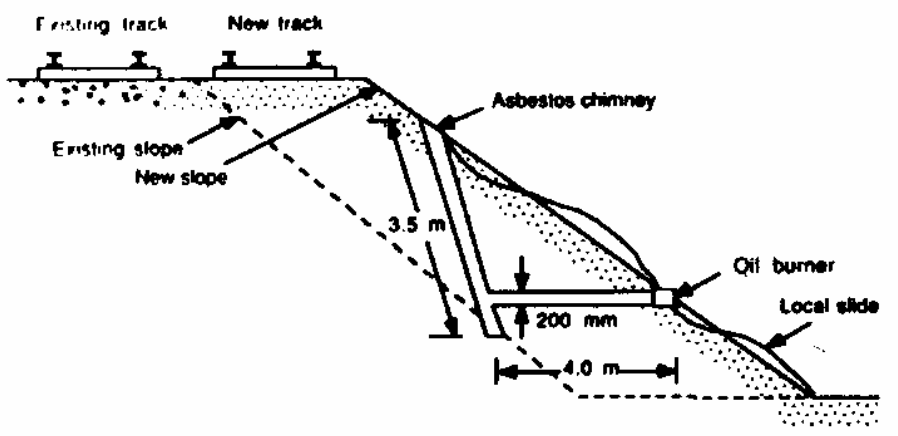

Figure 14. Kanazawa Railroad Embankment Site (Hausmann, 1990)

Approximately, 315 gallons of fuel were burned per hole, resulting in a 1-ft radius of treated area. Treated soil showed a strength improvement of 10 – 20 times the original strength, which was retained even after saturated with water. Ventilation was provided though a draught boring located near the top of the slope (Hausmann, 1990).

2.6.3 Modern Systems

Yurdanov (1978) developed an in-situ thermal treatment system that utilized electric heaters, in comparison to the previously described combustion types. Field tests were conducted on clay and loess deposits to create pile, column, and retaining structures. The heaters were used to blow hot pressurized air into the borehole with temperatures ranging from 500^{o}C to 1200^{o}C. Later the heaters were inserted directly down the hole. The soil was successfully fused to form independent structures.

In recent years, these technologies have been used for In-Situ Vitrification (ISV) treatment of waste materials. In-situ vitrification of waste was originally conceived at Pacific Northwest Laboratories (PNL) in 1980 using a grid of four gradmite/molybdenium electrodes that are configured in a square pattern. The ISV equipment was mounted on three standard road trailers with a containment hood to cover the entire area and collect by-product gases during the vitrification process. The generalized setup and vitrification sequence can be seen in Figure 15.

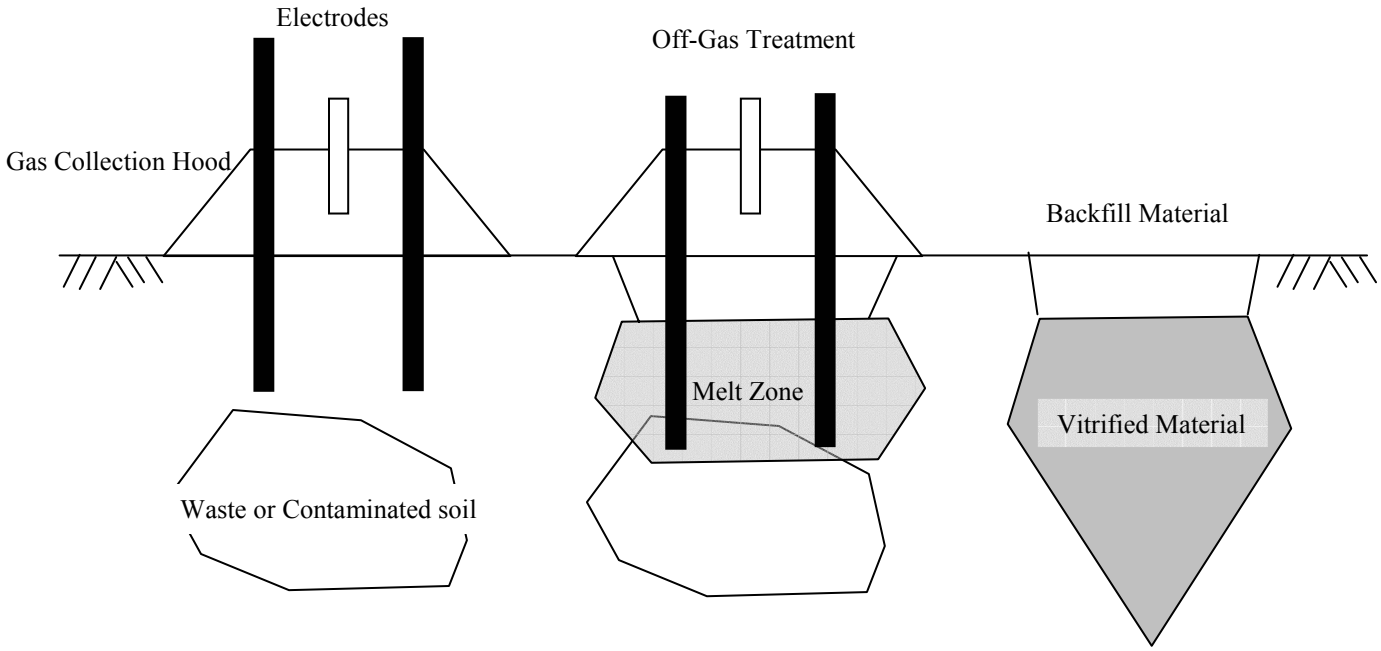

Figure 15. In-Situ Vitrification Setup (after Department of Energy)

The electrodes are embedded in the ground at a depth of 16 feet (5 meters) initially; then, during the process, the electrodes are advanced deeper. A high voltage current is passed through the electrodes to vitrify the enclosed soil mass within the square layout. Soils are heated to temperatures of approximately 2000^{o}C. The process is highly energy-intensive and requires approximately two weeks for meltdown. The resulting melt cools into a high durability glassy rock similar to obsidian with no defined fracture pattern (Byers, Fitzpatrick, and Holtz, 1991). Vitrification below the water table was not possible. The process resulted in the complete destruction of organic material, and most inorganic

contaminants were incorporated into the vitrified material. The vitrified material was found to be highly resistant to leaching, up to ten times stronger in compressive strength than unreinforced concrete, and unaffected by wet-dry or freeze-dry cycles. During the molten phase of the process, there was a significant reduction in the volume of 20-50%; almost all of the void spaces in the soil were removed. The surface subsidence had to be backfilled with clean fill material to the original grade. This work was jointly sponsored by the Department of Energy (DOE) and the Environmental Protection Agency (EPA). The first demonstration of the method to treat metal and organic-contaminated soil on a large scale was at the Superfund site at Butte, Montana. Further, a full-scale ISV experiments have been performed at the Hanford Nuclear Facility in Washington, the Parsons Chemical Superfund in Grand Ledge, Michigan (Figure 16), and the Wasatch Chemical site in Utah. Oak Ridge National Laboratories (ORNL) used a similar system to stabilize radioactive sludges in Tennessee.

Figure 16. In-Situ Vitrification Parsons Chemical Superfund in Grand Ledge, Michigan (after Department of Energy)

As seen from literature, thermal improvement of soils has been an exercise in time and money. Resulting strengths were at a minimum several times the original soil strength. Due to the small diameter of influence, the lack of consistency in results, the large

quantity of fuel consumed, and the difficulty in application, the beneficial effects outside the burn zone were rather limited. As such, thermal treatment was viewed as an unfavorable stability method. However, with the advent of technology and the invention of plasma systems, a complete magmatic transformation melting (temperatures exceeding 1600°C) of the soil is now technologically feasible.

2.7 Plasma Arc Technology

Plasma technology development began approximately 40 years ago as a means to provide an electrically generated energy source in the form of a high temperature gas. Plasma torches have been used for decades in many industrial applications. The technology is well established in metal manufacturing from metallurgical processing, such as material synthesis and surface coating, to the welding and cutting of metals. Plasma-arc furnaces have been used for waste destruction and disposal of hazardous, military, organic, and biological materials.

Plasma is often described as "the fourth state of matter." Electrical energy is applied to a gas (oxygen, argon, air, neon, etc.), which transforms the gas into plasma. Plasma is an ionized gas, which is composed of equal numbers of positive ions and electrons. Plasmas exhibit some properties of a gas but differ from a gas in that they are good conductors of electricity and magnetic fields. Natural occurrences of plasma include lightning and the Aurora Borealis. Plasma torches are devices that utilize plasma-produced heat for high-temperature operations. Based on the concept of Joule heat, this is the conversion of electrical energy to heat energy (Mayne and Beaver, 1996).

Four sizes of plasma torches exist and are ranked by the electrical energy input, DC Power, applied to the torch: 100-kw, 240-kw, 1-Mw, and 6-Mw (for industrial purposes). The torch's basic components can be seen in Figure 17.

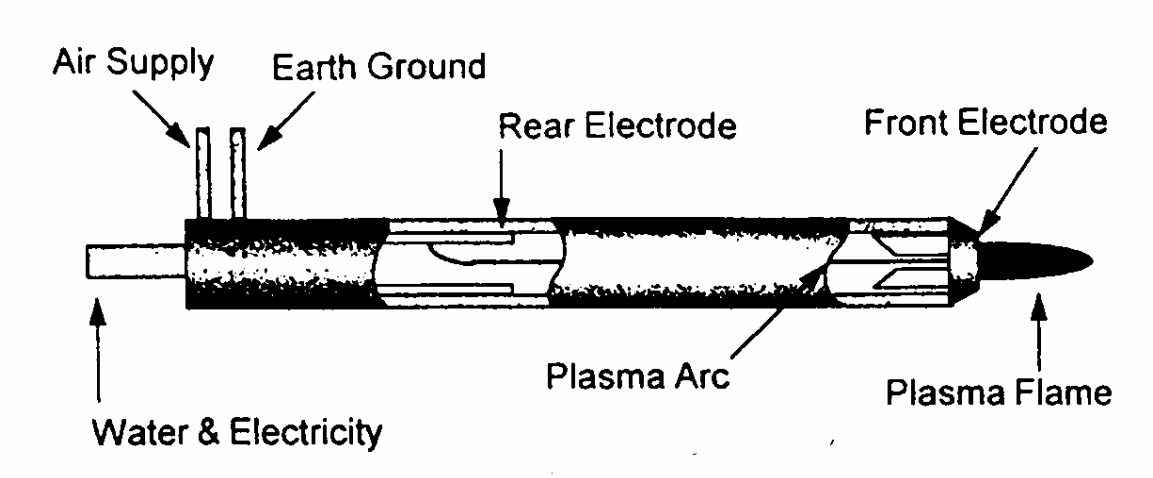

Figure 17. Reversed-polarity non-transferred plasma torch (Mayne, 1995)

Air (gas), electricity, and water are supplied through the top of the torch. Electrodes are located at the rear and near the tip of the torch. Temperatures at the electrode exceed all melting points; therefore, copper electrodes are replaced after 500 hours and most alloys can last 1000 hours. The plasma torch configuration can easily be modified for various gases at a wide range of pressures (from 20 atm to a low vacuum). Only one-tenth of one percent (0.1%) of the gas is actually converted to plasma. The electrical arc traversing between electrodes through an induced partially ionized gas generates the plasma temperatures. Movement of the arc and water-cooling are essential for the life of the electrodes.

Plasma torches have two configurations. The most commonly used is the transferred arc; the non-transferred arc is the less common alternative. The transferred arc flow of energy moves from one electrode to another. Applications normally involve a closed furnace or melter. The non-transferred arc can be directed at specific targets since the arc travels between electrodes that are system-contained and do not require a separate base electrode. Arcs generated at the back electrode are passed out of the torch and return to the front electrode in a "j-shaped" orientation (Mayne, 2000). The difference between these two systems is illustrated in Figure 18.

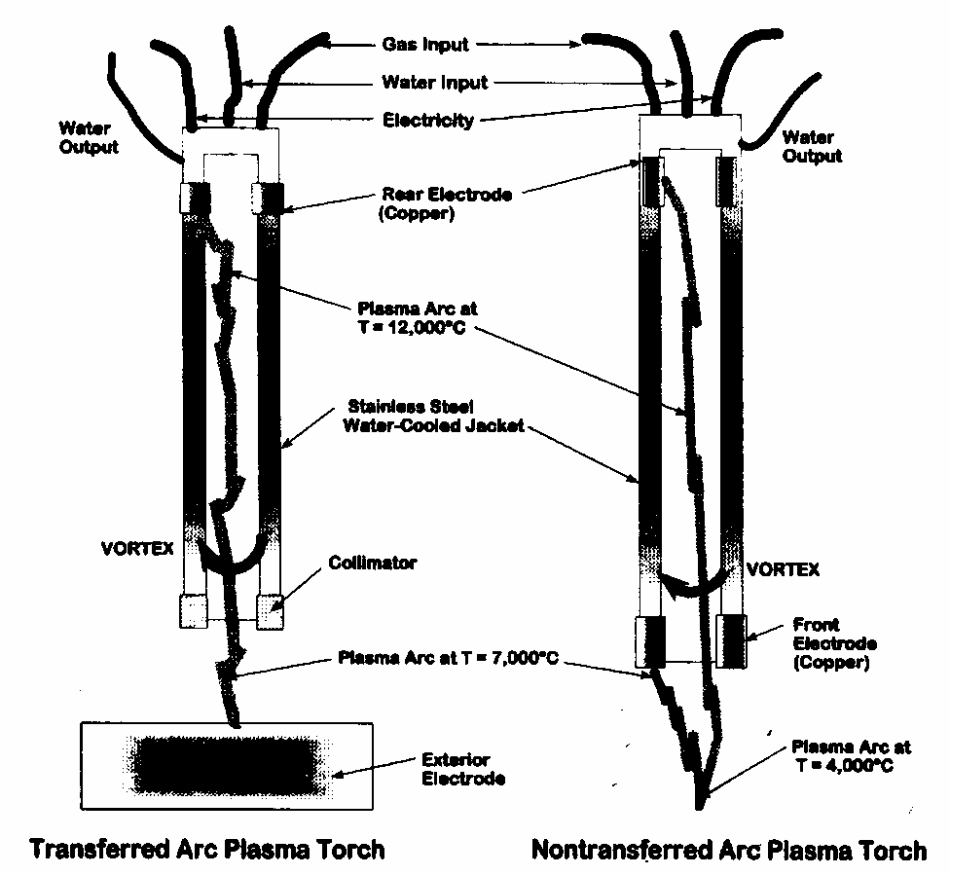

Figure 18. Transferred versus Non-transferred Arc Plasma Torches (Mayne, 2000)

The non-transferred plasma arc torch is that utilized for use in a mobile operation. The plasma arc torch mobile set-up consists of a trailer mounted control center and fuel supply; to ensure proper operation, all hoses and cables connected to the trailer should extend to a minimum distance of 250 feet. During vitrification, DC power is converted to AC power. The general layout of the control center can be seen in Figure 19.

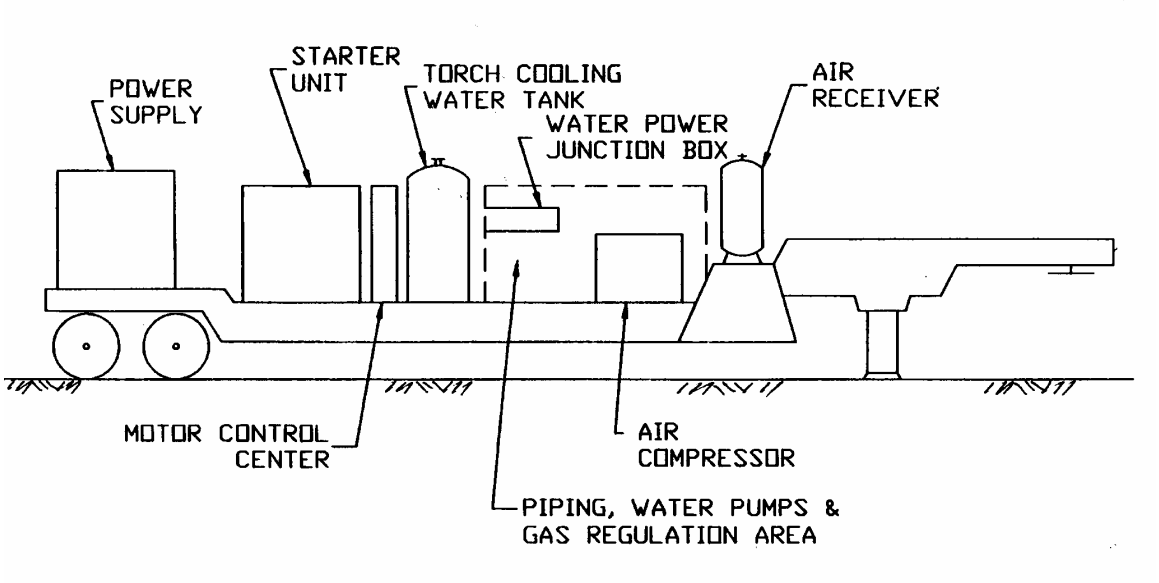

Figure 19. Mobile Plasma Trailer System Arrangement-53 foot (Berkovitz, 1996)

Off-gas hoods are used in applications where the burning of waste is involved. These hoods are necessary to ensure the safety of operators around fumes, Figure 20.

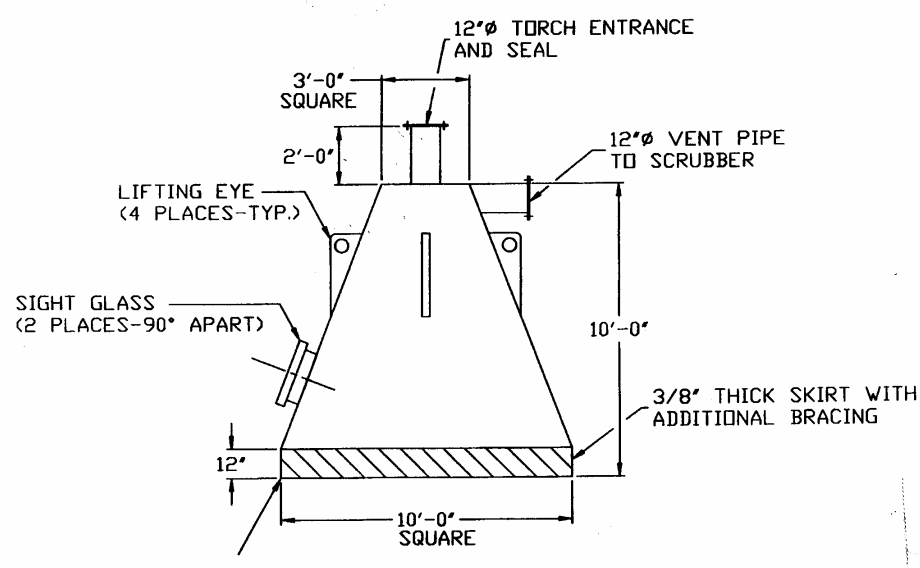

Figure 20. Gas Collection Hood (Berkovitz, 1996)

2.8 Plasma Vitrified Geomaterials

In waste remediation applications, the rationale for using plasma torches is their ability to destroy organic and biological components while decreasing the volume of waste and producing a non-leachable, glass-like slag. In soil improvement application, the rational

is to increase compressive strength, lower moisture sensitivity, and help with freeze cycles.

Over the past 10 years, several experiments were conducted at the Georgia Institute of Technology to observe the effects of initial water content, soil type, mineralogy, borehole to torch diameter, and engineering properties on the vitrified products. Plasma experiments using seven different soil types were studied. The results of the study are summarized in Table 1.

Table 1: Index Properties of Original Soil Materials Used in the Georgia Tech Vitrification Testing (Mayne, 2000)

Soil Type	USCS	D_{50}	Percent Fines	Clay Fraction	LL	PI
		(mm)	(%)	(%)	(%)	(%)
Tyndall Beach Sand	SP	0.23	0	0	NA	NP
Silica Blasting Sand	SP	0.71	0	0	NA	NP
Piedmont Sandy Silt	ML	0.07	51	5	37	NP
Georgia Kaolin	CL	0.003	79	38	41	20
Aiken Clayey Sand	SC	0.37	14	11	(150)[a]	(113)[a]
Goose Lake Clay	CL	0.011	87	25	39	19
Processed Kaolin	CH	0.002	100	85	79	41

[a] Material is nonplastic on complete sample, values are for the Percent Fines portions

Based on the results reported by Mayne (2000), it was found that both the compressive strength and the dynamic modulus increased, with respect to the original materials, by a factor of 2-3 orders of magnitude. As the energy consumption and mean grain size increased, so did the mass size of the rock that was produced. The Georgia Tech studies found that sands melted much more easily than clays. However, the system lost

efficiency when the borehole was enlarged and when clean sands were encountered, as these sands tended to cave in during the process. Conversely, increases in the system's efficiency were noted when the relative ratio of borehole-to-torch diameter was decreased (Beaver and Mayne, 1995). Characteristics of some of the vitrified material can be viewed in Table 2.

Table 2: Mass Produced from Plasma Georgia Tech Experiments (after Mayne, 2000)

Initial Soil Type	Initial Water Content (%)	Final Igneous Mass (lb)	Maximum Rated Capacity (kW)	Average Applied Power (kW)	Power Consumed (kW-hr)
Piedmont Silt (L)	18.3	83.8	200	180	180
Piedmont Silt (L)	15.4	108.0	200	172	172
Piedmont Silt (L)	30.9	88.2	200	181	181
Piedmont Silt (L)	17.9	68.3	100	74	74
Piedmont Silt (L)	29.7	57.3	100	71	71
Piedmont Silty Sand (L)	17.4	81.6	100	54	144
Piedmont Silty Sand (L)	23.7	13.2	100	70	17
Goose Lake Clay (L)	11.4	NR	100	53	113
20/30 Silica Sand (L)	0.0	18.1	100	90	NR
20/30 Silica Sand (L)	4.3	26.5	100	63	63
Tyndall Beach Sand (L)	4.1	46.3	100	62	75
Aiken Clayey Sand (L)	8.3	145.5	100	80	428
Aiken Clayey Sand (L)	10.0	88.2	100	68	294
Aiken Clayey Sand (L)	31.4	143.3	100	60	350
Aiken Clayey Sand (L)	8.3	196.2	100	96	624
Aiken Clayey Sand (L)	8.3	410.1	200	200	1100
Aiken Clayey Sand (L)	11.3	83.8	100	96	128
Plastic Kaolin (L)	50.0	52.9	100	80	100
Aiken Clayey Sand (F)	12.4	599.7	1000	650	870
Aiken Clayey Sand (F)	12.4	1199.3	1000	650	1740
Aiken Clayey Sand (F)	12.4	1250.0	1000	650-950	1423

L = laboratory chamber test; F = full-scale field experiment; NR = not recorded

Based on testing done by Beaver and Mayne (1995), Circeo and Mayne (1993), Mayer (1997), Schneider et. al. (1996), Celes (1999), Blundy et. al. (1996), and Mayne et. al. (1997), an empirical expression (Equation 2.5) was developed as follows (note that this equation was derived to yield kg):

$$M = S_s(P^*)^{0.7} \qquad \text{(Equation 2.5)}$$

where: M = mass of vitrified material (kg)

S_s = soil coefficient

$P^* = P/r_c$ = adjusted power consumption (kW-hr)

P = applied power consumption (kW-hr)

$r_c = d_b/d_t$ = closure ratio

d_b = final borehole diameter

d_t = torch diameter

Figure 21 shows the results of the laboratory burns in terms of mass of final rock as a function of power consumption.

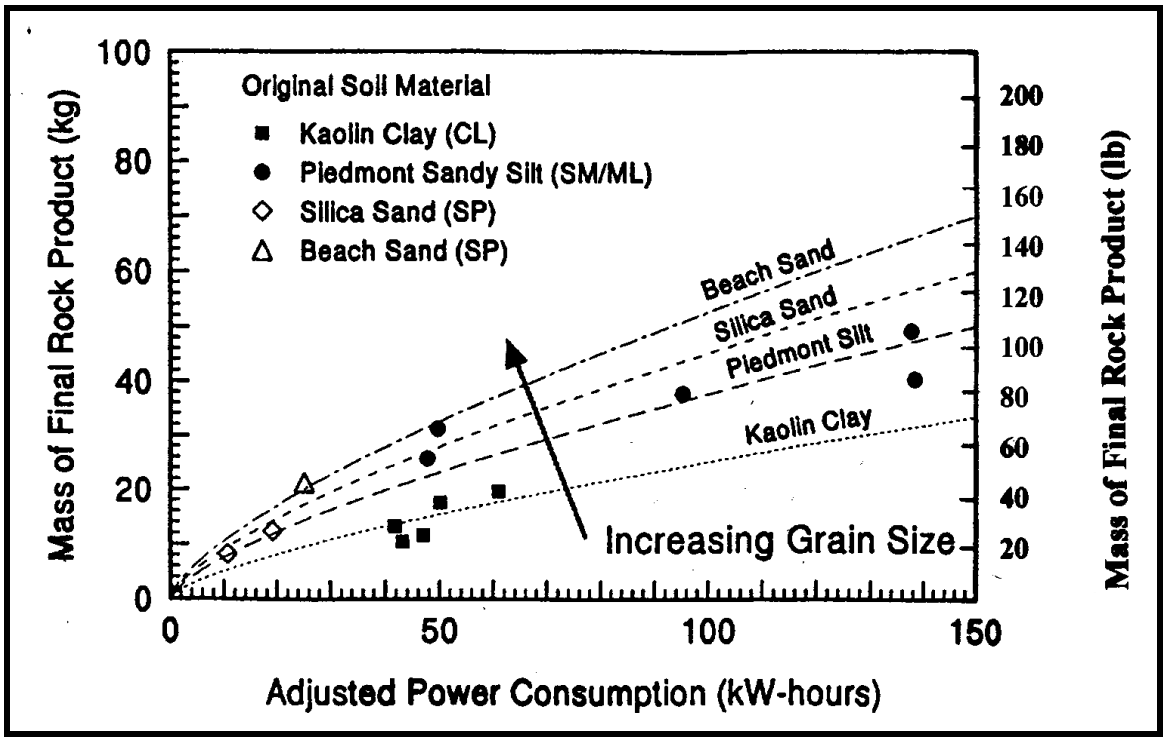

Figure 21. Mass of Rock Product to Adjusted Power (Beaver and Mayne, 1995)

As the power increased to 150 Kw-hour, the mass of rock produced was approximately 88 pounds (40 kg).

A larger diameter of the vitrified material was obtained when the ratio between the borehole diameter to the torch diameter (db/dt) was reduced. For a borehole diameter of 3 inches (75 mm), the diameter of the melt zone was measured to be approximately 14.2 inches (360 mm), as shown in Figure 22. This corresponds to a zone of influence of approximately 4.9 times the borehole diameter. As the ratio of borehole diameter to the torch diameter was increased to two, the melted zone diameter is reduced to approximately 1-foot (0.3m).

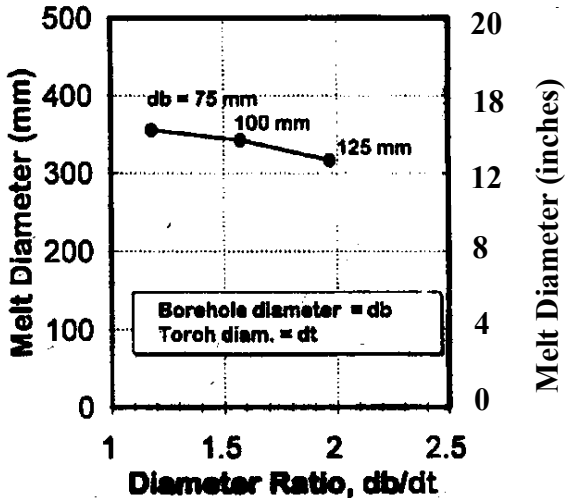

Figure 22. Melt Diameter to Borehole Diameter to Torch Diameter Ratio (Mayne, 2000)

Figure 23 shows the relationship between elastic modulus and uniaxial compressive strength of a vitrified material sample.

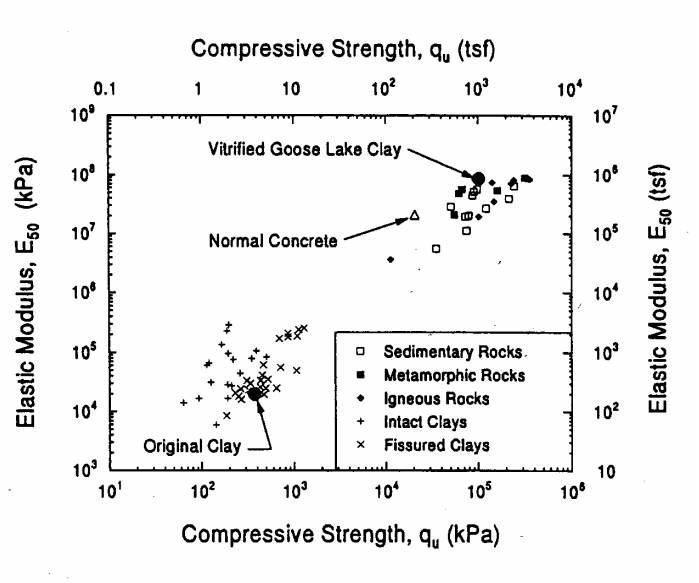

Figure 23. Elastic Modulus vs Compressive Strength of Various Soils and Rocks (Mayne, 2000)

3.0 SITE DESCRIPTION

The test site selected is located on US-1 in the southwestern part of Wake County, just south of Apex, North Carolina. The slide can be found three miles past the intersection of Highway 55 with US-1 at mile marker 91 on the northwestern side (right side of the road). The general location in Wake County can be seen as circled in Figure 24.

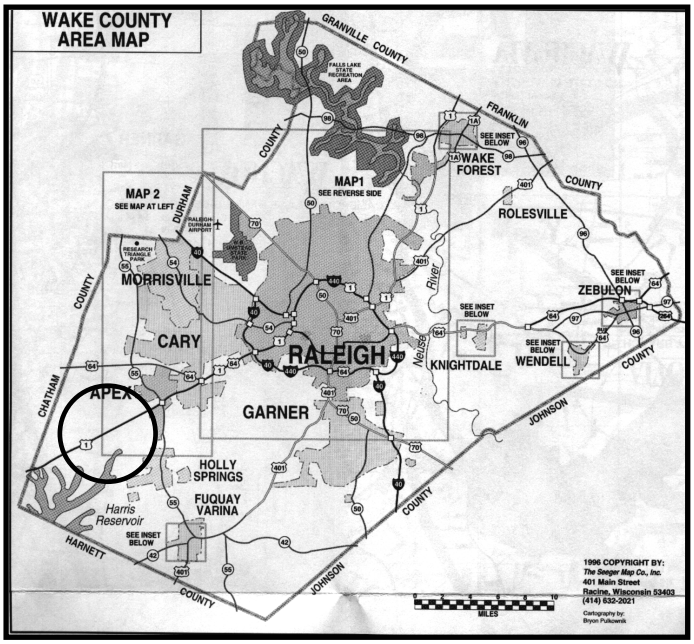

Figure 24. Site Vicinity Map, Wake County (The Seeger Map Co., 1996)

During a site visit, a total of four cut slope failures were noted in the immediate region. Slide features are somewhat obscured by erosion and vegetation, but they appear to all be rotational-compound slide failures. The original cut slope grade was 2 : 1 (horizontal : vertical). The slope failure spans approximately 65 feet, as depicted in Figure 25. The general area is mostly undeveloped with very few residential properties adjoining the site. Vegetation consists of medium to large pine and hardwood trees and dense underbrush. Within the limits of the highway right-of-way, larger vegetation has been removed so that only grass and underbrush remains. The only notable water-related feature is a storm ditch at the toe of the slope with a drain inlet. Topographic measurements conducted on

the slope site revealed that the slope is presently at 3 : 1 (horizontal : vertical), sloping downward towards the roadway, northwest to southeast, as shown in Figure 25.

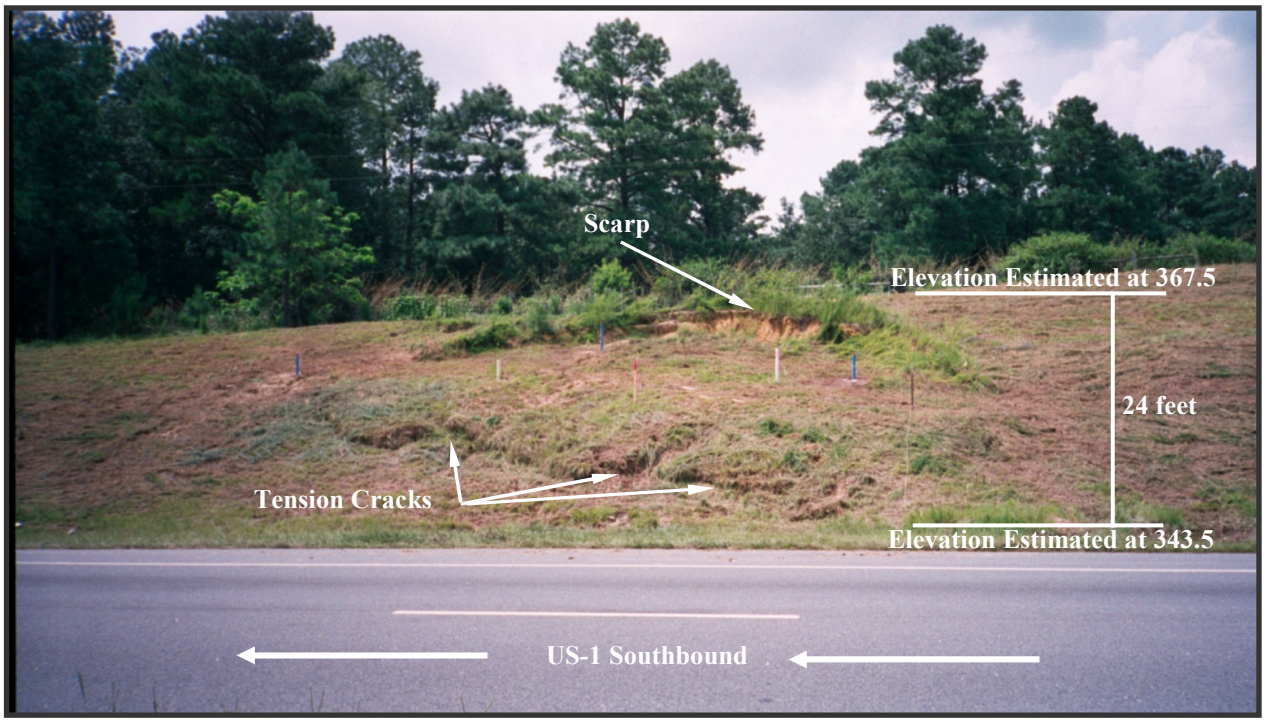

Figure 25. US-1 Slope Failure

3.1 Geologic Description

The test site resides within the Triassic Basins of North Carolina; more specifically, the site falls within the Chatham Group. A general map of the geologic belts of North Carolina is shown in Figure 26 below. The basin was formed during the Traissic and Jurrasic periods; eroded sediment from adjacent igneous and metamorphic formations filled in the lower lying areas (basins), over time forming sedimentary rocks. The *Wake County Soil Survey* places the area of study in the Mayodan-Granville-Creedmoor Association. The soft weathered formations are typical of sandstone, a mudstone, or a conglomerate. The surface soils are primarily residual high plastic clays with random sand lenses. The three major soil types are Mayodan, Granville, and Creedmoor; these soils range from sandy loams to silty loams to clays.

The soil and rock at the slope site are mainly residual silty clays overlying mudstone and sandstone from which they are derived, through chemical and physical mechanisms. The surficial soils are mostly residual high to low plasticity sandy or silty clay (CH-CL), with a few inclusions of clayey sand (SC), as classified in accordance with the Unified Soil Classification System (USCS). Mudstone and sandstone layers were classified to be partially weathered rock (PWR). The sandstones and mudstones were interlayered due to fluctuations of the water level when they were deposited. Based on review of the geologic map, the parent rock likely consists of layered conglomerate, fanglomerate, sandstone, and mudstone rocks, sedimentary in origin.

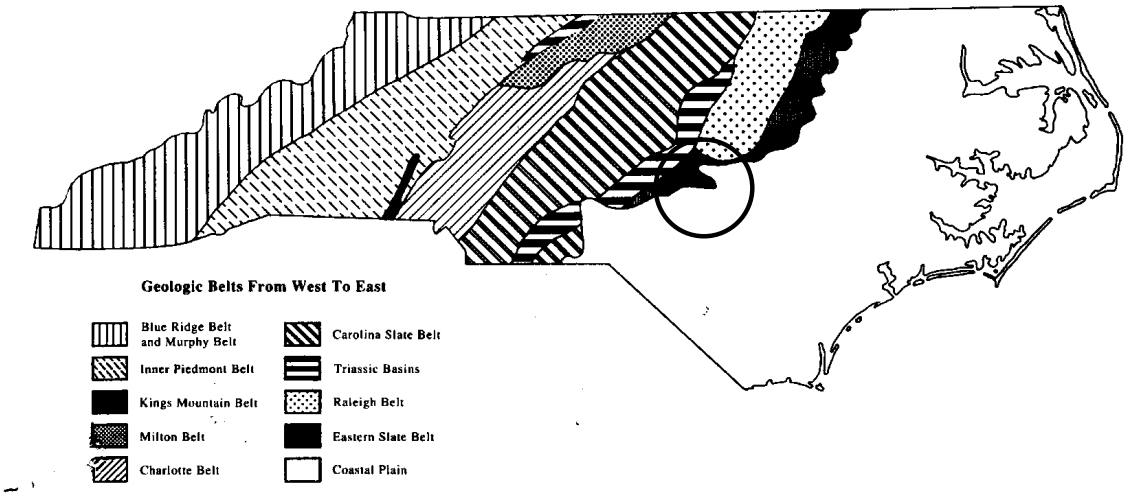

Figure 26. Geologic Belts North Carolina (NCGS, 1991)

3.2 Climate Description

Since numerous slides are rain-induced failures, the precipitation levels in the region were investigated. It was apparent from the onset of this study that water played a critical role in the US-1 slope failure. Rainfall in the region is heavy, with an average of 43.55 inches per year and a maximum-recorded rainfall of 59.14 inches in 1996; an overview of regional rainfall can be seen below, in Table 3 and Figure 27 (from Bill Reh, meteorologist for WLFL). Based on data obtained from the National Weather Service, the town of Raleigh experienced a maximum-recorded monthly rainfall of 21.79 inches in 1999 (data collected between1887 to 2002).

Table 3: Rain Fall Data Record in the past 10 years (From Bill Reh, WLFL)

Year	Average Rainfall* (in)
1991	35.46
1992	43.18
1993	38.05
1994	36.41
1995	48.51
1996	59.14
1997	40.81
1998	52.68
1999	50.64
2000	39.36
2001	34.78

*Average rain fall values take at the RDU Airport

The climate is moderate with an average winter temperature of about 40 degrees Fahrenheit and an average summer temperature of about 78 degrees Fahrenheit (Apex Chamber of Commerce).

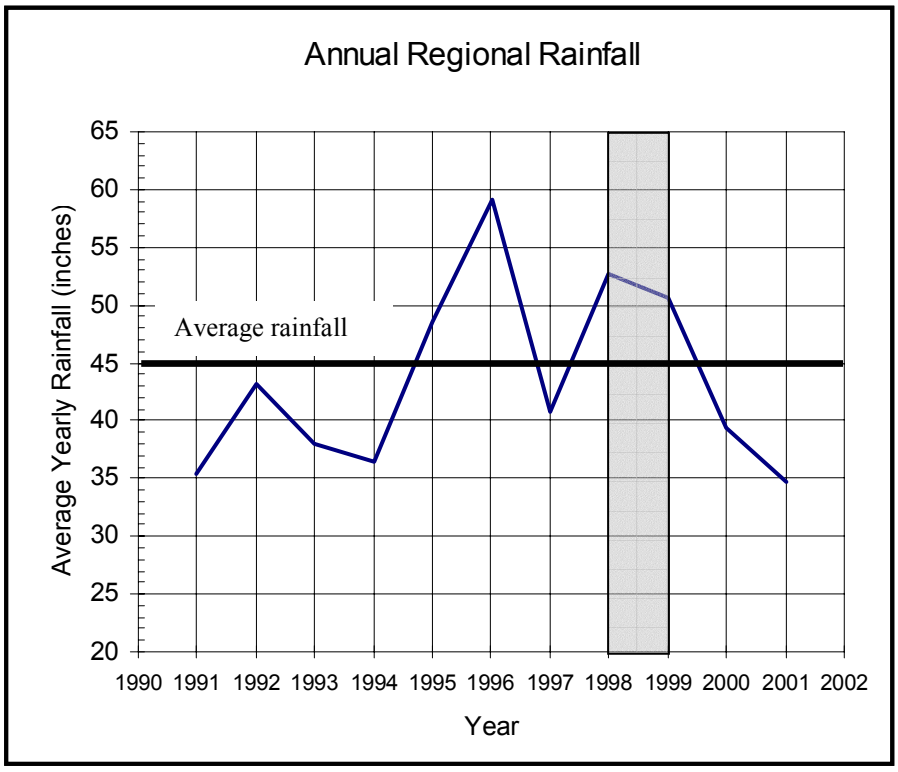

Figure 27. Annual Rainfall for the Area

It is hypothesized that the US-1 slope slide occurred during the 1998 to 1999 time period, as shown in Figure 27. It is important to note that the rain levels depicted are yearly and do not show seasonal or monthly fluctuation.

3.3 Site Seismic Information

The region is considered inactive relative to potential seismic and tectonic activity. Based on Figure 28, the site (circled on the figure) is located in a zone, which has a peak horizontal acceleration of approximately 3.0%g with a 10% probability of being exceeded in 50 years. Horizontal acceleration is expressed as a percent of gravity (%g) (USGS, June 1996).

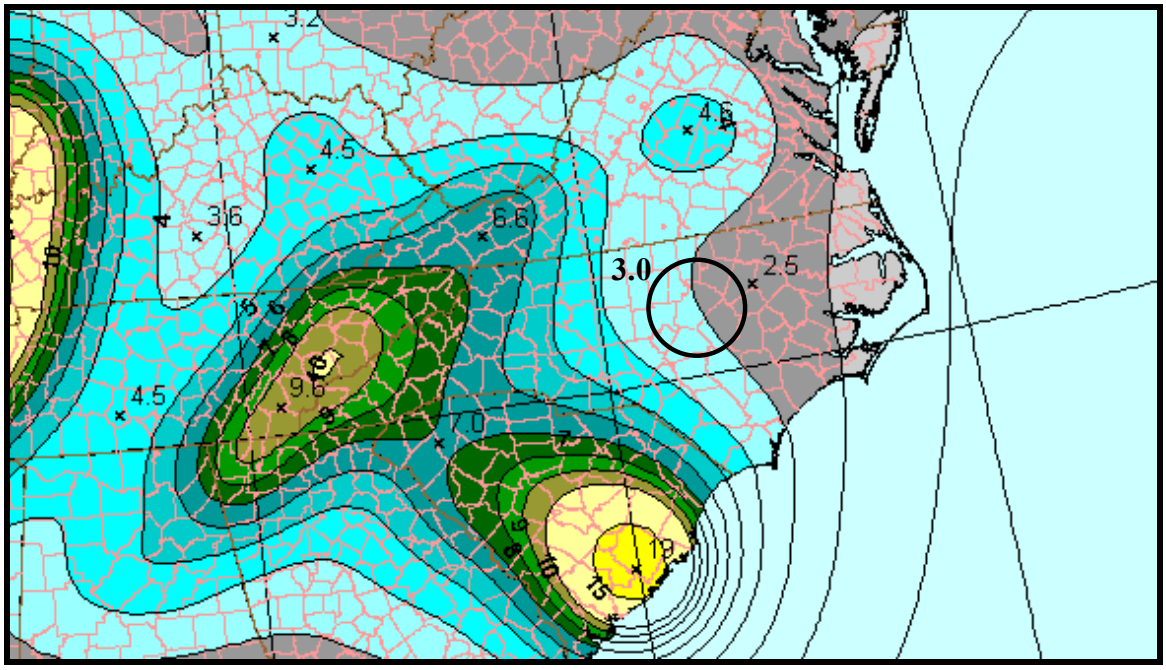

Figure 28. National Seismic Hazard Maps (USGS, June 1996)

No seismic activity was considered in the cause of the slope failure. Therefore, it was not taken into account in the modeling phase of this work.

4.0 CHARACTERIZATION OF TEST SOILS

This chapter outlines the field explorations undertaken at the US-1 site, between the years of 1998 and 2000. Early investigations were conducted by the North Carolina Geological Survey (NCGS). Later, in March and July of 2000, subsurface investigation and base line geophysics testing were completed by the North Carolina Department of Transportation Geotechnical testing Unit (NCDOT), Georgia Tech, and North Carolina State University, respectively.

4.1 NCGS Subsurface Exploration

The North Carolina Geological Survey's (NCGS) evaluation consisted of shallow hand auger bores and an extensive survey of the topographic features of the slope. They identified a possible failure plane along the interface of two weathered rock sections, as seen in Figure A1, in Appendix A. The inclination of the failure plane ranges from 10 – 15 degrees, prevalently about 12 degrees on the slope of study. Stratigraphy for the area, per the NCGS investigation, revealed the following:

- a conglomeratic layer of sandstone that turns to a silty sand with clay,
- a micaceous mudstone that contains soft clay lenses and laminae where the slip plane is postulated to be, and
- a micaceous sandstone yielding to a siltstone towards its base.

Further investigations by the NCDOT Geotechnical Unit and slope stability analyses strongly supported the NCGS hypothesis.

4.2 Current In-Situ Testing

The NCDOT Geotechnical Unit conducted subsurface investigations and inclinometer installation activities at the site during the months of March and July 2000. The subsurface investigation consisted of a total of five soil test borings. Standard penetration tests (SPT) and soil sampling were performed at each of the borings. Figure 29 shows locations, dates, and type of instrumentation installed at the slope site.

Figure 29. US Route 1 Borehole Locations

Borings were advanced to depths of 16.5 to 30 feet, with most terminated at elevations in soft weathered rock. Continuous NXWL casing was used in conjunction with an automatic hammer CME550 drill rig. Standpipes and inclinometers were installed during the exploration to monitor on-going slope movement, if any. A generalized profile was developed from the NCDOT boring logs, as seen in Figure A2 in Appendix A. Elevations were taken from the survey conducted by Georgia Tech and referenced to NCGS Monument, "Patrick".

Both disturbed and undisturbed soil samples were obtained from the site. Shelby tube samples were extracted at BH-1 and BH-2 in March 2000. These undisturbed samples were used for triaxial, direct shear, and consolidation testing. Split-spoon samples and soft weathered rock cores were taken at BX-1 and BX-2. At boring BX-3, material was augured out and bulk sampled. N-values recorded during standard penetration testing ranged from 3 to 44 blows per foot in the overlying soil and 100 plus blows per foot for the soft weathered rock regions. Table 4 shows idealized blow count

profile as constructed from the field studies conducted by the NCGS and the March / July 2000 borings by the NCDOT.

Table 4: Idealized Blow Count Profile for the US-1 Site

Layer	Soil Description	Average Blow Counts (BPF)
1	soft clay	N =3
2	stiff clay	N = 10
3	hard clay	N = 32
4	SWR (sandstone)	N = +100
5	SWR (siltstone)	N = +100

Groundwater was not encountered within any of the borings at the time of drilling operations. However, it should be noted that borings were performed during a dry period of the year when groundwater levels are typically low. Water level elevations can be expected to fluctuate due to seasonal variations in rainfall, evaporation, and other factors.

4.3 Georgia Tech Geophysical Exploration

Geophysical characterization of the site profile was conducted between the months of March and December. Georgia Tech conducted these geophysical tests as part of the baseline, pre-classification testing program. The following tests were conducted: Magnetics/Electromagnetic Conductivity, Earth Resistivity, and Ground Penetrating Radar (GPR). Though the data obtained displayed good pre-vitrification profiling of the site, these data are of little assistance on this project due to the fact that the field application of PAV was canceled. If the field PAV columns are implemented, then the geophysics data will be invaluable for use in comparison to post-site profiling. The complete geophysics data are presented in Appendix B of this report.

4.4 Inclinometer Data

The NCDOT Geotechnical Unit conducted slope monitoring using slope inclinometers. The first measurements are considered as a baseline for comparison. Later measurements would determine the actual failure plane as well as the slippage rate.

Three 70-mm diameter inclinometer casings were placed in boreholes BX-1, BX-2, and BX-3 during the July drilling. Starting August 28, 2000, data were collected by the NCDOT using a digital inclinometer probe at least once every two weeks. Data were downloaded to the DigiPro Software. (Figures C.3 through C.5, Appendix C, were developed using this software.) Extensive slope monitoring found no clear indication as to the location of the slip plane. It had been postulated that the slope failure was brought on by the infiltration of water into the mudstone layer; an action that would result in weakening of the stone.

5.0 LABORATORY INVESTIGATION

The focus of this section will be to discuss the results of testing that was performed on samples obtained from the US-1 slope site. Testing was performed at both Georgia Institute of Technology and North Carolina State University.

5.1 Overlying Soil

Laboratory testing consisted of index properties and shear strength tests. Laboratory test results indicated that moisture contents tended to vary from about 20 to 60 percent. Moisture contents decreased with depth. Atterberg Limit tests on the material indicated liquid limits ranging from 41 to 66% and plasticity indices varying from 10 to 34%. The surficial soils are residual and are derived from rock similar to the Triassic sandstone and mudstone beneath. The site soils were classified mostly to be high to low plasticity silty clays (CH-CL). Table 5 details the laboratory findings regarding the soil samples taken at the US-1 site.

The peak shear strength of the soil was obtained by conducting consolidated undrained triaxial tests on "undisturbed" specimens according to ASTM D 4767. A fully automated Geocomp Load Trac system, located in the Georgia Institute of Technology, was used for conducting the tests. Due to the limited number of undisturbed specimens, only two triaxial tests were executed. Specimens 1 and 2 were extracted from BH-1 (from depths 3 ft to 5 ft, and from 5 ft to 7 ft, respectively.) Test results are shown in Figure 30.

Table 5: Results of Laboratory Testing on Overlying Soil ~ March drilling of BH-1 & BH-2, July drilling of BX-1 & BX-2

Sample	Depth (ft)	N_{avg} (BPF)	Soil Description (field)	USCS	LL	PI	CF (%)	w_{nat} (%)
Drill BH-1								
J	1.5	3	soft silty clay	CH	66.16	29.66	48.8	--
F	3.0	5	firm silty clay	CH	58.09	24.59	37.4	43.93
G	5.0	7	firm silty clay	CH	55.94	22.88	--	39.59
E	7.0	38	hard silty clay	CL	45.76	14.68	--	28.53
L	9.0	44	hard silty clay	CL	41.80	15.5	30.93	--
Drill BH-2								
H	1.0	2	very soft silty clay	CH	58.55	23.48	45.2	34.98
A	3.0	4	soft silty clay	CH	60.19	24.34	--	36.89
B	5.0	4	soft silty clay	CH	54.05	21.75	--	47.72
C	7.0	8	firm silty clay	CH	55.23	22.45	--	30.17
Drill BX-1								
SS1	2.9	4	soft silty clay	CH	59.8	27.6	--	23.39
SS2	7.9	9	stiff silty clay	CH	56.6	22.7	--	23.21
SS3	11.2	18	very stiff silty clay	CH	58.0	19.9	--	23.82
SS4	12.9	21	very stiff silty clay	CL	42.1	10.0	--	22.83
Drill BX-2								
SS5	3.6	3	soft silty clay	CH	63.9	33.9	--	38.78
SS6	8.6	11	stiff silty clay	(CH)	--	--	--	24.81
SS7	9.5	20	very stiff silty clay	(CL)	--	--	--	25.11
SS8	136	32	hard silty clay	(CL)	--	--	--	14.43

Note: All soils are classified residual. (CH) = visual classification, while CH = lab classification, and -- = test not performed

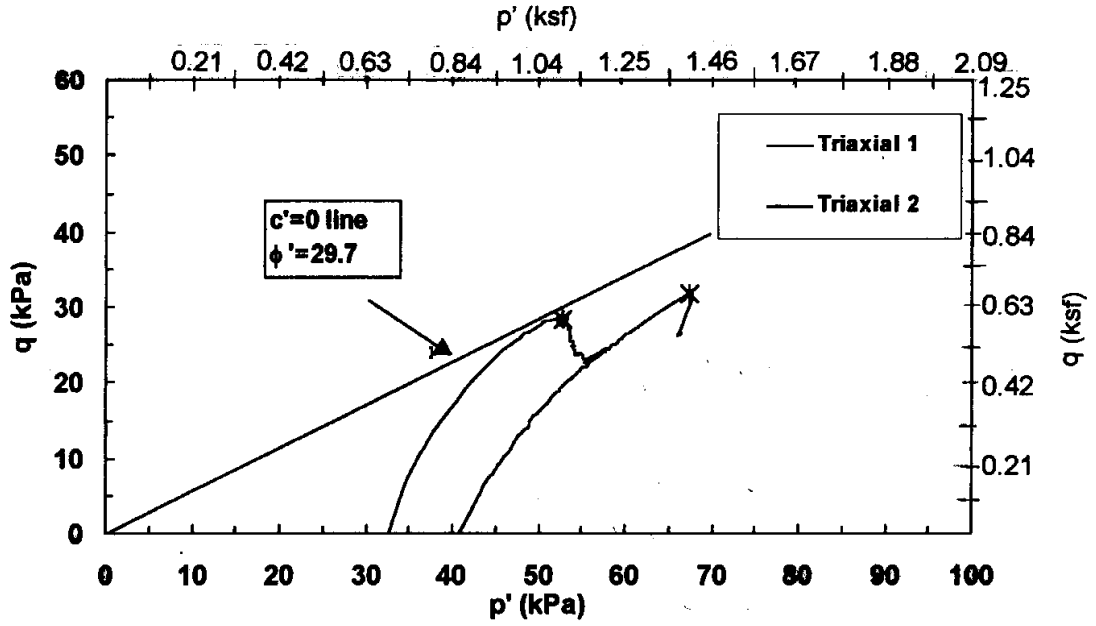

Figure 30. Triaxial test results for silty clay (Georgia Tech, 2001)

Direct shear tests were conducted using an automated ShearTrac testing machine located at the Georgia Institute of Technology. Tests were conducted on five specimens by varying the normal stress. Based on test results at failure, the Mohr-Coulomb failure envelope, shown in Figure 31, was plotted for the peak shear strength. The angle of internal friction was evaluated to be 25.6°. The fully softened shear strength of the clay was obtained by testing remolded specimens using the direct shear test. Using the failure stresses, a Mohr-Coulomb failure envelope was developed. The fully softened angle of internal friction was estimated to equal to 24.4°, as shown in Figure 32.

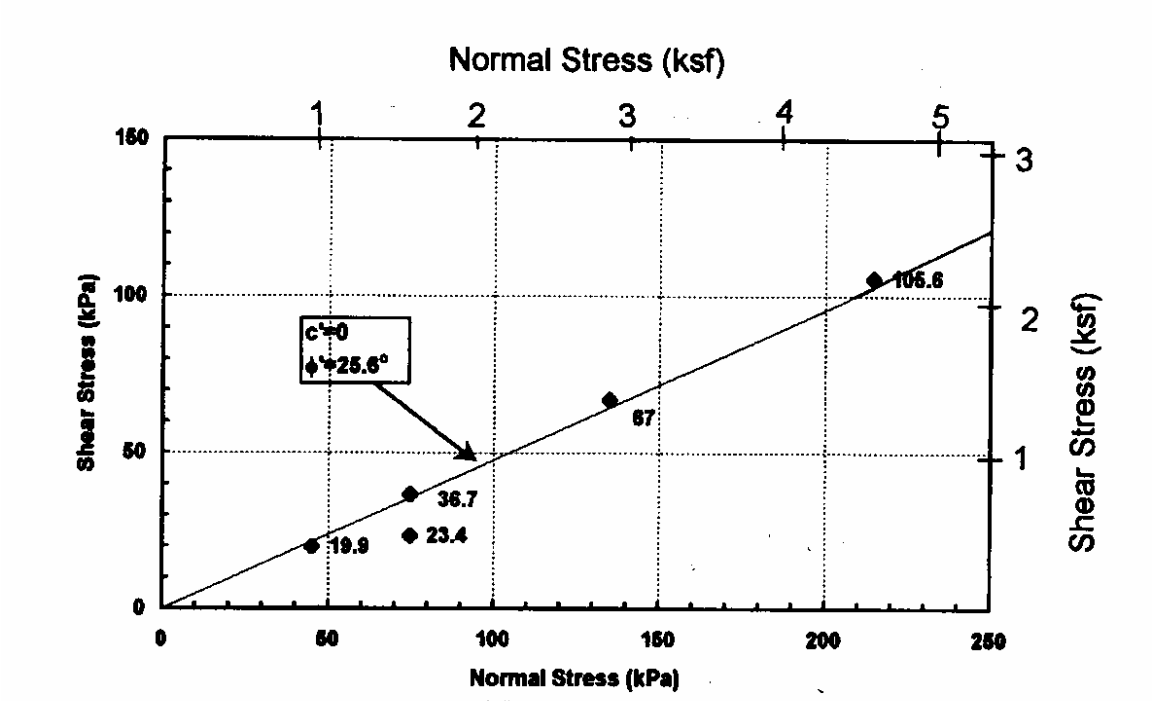

Figure 31. Peak Shear Strength of Silty Clay Based on Direct Shear (Georgia Tech, 2001)

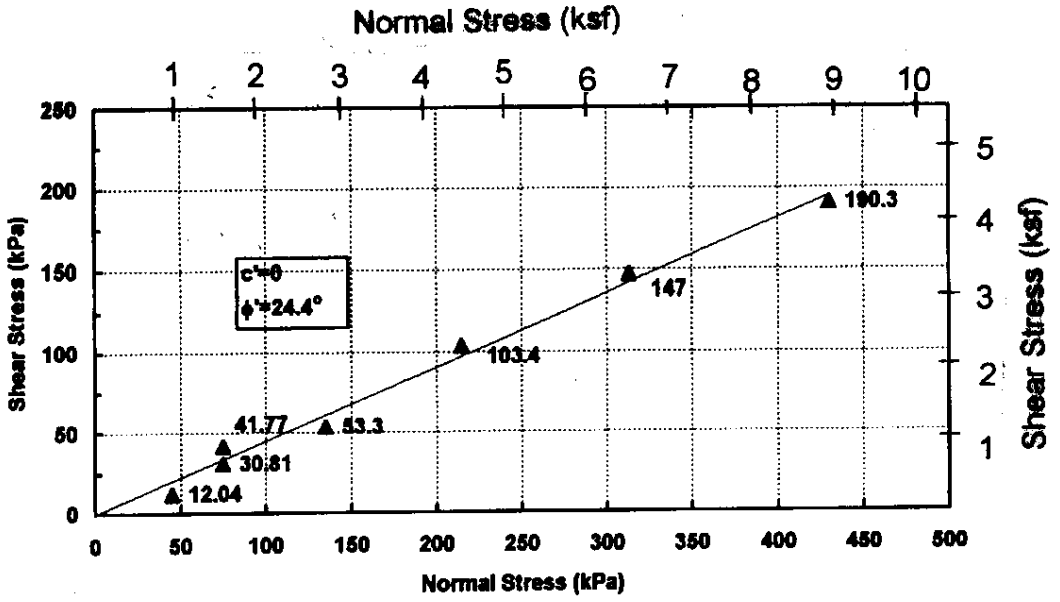

Figure 32. Fully Softened Shear Strength Based on Direct Shear (Georgia Tech, 2001)

The residual shear strength was evaluated using the ring and direct shear tests. The ring shear testing device is a Bromhead manufactured by Wykeham Farrance company and is located at North Carolina State University in Raleigh, NC. Three specimens from BH-1 and BH-2 were tested. Figure 33 summarizes the test results. The average residual angle of internal friction was assessed to be 17.5°.

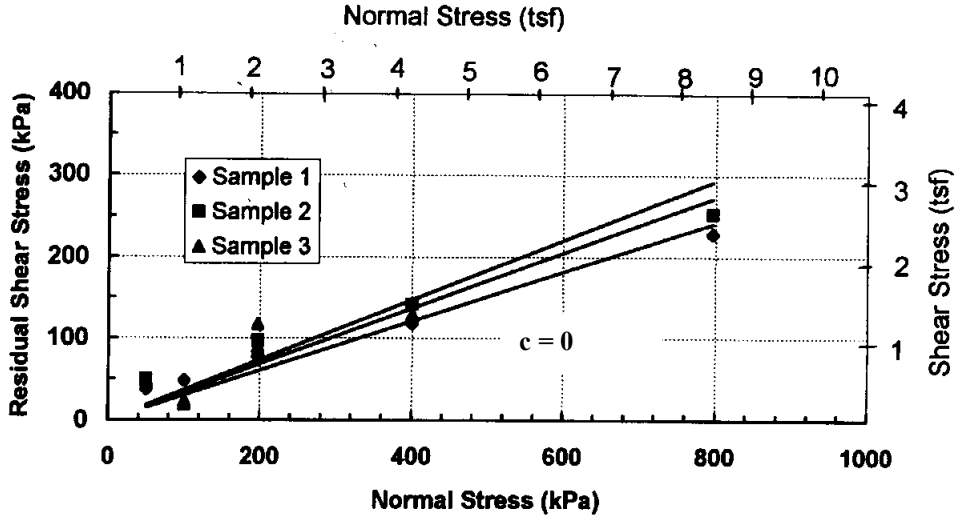

Figure 33. Ring Shear Residual Shear Strength Test Results on Silty Clay (Georgia Tech, 2001)

Residual shear strength was also evaluated from the direct shear results conducted on intact and remolded specimens. Test results are shown in Figure 34. The values of the internal angles of friction were evaluated to be 21^{o} and 18.6^{o} for the intact and remolded specimens, respectively.

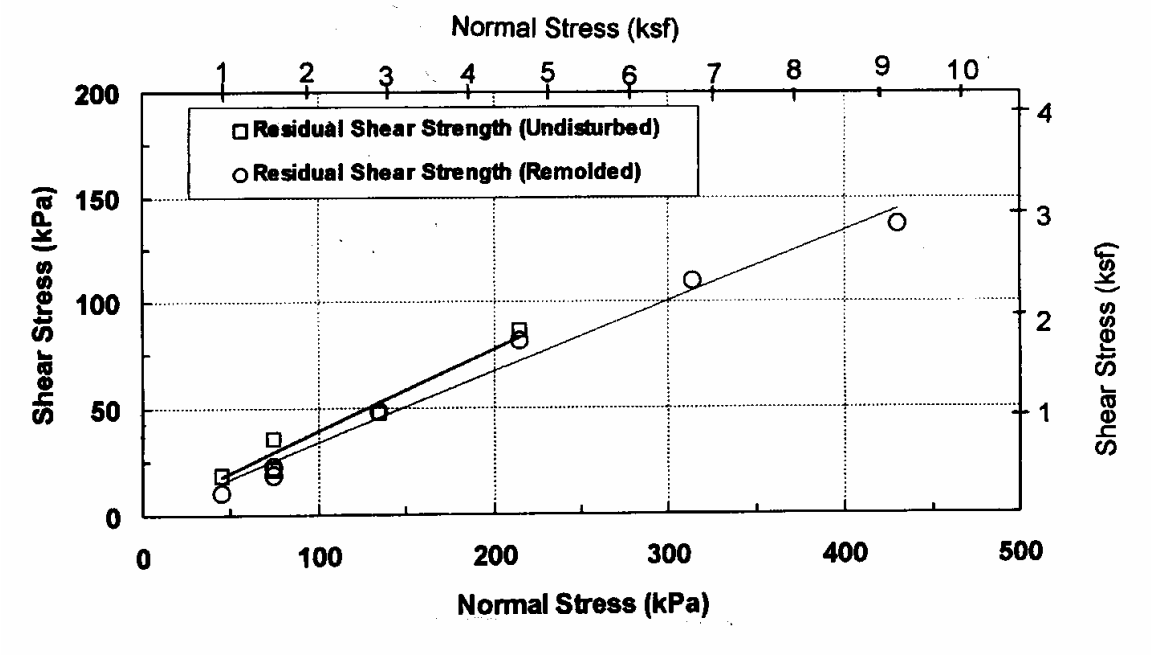

Figure 34. Direct Shear Residual Shear Strength Test Results on Silty Clay (Georgia Tech, 2001)

Table 6 summarizes the values of the internal angle of friction for the residual silty clay from the US 1 slope site under study.

Table 6: Summary of internal friction angles for silty clay

Test	ϕ'_{peak}	$\phi'_{softened}$	ϕ'residual
Triaxial	29.7	--	--
Direct Shear (intact)	25.6	--	21.1
Direct Shear (remolded)	--	24.4	18.5
Ring Shear	--	--	17.5

The clay fraction of the test site material exhibited a range from 30% to 49%; this corresponds to a residual ring shear friction angle of 10 to 20 degrees, according Figure 35, which is consistent with the results obtained in this study.

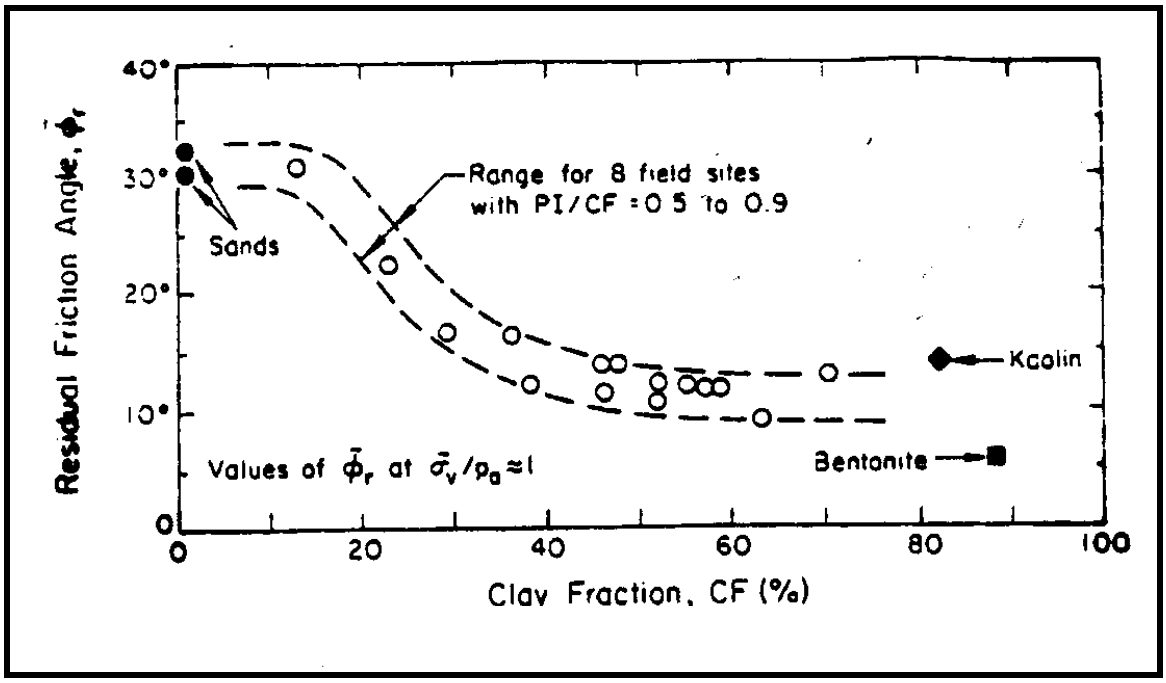

Figure 35. Residual Friction Angle from Ring Shear Tests
(Kulhawy and Mayne, 1990)

The undrained shear strength parameter for the overlying soil were developed using empirical correlations, triaxial tests, and direct shear testing. Three methods were employed: Navy (chart), AASHTO (chart), and Vesic (*c = 100N*) in order to estimate the undrained shear strength (S_u) for the idealized profile. The estimated values are shown in Table 7.

Table 7: Undrained Shear Strength for the Idealized Profile of Overlying Soil

Soil Description	N_{avg}	AASHTO	Vesic* (1977)	Navy**	Used S_u
	(BPF)	(psf)	(psf)	(psf)	
soft silty clay	3	375	300	400	300
firm silty clay	6	750	600	600	600
stiff silty clay	10	1200	1000	1300	1200
hard silty clay	32	4100	4300	4000	4000

*Vesic (1977), c = N100, uncorrected, for N < 20
**Navy chart gives unconfined compressive strength q_u, $S_u = q_u / 2$, used Terzaghi & Peck's line

5.2 Soft Weathered Rock

Weathered rock samples were cored from depths of 17.0 to 33.0 feet below the surface. A total of 10 samples were chosen for testing. The rock quality designation (RQD) for the weathered rock mostly ranged between 42 and 80. Table 8 summarizes the laboratory findings regarding the soft weathered rock samples taken at the US-1 site.

Table 8: Soft-Weathered Rock ~ July drilling of BX-1 and BX-2

Sample	Depth	RQD	REC	Type	Slake	UCS	Tensile	LL	PI
	(ft)	(%)	(%)		(%)	(psi)	(psi)		
Drill BX-1									
5	17.1 - 18.7	42	88	Sandstone	0.0	--	--	NP	NP
4	19.4 - 20.6	58	94	Sandstone	18.4	175	21	NP	NP
3	21.3 - 22.7	58	94	Siltstone	38.0	--	--	33.5	8.2
2	24.4 - 25.9	80	96	Siltstone	59.7	1845	218	29.1	5.8
1	25.9 - 27.9	80	96	Siltstone	42.2	2484	205	30.5	6.3
Drill BX-2									
E	20.0 - 22.4	78	92	Sandstone	6.1	--	--	NP	NP
D	22.4 - 25.7	78	92	Sandstone	11.2	190	26	NP	NP
C	26.3 - 29.8	40	60	Siltstone	2.1	1247	241	29.8	6.3
B	29.8 - 31.7	54	98	Siltstone	45.1	--	--	32.2	7.4
A	32.0 - 32.6	54	98	Siltstone	43.0	--	--	30.0	7.1

Note: Samples US1-A, US1-B and US1-3 are similar materials. The same is true for US1-4, US1-5 and US1-D. Again, the same is true for US1-1, US1-2 and US1-C. The material from these cores was so soft that many tests could not be conducted. This can be seen in the blank regions indicated. The notation -- indicates that laboratory testing was not performed.

For the soft weathered rock, the undrained shear strength was estimated by methods outlined in AASHTO's "Standard Specifications for Highway Bridges" using RQD and uniaxial compressive strength. A summary of the results is shown in Table 9.

$$S_u = C_m / 2 \qquad \text{(Equation 5.1)}$$

$$C_m = \alpha_E (C_o) \qquad \text{(Equation 5.2)}$$

$$\alpha_E = 0.0231 \text{ (RQD)} - 1.32 \geq 0.15 \qquad \text{(Equation 5.3)}$$

where:

C_m = uniaxial compressive strength of rock mass

C_o = uniaxial compressive strength of intact rock (test lab)
α_E = reduction factor that accounts for discontinuities based on RQD

Table 9: Undrained Shear Strength (S_u) of SWR

Soil Description	S_u (psf)	ϕ' (degree)
SWR (sandstone)	1950	40
SWR (siltstone)	13500	35

Reference: AASHTO

The effective internal friction angles were estimated for the soft weather rock.

6.0 LABORATORY VITRIFICATION

A laboratory vitrification test was conducted on soil extracted from the slope site using a backhoe (by the NCDOT). The soil was then placed and sealed in 55-gallon drums to prevent changes in moisture content and transported to the Georgia Tech Plasma Applications Research Facility (PARF) in Atlanta. The slope material was composed of residual plastic clay resulting from the weathering of the underlying mudstone layer.

6.1 Pre-Vitrification Tests Setup

The soil was compacted at its natural moisture content in cylindrical steel chamber 36-inches in diameter and height. A ¾-in thick insulation was placed on the inside bottom of the chamber. Soil was placed in 15 layers, each layer being compacted with a 17.5 pound (8-kg) weight at 75 blows/layer. The soil's water content was monitored at each lift, approximately 25% of the full depth. It is important to note that the slope stratification was not reproduced. The soil tested was a mixture of the soil obtained and therefore a heterogeneous mixture. A metallic 4-inch diameter stovepipe (borehole) was placed at the center of the chamber; through this borehole, the torch was placed into the ground during vitrification. The hole's final elevation was 6-inches off the bottom of the container. The average total and dry unit weights were 109.1 and 86.2 lb/ft^3, respectively. Figures 36 and 37 show a schematic diagram of the chamber setup and a photograph of the actual chamber. Six thermocouples (Omega) were placed through pre-drilled holes in the chamber wall; these holes were arranged in two rows, at 12 inches and 18 inches, respectively, off the bottom of the container. The embedment lengths were 2, 4, and 6 inches into the chamber.

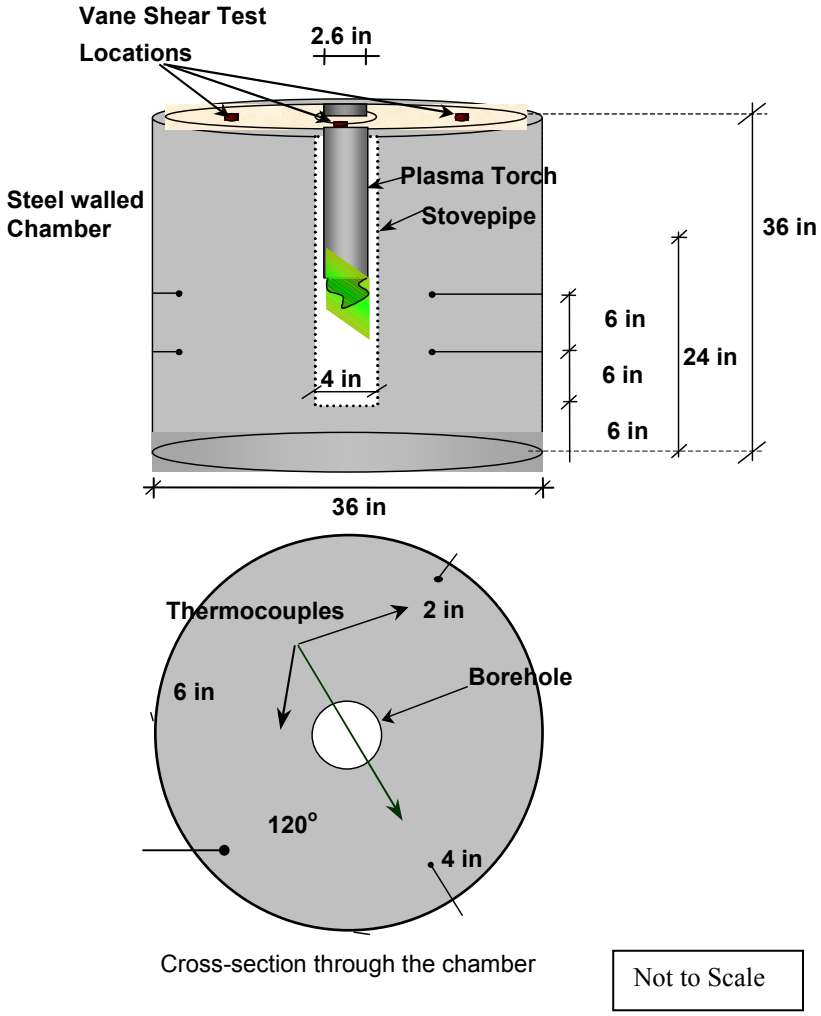

Figure 36. Chamber Setup for Plasma Vitrification of Route 1 Clay (Georgia Tech, 2001)

Peak and remolded soil strengths versus depth were determined using a laboratory shear vane device. Measurements were made in 4-inch increments, starting from the top of the chamber to 30-inch in depth. Knowing the measured torque at failure, the undrained shearing resistance was calculated. To determine the remolded shear strength, the blade was rotated rapidly to remold the soil and the shearing strength was measured again. Peak shear strength values ranged from 1.04 to 2.25 ksf, increasing with depth. Remolded shear strength values ranged from 0 to 1.04 ksf, increasing with depth.

Figure 37. Photograph of Test Chamber Setup (Georgia Tech, 2001)

6.2 Laboratory Burn

Vitrification of the US-1 slope material was conducted on November 29, 2000; the burn started around 8:30 am and proceeded for 70 minutes, during which time the material was burned constantly. The vitrification was conducted using the 100-kilowatt torch, initially located 6-inches off the bottom of the chamber. The torch was turned on and allowed to run for 10 minutes in its initial position, subsequently raising it every 15 minutes with an average withdrawal rate of (0.2-in/min).

at 10 minutes – up 3.5 inches

at 25 minutes – up 3.5 inches

at 40 minutes – up 3.5 inches

at 55 minutes – up 3.5 inches

This was done to prevent the torch from over heating the tip and to evenly distribute the heat throughout the soil mass. Voltage and current intensity were recorded every 5 minutes for energy consumption calculations. The average energy consumption during the experiment was 97 kWh. Temperature readings were measured at regular time intervals. For additional photos of the vitrification see Appendix.

6.3 Post Vitrification Testing

After the test completion, magma was allowed to cool for 48 hours before opening the chamber. No significant subsidence was observed. Originally, the mass of the soil was 2041.5 lbs. After vitrification, the total mass of the vitrified and unvitrified soil dropped to 1993.0 lbs. The weight loss could be attributed to drying of the soil surrounding the vitrified zone. The vitrified column weighed 103.6 lbs. Figure 38 shows a photograph of the vitrified end product.

Figure 38. Vitrified Column of Weathered Mudstone Created using 100-kW Torch (Georgia Tech, 2001)

Table 10 shows the final mass, power and energy consumption, specific energy requirement (SER), and the maximum diameter of the vitrified soil. It should be mentioned that the specific energy requirement is defined as the amount of energy required for the formation of a unit mass of the vitrified material.

The mass of vitrified column from US 1 weathered mudstone laboratory burn is in good agreement with previous experiments in the existing database. Figure 39 shows the correlation between the vitrified mass and the energy put into the soil.

Table 10: Vitrification Test Results using 100-kW Torch

Test Code	Running Time	Vitrified Mass	Power Consumption	Energy Consumption	SER	Maximum Diameter
	min.	lbs (kg)	kW	kWh	lb./kWh (kg./kWh)	in (cm)
NC-1	70	104 (47)	83	97	1.1 (0.48)	15 (38)

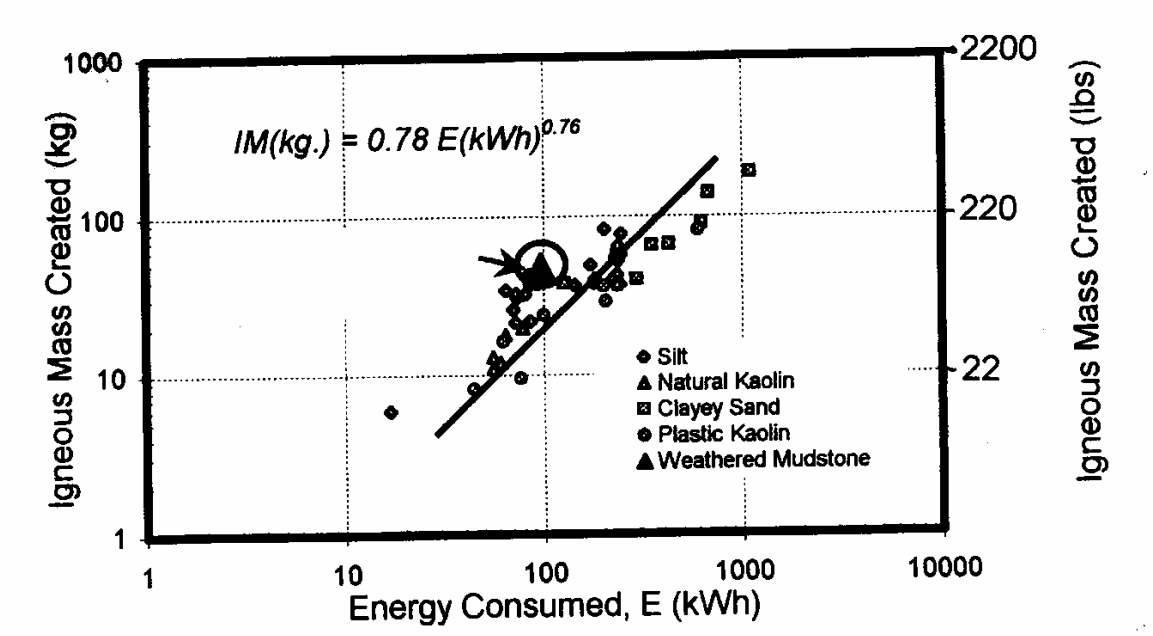

Figure 39. Mass of Vitrified Column Versus Energy Consumption (Georgia Tech, 2001)

Based on previous chamber test results, the following empirical expression between the created igneous mass and energy consumption is formulated, as described before equation 2.5, where the soil coefficient equals 0.78. This expression is given in Equation 6.1; note that this equation results in kg:

$$IM = 0.78\ E^{0.76} \qquad \text{(Equation 6.1)}$$

where:

IM = igneous mass created (kg)
E = energy consumed (kWh)

6.3.1 Unit Weight

The unit weight of the vitrified material was calculated to be 159.15 lb/ft^3. This represented a 46% increase in unit weight relative to the original soil.

6.3.2 Initial Small-Strain Stiffness

Non-destructive ultrasonics were used to measure the shear and compression wave velocities of the rock, at Georgia Institute of Technology. Though cubical specimens were trimmed from the larger rock mass, they were too small to use without having the measurements affected by the boundary conditions. Therefore, the test was conducted on irregularly shaped samples with two trimmed parallel sides.

The test setup consists of a pulse generator unit, transducer, and an oscilloscope. According to ASTM D 2845, a mechanical wave is generated and transmitted through the specimen. A receiver receives it on the other end of the rock. The transmitter is connected to a trigger that marks the time the wave is generated. The timing is stopped when the wave is detected by the receiver geophone and the travel time is obtained. The travel velocity is then calculated by dividing the specimen height by the travel time. The specimen was tested using both compression and shear waves. The shear and compression wave velocities were measured to be 9000 ft/s and 15,426 ft/s, respectively.

Using Equation 6.2, the shear modulus was calculated to be 2780 ksi. Using a Poisson's ratio of 0.12, the elastic modulus was found to be 3115 ksi.

$$G_0 = \rho V_s^2 \qquad \text{(Equation 6.2)}$$

where:

G_0 = strain shear modulus

ρ = soil density

V_s = shear wave velocity

6.3.3 Compressive Strength Tests

The compressive strength of the cooled rock-like product was measured by a uniaxial compression test using a SATEC compression machine, at Georgia Institute of Technology. The specimen was loaded at a constant rate of 0.2-in/minute. A sample was trimmed, using a diamond saw, into a cube 0.7 in X 0.7 in X 1.5 in and the loading faces were cut parallel. Specimen is shown in Figure 40. The sample started shattering but did not completely fail when the compression machine capacity was reached. The peak load was 15.1 kips. Accordingly, the compressive strength would be higher than 4845.6 ksf or 33.65 ksi. The stress-strain curve is shown in Figure 41.

Figure 40. Photograph of the Vitrified US 1 Clay Compression Test Specimen (Georgia Tech, 2001)

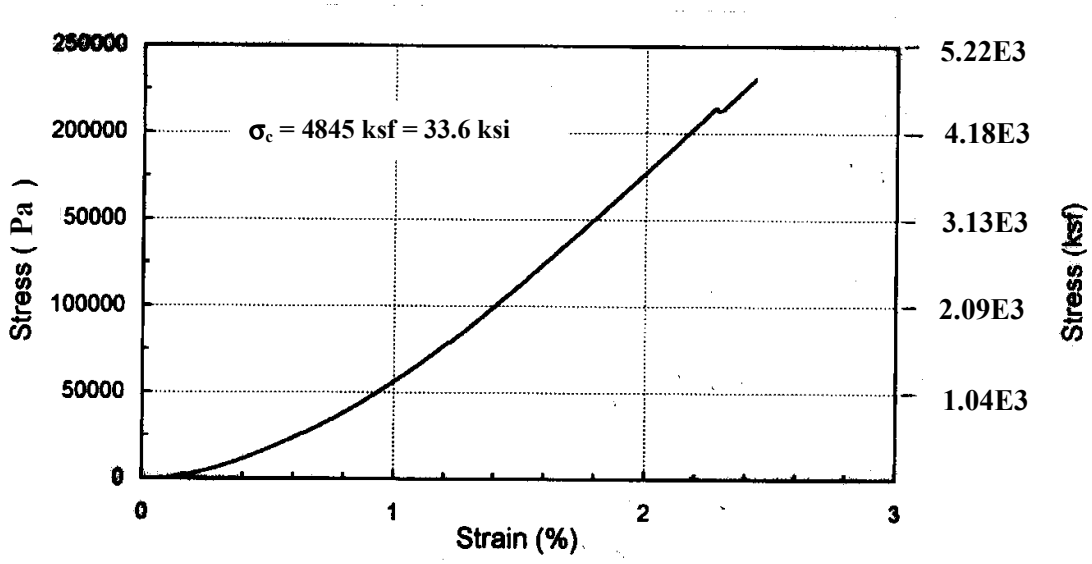

Figure 41. Stress-Strain Curve for the Uniaxial Compression Test Conducted on the Rt 1 Vitrified Clay (Georgia Tech, 2001)

Figure 42 shows the improvement in soil stiffness and compressive strength due to vitrification. Soil shear wave velocities were measured using down-hole tests while ultrasonic laboratory testing was used to determine the shear wave velocity in the intact vitrified material. The peak compressive strengths for two soil specimens extracted from borehole BH-1 were determined using triaxial tests, as previously described in section 5.1. The samples were tested at confining pressures of 0.691 and 0.849 ksf. The strength of the vitrified material was measured by uniaxial compression testing.

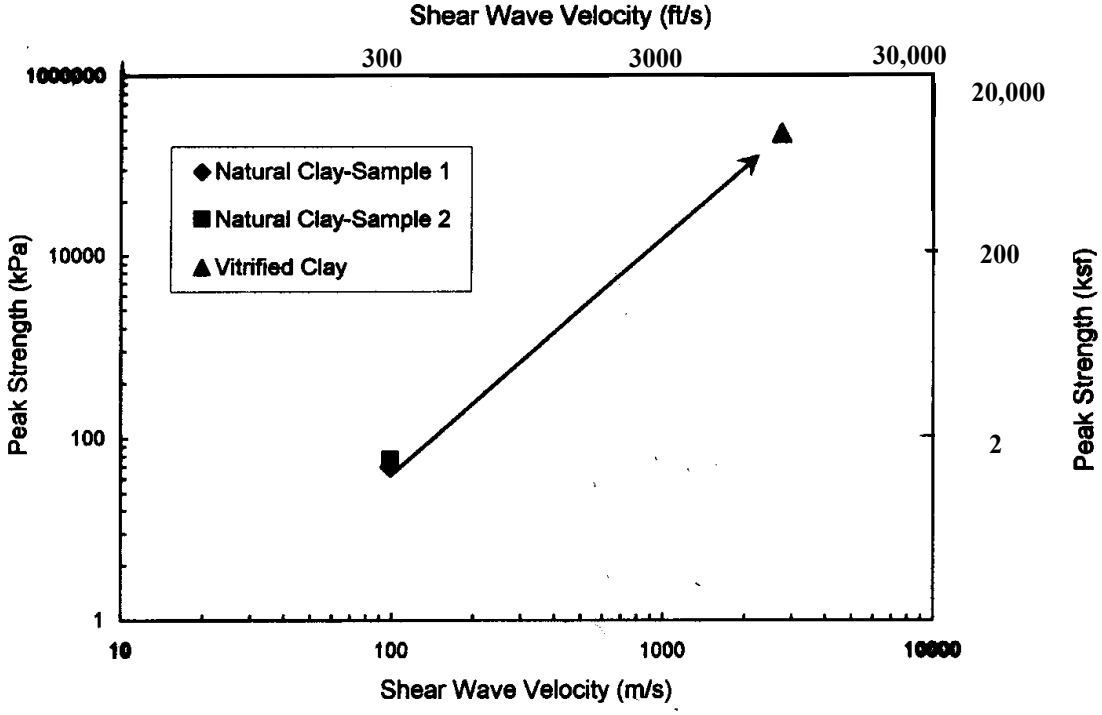

Figure 42. Improvement in Soil Stiffness and Compressive Strength through Plasma Vitrification (Georgia Tech, 2001)

7.0 SLOPE STABILITY MODELING

This section details the development and analyses conducted on the effects of PAV columns being placed within the US-1 slope. First, details are offered as to how the models were developed and then the results of the parametric study are presented for review.

7.1 Overview of Development of Slope Stability Models

Field explorations of the slope consisted of standard penetration testing (SPT) and hand auger borings. Samples were collected during the drilling for laboratory classification. Furthermore, inclinometers were installed at the site to determine the location of the possible slip plane and the possibility of further movement extensive inclinometer monitoring found no clear answer to the location of the slip plane. From this information, an idealized model of the slope was developed in stability software packages, XSTABL and Rotational Equilibrium Analysis of Multilayered Embankments (REAME), both of which utilize the limit equilibrium method. In addition, lateral loads applied to the PAV columns had to be considered. To develop the slope stability models, using borings and lab data to establish the ideal soil profile. In these analyses, both the circular and non-circular failure surfaces were considered. The initial slope stability shear strength parameters are summarized from previous sections can be seen in the Table 11 below:

Table 11: Developed Soil Parameters

Soil Layer	γ	Total Stress S_u	Effective Stress ϕ'
	(pcf)	(psf)	(degrees)
soft silty clay	100	300	17.5
firm silty clay	110	600	17.5
stiff silty clay	115	1200	25.6
hard silty clay	130	4000	29.7
SWR (sandstone)	140	1950	40
SWR (mudstone)	140	13500	35

*Note: values from previous section, unit weights were estimated

The following idealized (original) slope geometry was constructed from the field studies conducted by the NCGS and the NCDOT, and laboratory values determined by Georgia Institute of Technology and North Carolina State University, Figure 43.

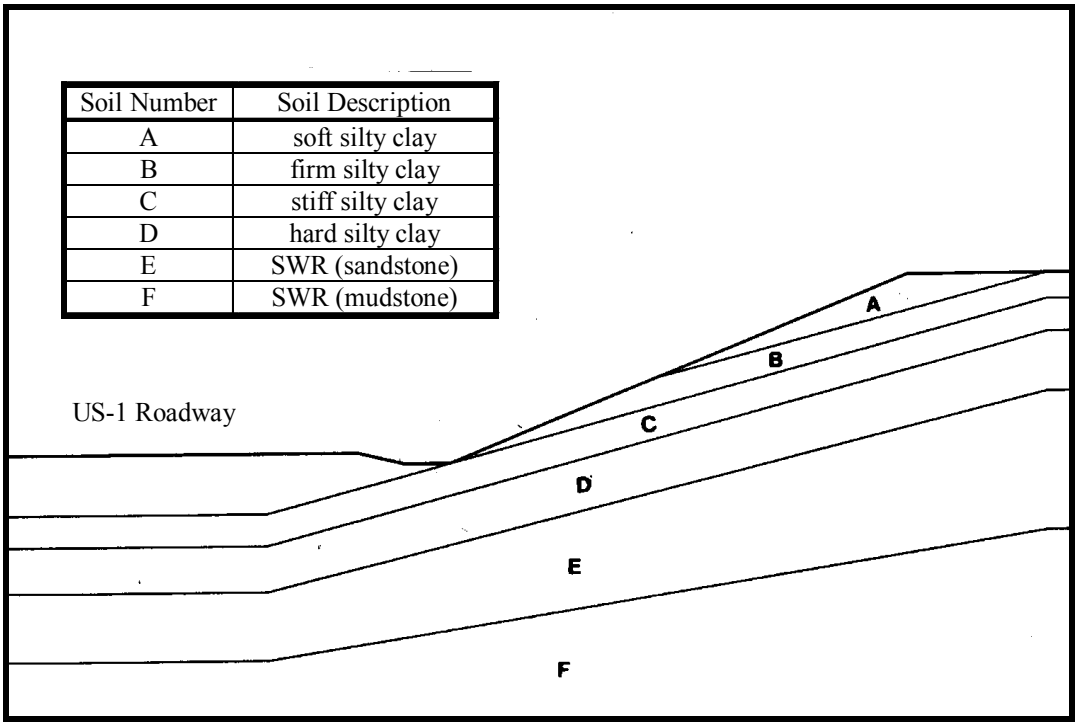

Figure 43. Original Slope Geometry

The following general assumptions were made in developing the US-1 slope methods:

- Excavation at this site reduced the resisting forces and influenced the overall long-term equilibrium of the slope
- No seismic activity
- The presence of mudstone, which can act as slip surfaces, particularly when wet (highly slakable material)
- Unfavorable dipping of the strata
- Unusually high rainfall amounts during the failure period
- Ground water level (piezometer surface) 2/3 of the slope height; although no ground water was encountered at the time of the subsurface exploration

- No cracks were assumed to exist before initial failure (no forces caused by water-filled cracks were induced at initial failure)
- The factor of safety was one at failure (FS = 1)
- Only the fused soil zone of the column is considered, Figure 44. The fused zone is assumed from the ground surface down, neglecting the backfill area.

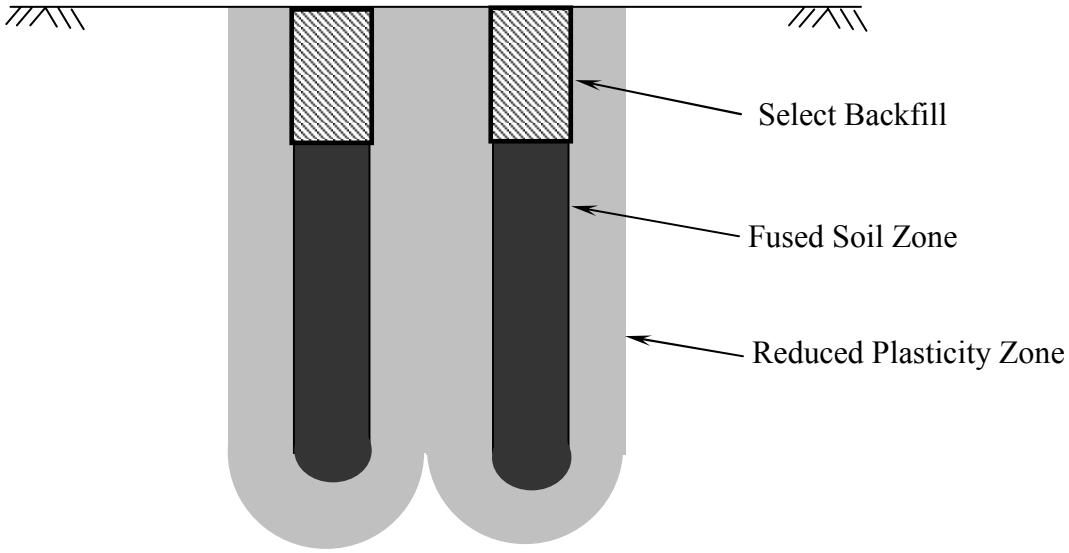

Figure 44. PAV Column Components

7.2 Groundwater Studies

Pore pressure changes are the most important parameter to evaluate the effect of the stability of cut slopes and excavations. They are functions of the rate of infiltration, rainfall period and intensity, the geometry of the slope, porosity, and degree of saturation of the soil. It had been postulated that the slope failure was brought on by the infiltration of water in the mudstone (PWR) layer, known for potential short-term physical disintegration or slaking when exposed to water. Groundwater was not encountered within any of the borings at the time of drilling operations. However, rainfall amounts were less than those experienced in previous years; therefore, the effect of water on the plane was not clearly seen. Water level elevations can be expected to fluctuate due to seasonal variations in rainfall and other factors. Standing water was viewed in the ditch at the toe of the slope. Groundwater studies were conducted at three perched levels: one at the elevation of the toe of the slope, one located one-third of the distance up the slope,

and the final level two-thirds of the distance up the slope. On effective stress analysis was then conducted. The water level that yielded the lowest factor of safety, the most critical, was used in subsequent modeling. Therefore, the ground water level (piezometer surface) was taken at 2/3 the height up from the elevation of the toe. Effective stress analysis may be simulated by specifying a piezometric surface.

7.3 Back Analysis

"When slope failures occur, the shear strength of the soil is mobilized along the full length of the slip surface. An estimate of this mobilized strength can be made by performing what has come to be called a back analysis" (Duncan and Stark, 1989). A back analysis of the US-1 slope was performed according to these methods presented by Duncan and Stark. The analysis was done using the slope stability programs, and a trial and error process. The main purpose of back analysis was to estimate indirectly the shear strength parameter at the time of failure. By holding the factor of safety at one (FS = 1). Using the presumed ground water level at failure (2/3), ignoring seismic loading, and assuming an effective stress condition ($c' = S_u = 0$), the internal friction was determined (Duncan, 1989). Although the effective friction and pore water pressures are not known for the failure envelope, reasonable approximations for these values can be determined. The final effective strength parameters can be seen in Table 12. The circular slope stability analysis results from XSTABL can be seen in Figure 45 and REAME in Figure 46.

Table 12: Soil Parameters at the Time of Failure from Back Analysis

Soil Layer	γ (pcf)	c' (psf)	ϕ' (degrees)
soft silty clay	100	0	15
firm silty clay	110	0	15
stiff silty clay	115	0	25
hard silty clay	130	0	25
SWR (sandstone)	140	0	37
SWR (mudstone)	140	0	30

Since the long-term stability of the slope was the component in question, it seemed plausible to conduction an effective stress analysis. Such analysis requires both the effective strength parameters of the soil (determined) as well as the distribution of pore pressure in the slope (2/3 location of phreatic surface).

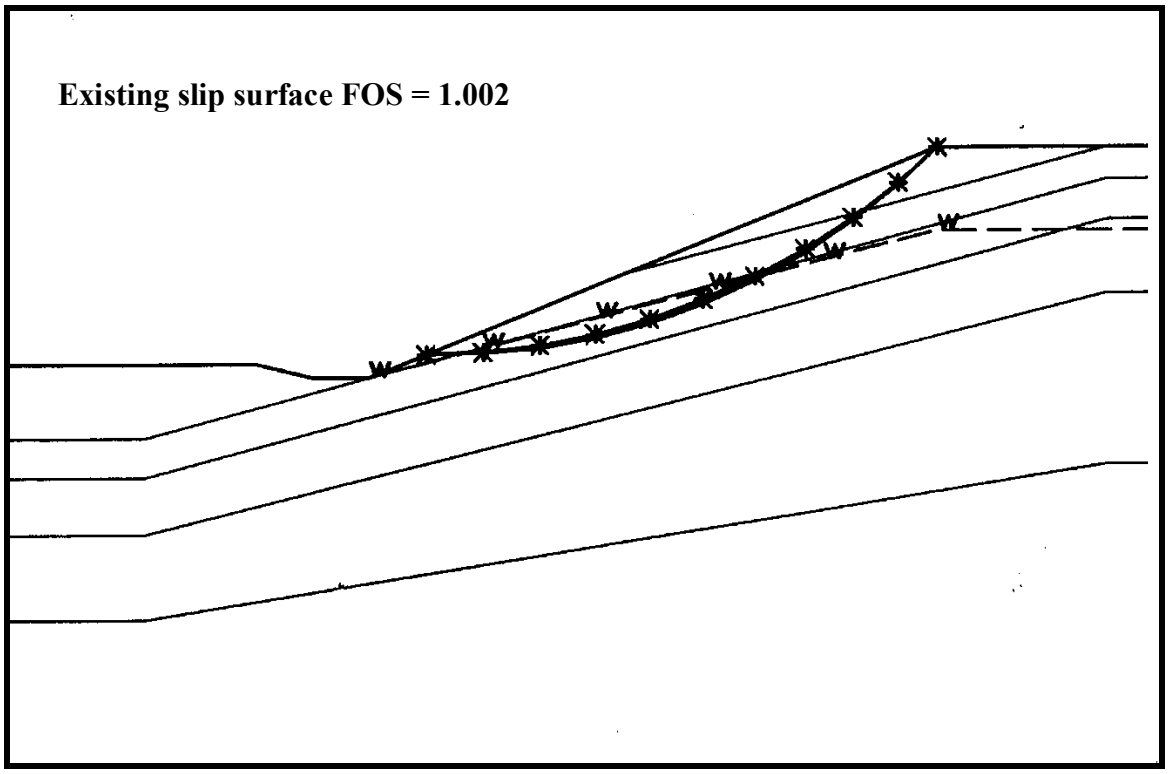

Figure 45. Results of the Back-Analysis from XSTABL

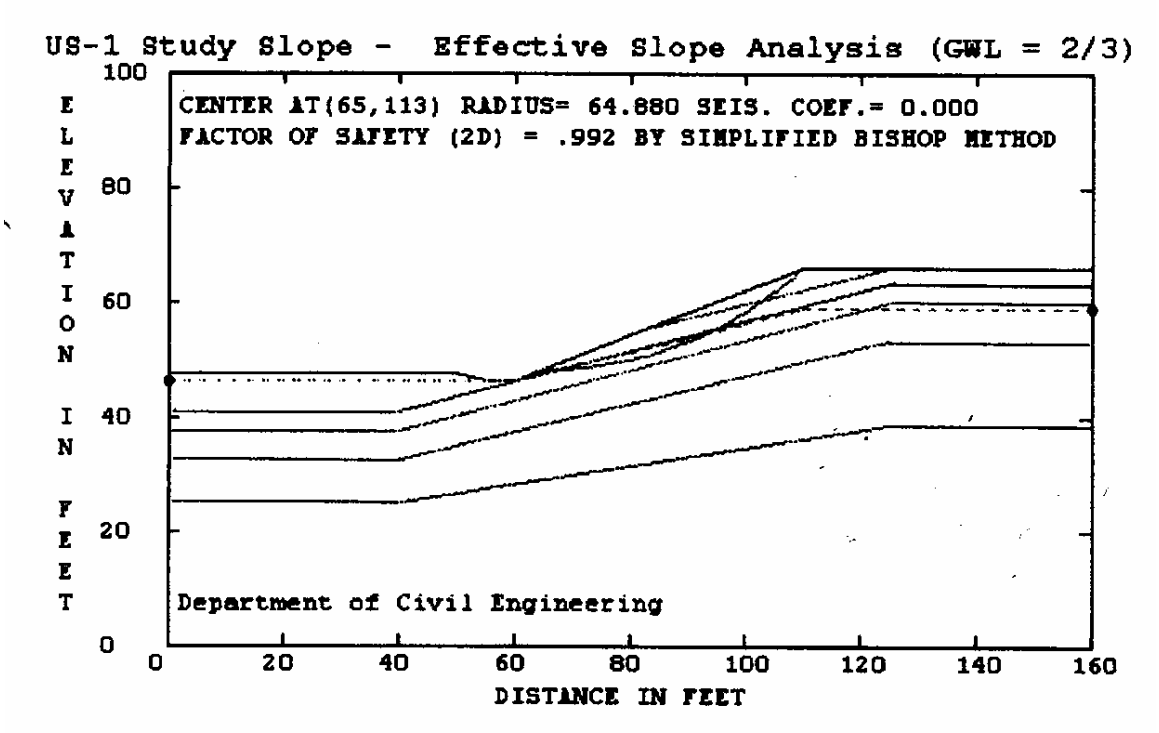

Figure 46. Results of the Back-Analysis from REAME

Both programs yield similar results using the same effective strength parameters and ground water levels. Note that the back analysis method does not give unique values, may different solutions can yield the same factor of safety. Unique shear strength parameters can only be determined if the pore pressure at the time of failure is known.

7.4 Slip Plane Analysis

Finally, we conducted a compound slope analysis to find the weakest plane within the profile, due to the unfavorable dipping of the strata. This was achieved with the REAME program, using the effective stress parameters and a compound failure surface with a presumed weak plane of movement, Modified Spencer Method. Figures 47, 48, and 49 depict the interface compound slip analysis. The first case shows slippage along the plane, which is at a similar location as the circular failure and field finding. The interface checks for the latter two cases yield that the slope has a higher probability to failure above the plane than at it.

Table 13: Slip Plane Analysis Results

Slip Plane Interface	FS
firm silty clay and stiff silty clay	0.711
stiff silty clay and hard silty clay	1.025
hard silty clay and soft weathered rock	1.037

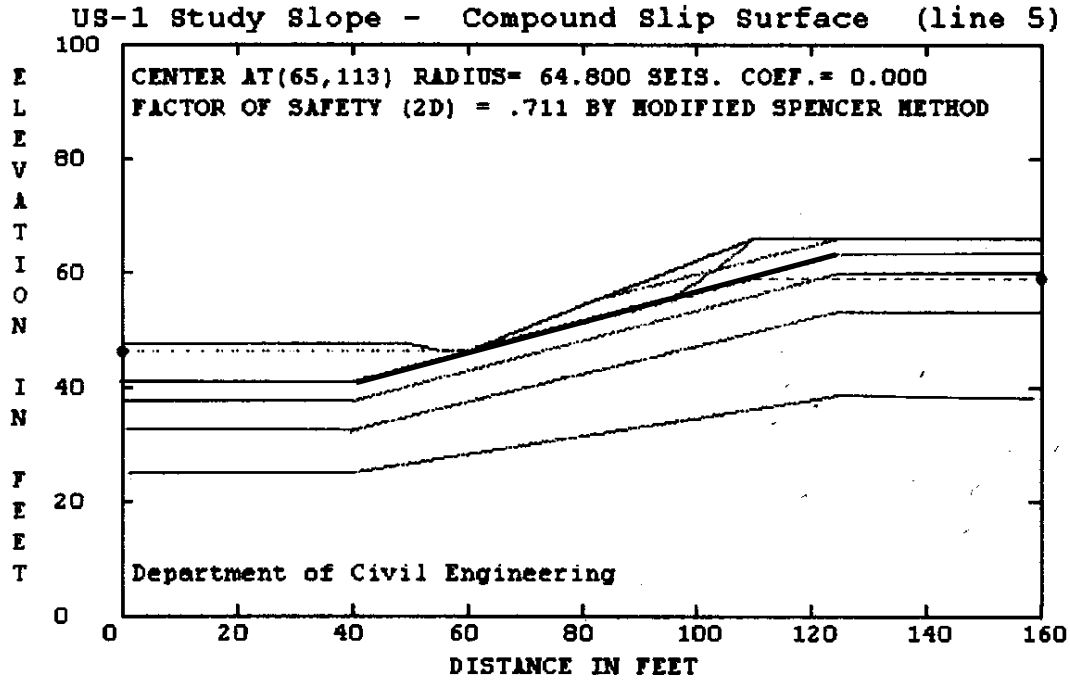

Figure 47. Interface between firm silty clay and stiff silty clay

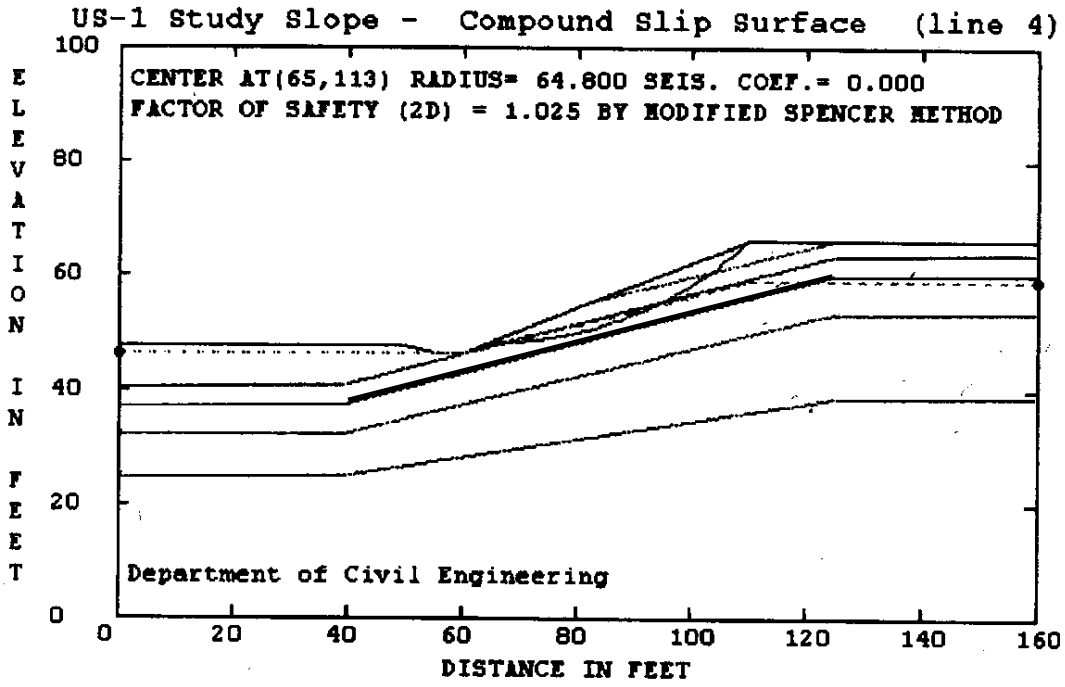

Figure 48. Interface between stiff silty clay and hard silty clay

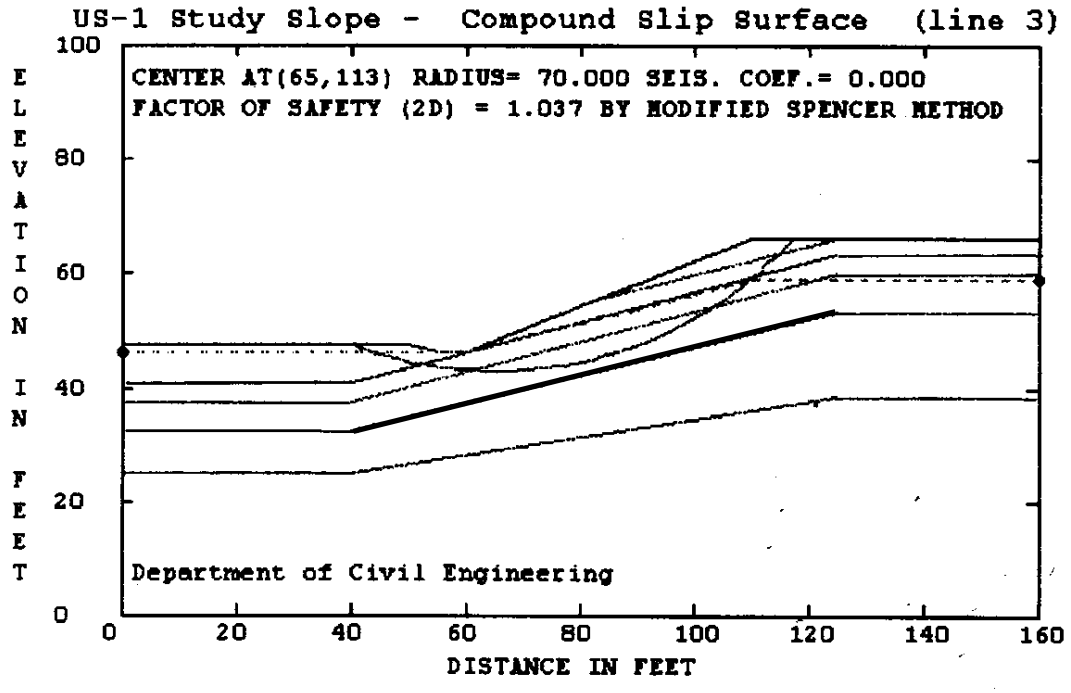

Figure 49. Interface between hard silty clay and soft weathered rock

7.5 Plane Strain Condition and Column Spacing

XSTABL and REAME both utilize the limit equilibrium method in a plane strain setting. Therefore, when the PAV column layer is entered into the program, it is modeled infinitely in each direction or like a wall. The diameter of the column must be reduced based on the following equation:

$$t = \frac{\pi D^2}{\ell 4} \qquad \text{(Equation 7.1)}$$

where: t = reduced column width (modeling thickness of a wall)

D = true column diameter

ℓ = column spacing (tributary area length)

This equivalent system (average area) of diameter takes into account the slope stability software's inability to model in three dimensions. The following figure (Figure 50) shows the methodology.

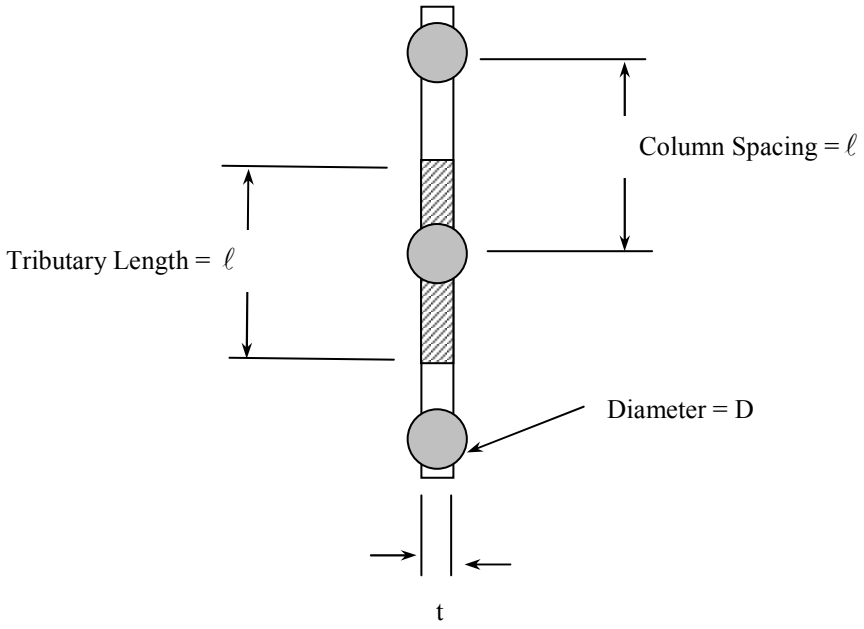

$$t \times \ell = \frac{\pi D^2}{4}$$

$$t = \frac{\pi D^2}{\ell 4}$$

Figure 50. Equivalent System for Plane Strain Problem

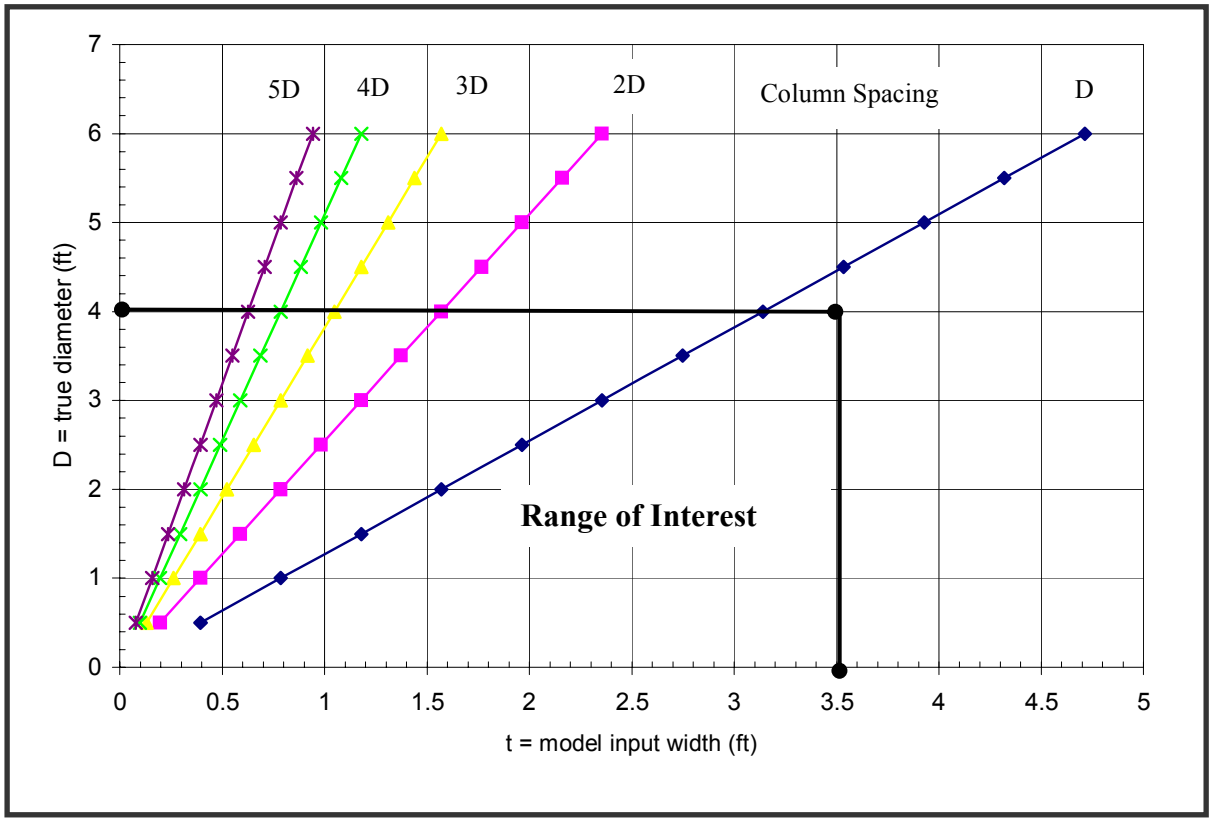

Figure 51. Equivalent System Graphical Representation

Figure 52, shows the range over which the PAV columns were of interest.

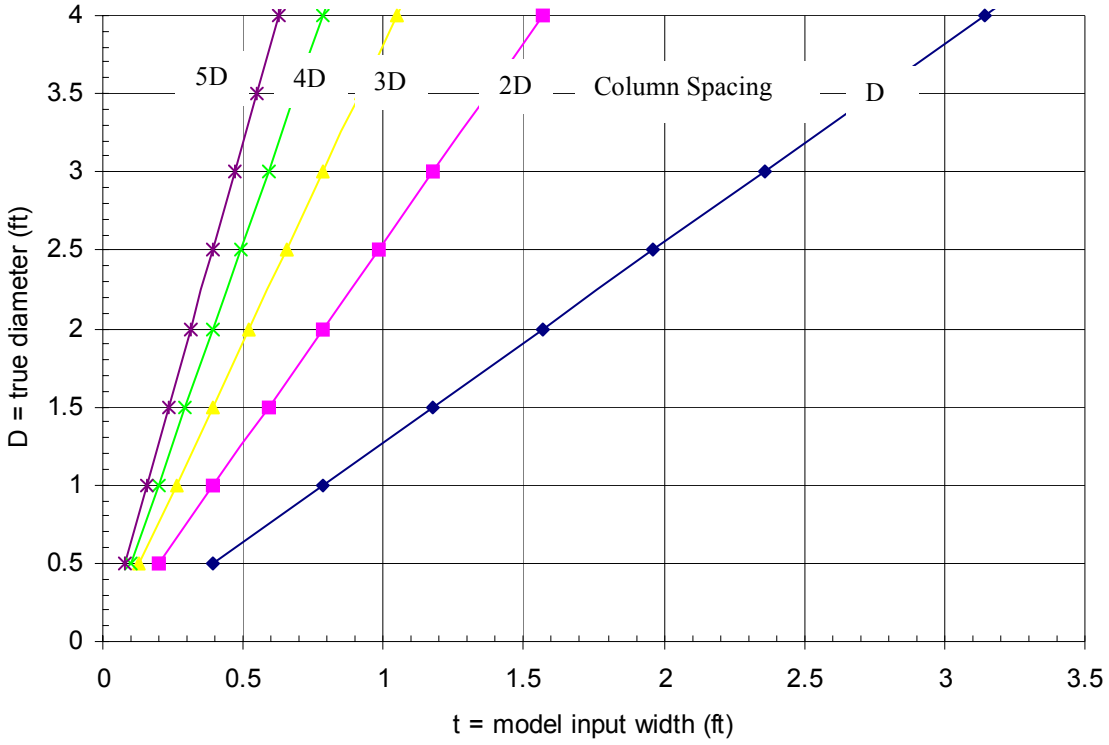

Figure 52. Equivalent System Graphical Representation Range of Interest

It is important to note that an optimal spacing must be determined or assumed. The two extremes cases are when the columns are either side-by-side, with no spaces between, thus acting as a wall, or so widely spaced that no interaction occurs. Next, the mode of failure for the soil around the columns must be postulated, a passive wedge failure was assumed, as seen in Figure 53. The optimal spacing results in the overlapping zones of resistance against the failure wedges, as depicted in Figure 54.

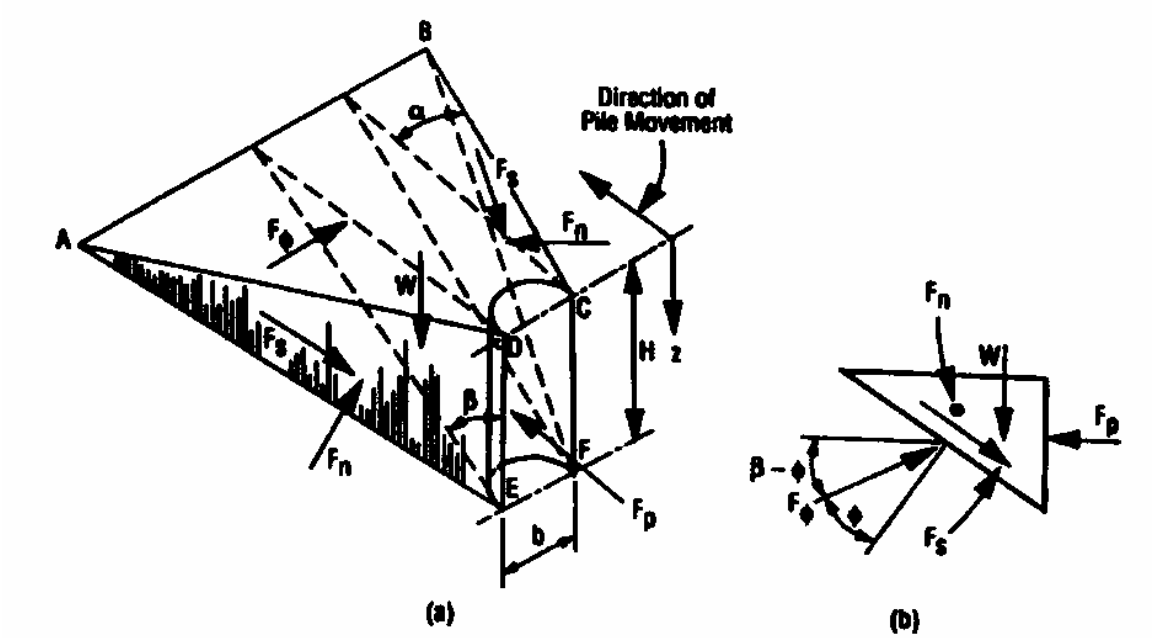

Figure 53. Typical shape and Forces for Wedge Failure (Reese, Wang, Fouse, 1992)

Therefore the lateral force from the moving soil mass is reduced based on the center-to-center spacing of each column. Studies suggest that reduction in lateral force is negligible if the spacing is greater than three times the column's diameter, results of test can be seen in Figure 55.

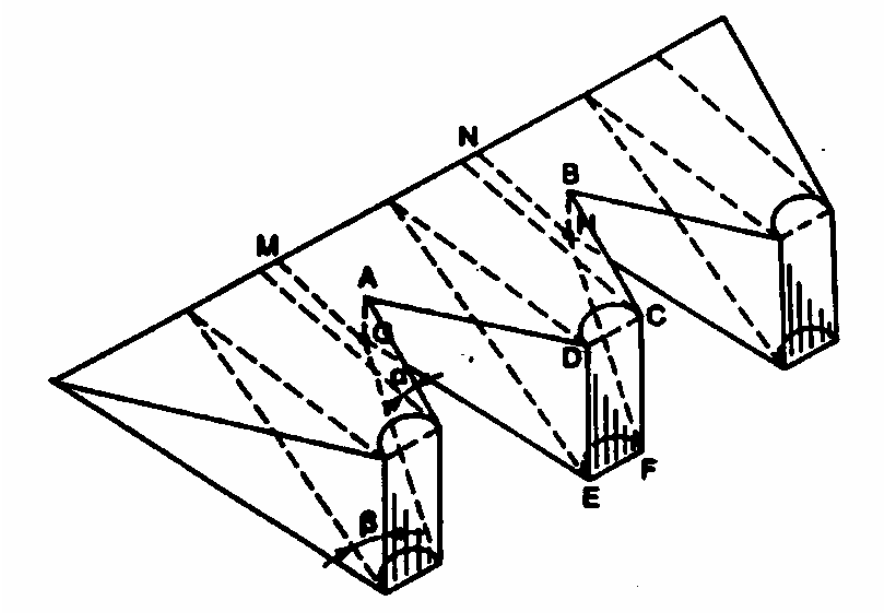

Figure 54. View of Wedge Failure for Spaced Columns (Reese, Wang, and Fouse, 1992)

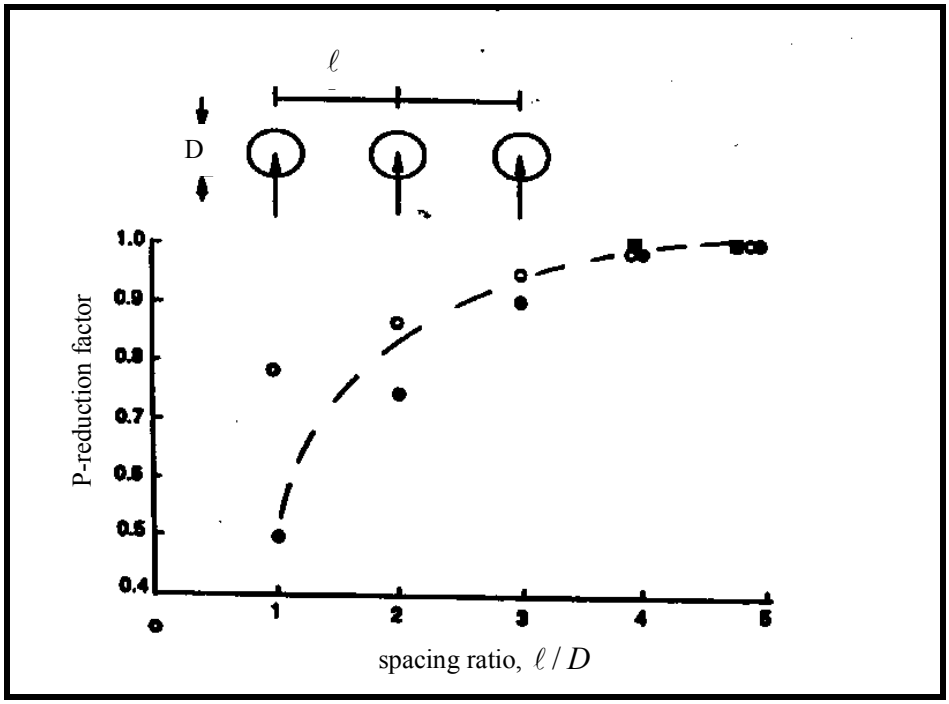

Figure 55. Given Reduction Factor for Piles (Reese, Wang, and Fouse, 1992)

Table 14: Model Improved-Zone of Thickness and True Diameter

D = true diameter (feet)	Horizontal Spacing (ℓ) D	2D	3D	4D	5D
D = 1	t = 0.79	t = 0.39	t = 0.26	t = 0.20	t = 0.15
D = 2	t = 1.57	t = 0.79	t = 0.52	t = 0.39	t = 0.31
D = 3	t = 2.36	t = 1.18	t = 0.79	t = 0.59	t = 0.47

t = model wall thickness (feet)

7.6 Plasma Arc Vitrified Column Properties

Column properties where based on the Georgia Tech US-1 laboratory vitrified specimen. The following soil parameters where used in the slope stability program to represent the vitrified columns.

Unit Weight (supplied from Georgia Tech Lab)

$\gamma = 160$ pcf

Friction Angle (assumed)

$\phi = 45^o$

Cohesion (estimated after AASHTO Specifications, Below)

c = 360,000 psf

The following outlines the methodology used in determining parameters for the slope stability program. The shear strength was estimated by methods outlined in AASHTO's "Standard Specifications for Highway Bridges" using RQD and uniaxial compressive strength.

$$S_u = C_m / 2 \qquad \text{(Equation 5.1)}$$

$$C_m = \alpha_E (C_o) \qquad \text{(Equation 5.2)}$$

$$\alpha_E = 0.0231 (RQD) - 1.32 \geq 0.15 \qquad \text{(Equation 5.3)}$$

where:

C_m = uniaxial compressive strength of rock mass

C_o = uniaxial compressive strength of intact rock (test lab)

α_E = reduction factor that accounts for discontinuities based on RQD

Note in-situ test results for RQD are not available, therefore used $\alpha_E = 0.15$ which is conservative. The uniaxial compressive (C_o) strength of the vitrified rock was determined to be 33,649 psi. Therefore, resulting in an estimated rock mass uniaxial compressive strength (C_m) of 5047 psi and shear strength (S_u) of 2523 psi or 360,000 psf. The modulus of elastic (E) was determined to be 3,114,830 psi. The following Figure 56, shows the relationship between elastic modulus and uniaxial compressive strength of

intact rock. Entering the chart with the vitrified rock's results one can see that the vitrified material plots close to those of metamorphic and igneous rocks.

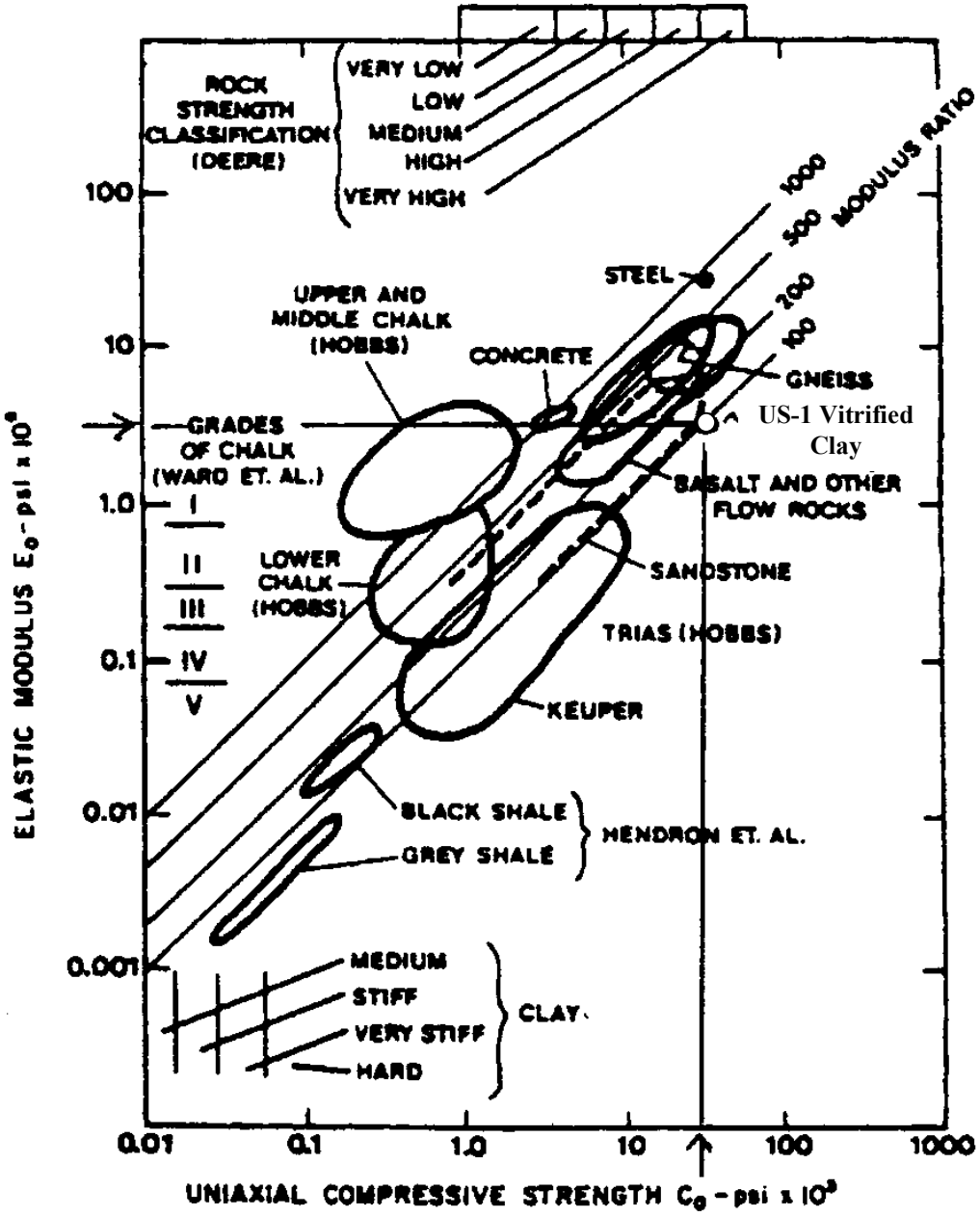

Figure 56. Elastic Modulus vs Uniaxial Compressive Strength of Intact Rock (AASHTO, 1989)

7.7 Parametric Study

Parametric studies were performed on the diameter, length, distance up slope, and horizontal spacing along the slope. This section summarizes the results obtained when varying the PAV column geometries (location). This parametric study was only developed for the US-1 slope site to help in the determination of PAV columns at optimum locations.

The PAV column was moved at different distances from the toe of the slope. The distance, length, and diameter of the PAV columns were varied and the program was run, as follows:

Distance (s): 0, 5, 10, 15, 20, 25, 30, 35, 40, 45 feet
Length (L): 10, 20 feet
Model Wall Thickness (t): 0.2, 1, 2 feet

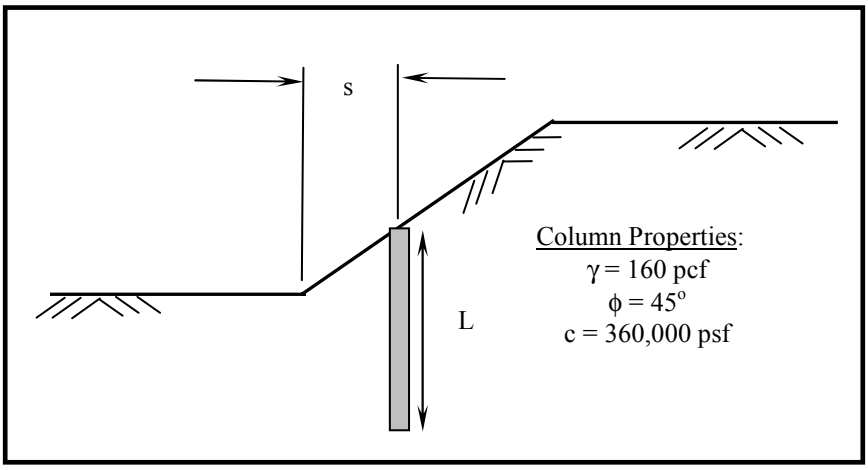

Figure 57. Diagram of PAV Column Geometry

Slope stability studies were conducted with three failure types considered, as follows:

1. Failure occurring on the existing slip plane (Figure 58);
2. Deep failure where a new slip surface is developed below the column (Figure 59); and,
3. Shallow failure (surficial or sloughing) that occurs in front and behind the PAV column (Figure 60).

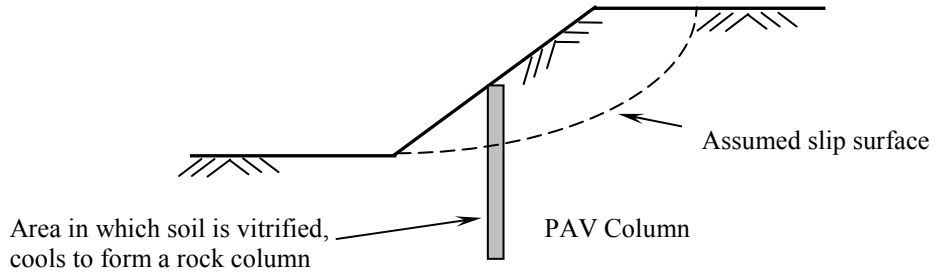

Figure 58. Pre-Column Insertion Critical Slip Surface Model

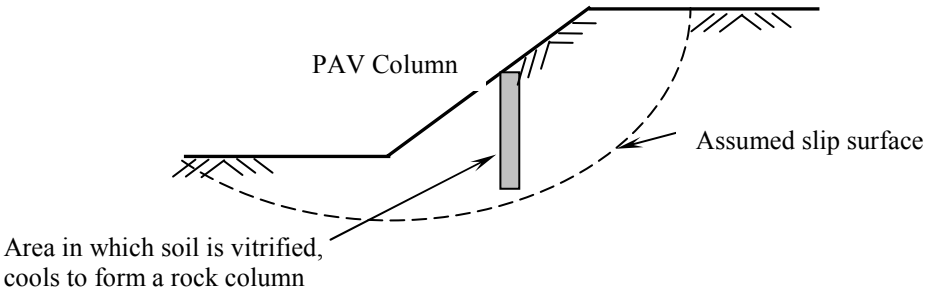

Figure 59. Deeper Slip Surface Model

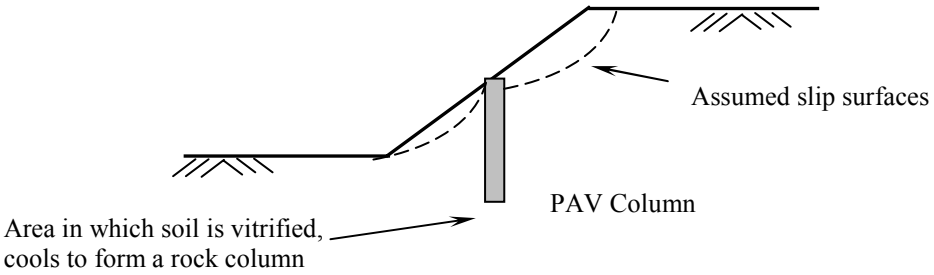

Figure 60. Shallow Slip Surfaces Models

Pre-Column Insertion Failure Surface

Analyses revealed that these failures are very unlikely to propagate through the PAV burn zone. Once the PAV column intersected the slip plane, the factor of safety increased almost boundlessly. After repeated trials with identical results, efforts to produce models in this category were suspended. Lateral pile analysis will be the limiting factor in this situation.

Shallow Failures

Analyses revealed that these failures are a function of column location. Most failures were surficial or sloughing in nature. Closer spacing of columns could help with surface slips. Further, the use of good vegetation cover should be able to stabilize this problem. Changes in PAV column diameter and length showed to be negligible in improving the factor of safety. As the column was advanced up the slope, the factor of safety for failures at the front of the column started to decrease. Factors of safety for circular surfaces to the rear of the column improve with the advancement of the PAV column up slope

Deep Failures

Modeling revealed that these failures are a function of both length and location of the column. Ultimately, stabilized zone diameter does not affect the factor of safety. Columns have their best effect at the slope's boundaries (at the toe or at the crest); these locations force the slip surfaces deeper, which increases the factor of safety.

The following table (Table 15) summaries the results of the parametric studies a function of failure type.

Table 15: Summary of Parameter Effects on Factor of Safety

Slip Surface Failure Mode	Slope Distance (S)	Column Diameter (D)	Length Column (L)
Shallow Front	decrease	no change	no change
Shallow Rear	increase	no change	no change
Pre-column	*	*	*
Surface			
Deep	decrease	no change	increase

* Generally, any column location increases the factor of safety.

Figure 61 shows the resulting factor of safety of the 24 feet-high slope as the PAV column changes diameter, length, and slope location. Note that column diameter has no true effect on the factor of safety in the slope stability program. This is due to the extremely high strength of the vitrified soil zone. The column's up-slope distance and length have the greatest effect on the factor of safety.

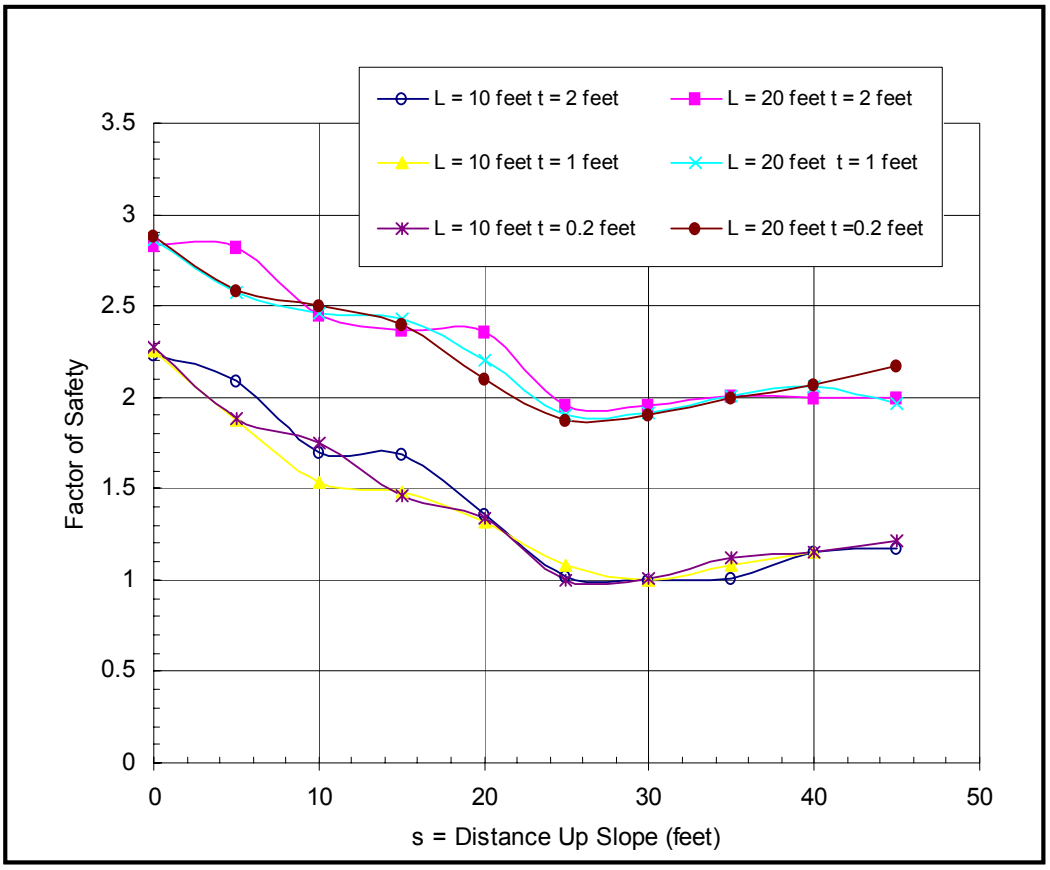

Figure 61. Influence of PAV Column Location on the Factor of Safety for Deep Surfaces

As the column location progresses up the slope, circular failures develop at the front of the column (Figure 62). The factor of safety decreases as more space is provided for the circle to develop.

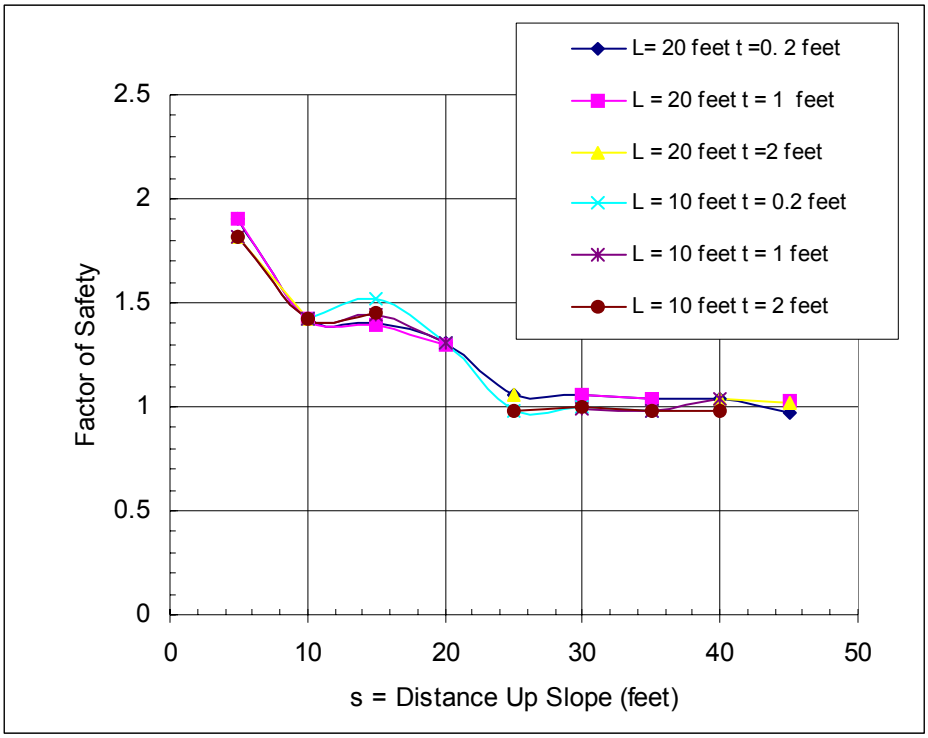

Figure 62. Influence of PAV Column Location on the Factor of Safety for Frontal Surfaces

Factors of safety for circular surfaces to the rear of the column (up slope) improve with the advancement of the PAV column up slope (Figure 63).

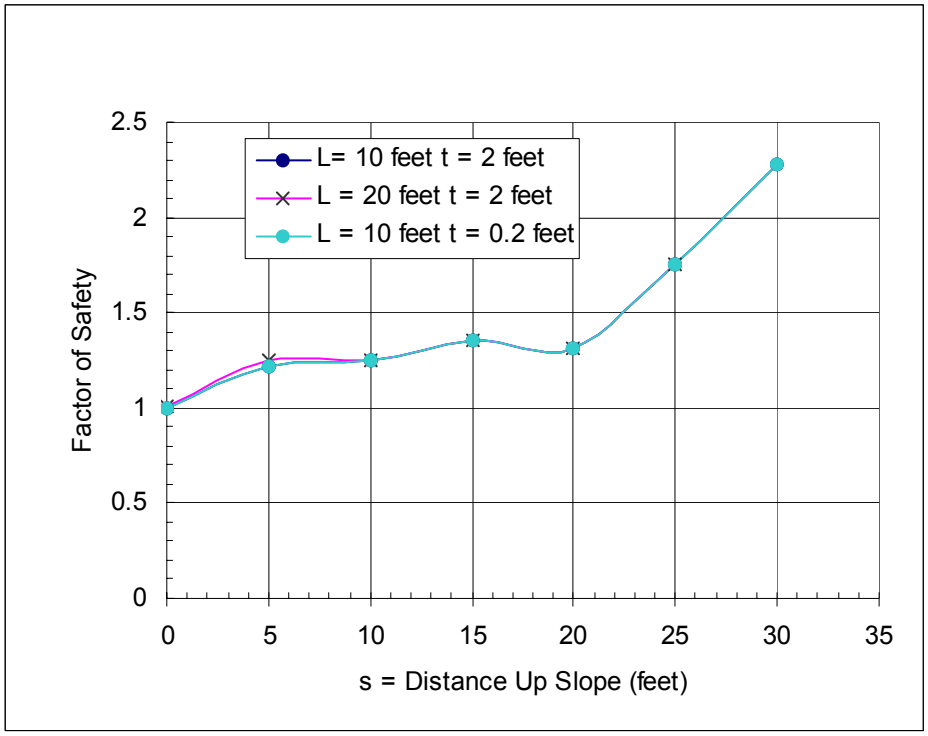

Figure 63. Influence of PAV Column Location on the Factor of Safety for Rear Surfaces

It is important to note, that column diameter and length do not affect the resulting factor of safety against frontal and rear slope failures. Thus, for these mechanisms the factor of safety becomes a function of the location of the column in the slope, i.e. the distance up-slope. Determination of the position of the column is shown in Figure 64.

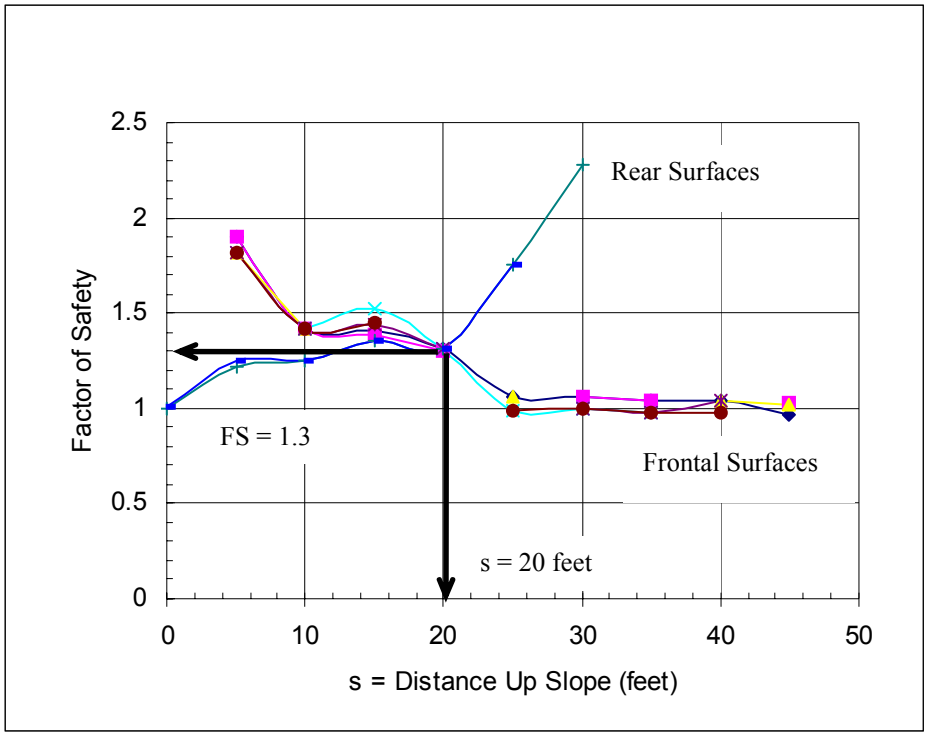

Figure 64. PAV Column's Optimum Factor of Safety

Optimum location is selected at the intersection on the front and rear factor of safety lines. Design is dictated by the development of the shallow surfaces to the front and rear, as the column changes position. Therefore, columns of 1-foot in true diameter with a length of 10-feet and at a distance of 20-feet up the slope from the toe was found to be the optimum location for a PAV column based on the slope stability analyses performed. The slope stability results are inconclusive, lateral analyses will dictate the final design.

A parametric study of the shear strength parameters within the PAV column was conducted. Initial values were based upon the Georgia Tech laboratory burn data and varied within one of the simulations. As the shear strength parameters decreased, the factor of safety decreased. To maintain the same factor of safety, column lengths or diameter had to be increased. In all cases, parameters changed as expected.

7.8 Lateral Analysis

As noted, it is the existing slip surface that shows great improvement with the installation of PAV. Also, slope stability models show that a 10-ft long, 2-ft diameter PAV column at 20 feet up the slope to be the optimum location. However, the data are inconclusive; the determining factor is the PAV's ability to resist the lateral forces (pressure) applied to it by the slope. It may be shown that a longer or wider column is needed. Figure 65 shows a typical distribution. Note that h_p is the distance to the slip surface from the ground surface.

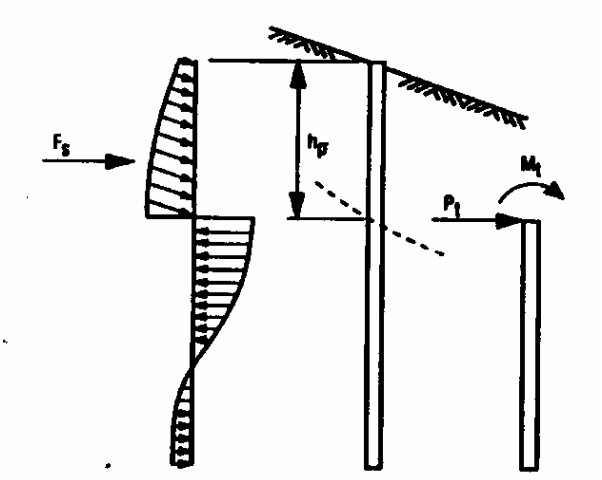

Figure 65. Forces from Soil Against a Pile in a Sliding Mass
(Reese, Wang, and Fouse, 1992)

Assuming a Broms' distribution acting on the columns, two failure modes are considered:

- a soil failure (short columns)
- development of a plastic hinge (longer columns) (see Figure 66)

The PAV column is considered free headed. No restraints are applied.

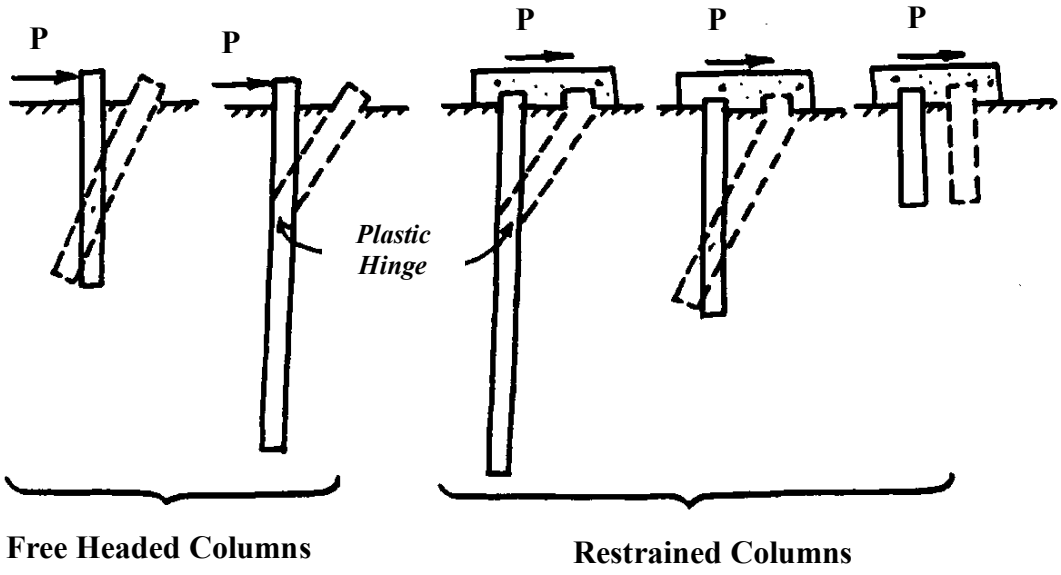

Figure 66. Failure Mechanisms of Laterally Loaded Piles (after Broms, 1965)

Broms assumed that ultimate lateral resistance is equal to three times Rankine's passive pressure ($\ell = 3D$). The following equations were used to estimate the amount of lateral force being applied to the columns. Column spacing (ℓ) were varied between D and 3D.

$$p_z = \ell \gamma h_p k_p \qquad \text{(Equation 7.2)}$$

$$k_p = \tan^2(45+\phi/2) \qquad \text{(Equation 7.3)}$$

$$P = p_z(\tfrac{1}{2}h_p) \qquad \text{(Equation 7.4)}$$

were:

p_z = lateral pressure (stress) on the column

K_p = Coefficient of passive earth pressure

P = lateral force applied to the column form the soil mass (Load)

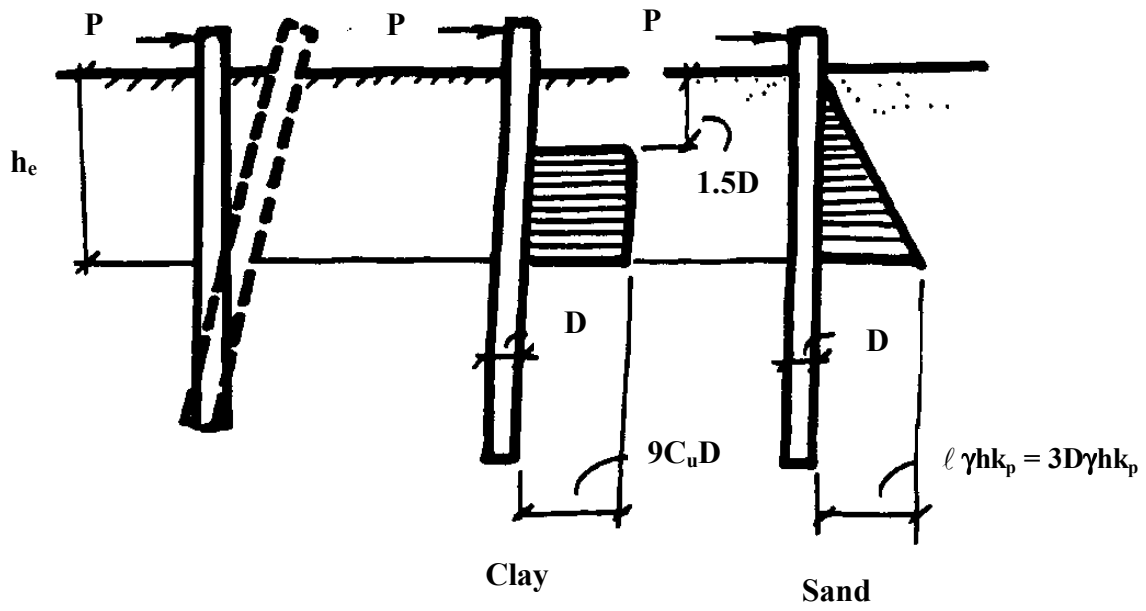

Figure 67. Assumed Earth Pressure Distribution for Laterally Loaded Piles (after Broms, 1965)

Using Broms' earth pressure distribution, the loading condition change with changes in diameter and horizontal spacing (ℓ) using Equations 7.2 to 7.4. The lateral loads were determined at different horizontal spacing as seen in Table 17.

Some generalized assumptions had to be made so that lateral loads could be determined. The soil was considered as a homogeneous mass, using a unit weight of 120 pcf with a internal friction angle of 20 degrees and cohesion intercept of 0. A height (h_p) of 5 feet from the ground to the pre-column insertion failure surface, was taken at the optimum location determined in the slope stability analysis.

Knowing the load values, a lateral analysis was conducted using LTBase (Gabr and Borden, 1987). A soil profile for LTBase was developed as follows, Table 16:

Table 16: Soil Parameters used for LTBase Input

Layer (feet)	Soil Layer	γ (pcf)	S_u (psf)	ϕ (degrees)	k (lb/in^3)
0 – 5	firm silty clay	110	0	15	20
5 – 8	stiff silty clay	115	0	25	20
8 – 14	hard silty clay	130	0	25	20
14 – 25	SWR (sandstone)	140	0	37	95
25 - down	SWR (mudstone)	140	0	30	40

Modulus of subgrade reaction (k) values were estimated from Figure 68; for American Petroleum Institute, using the above friction values.

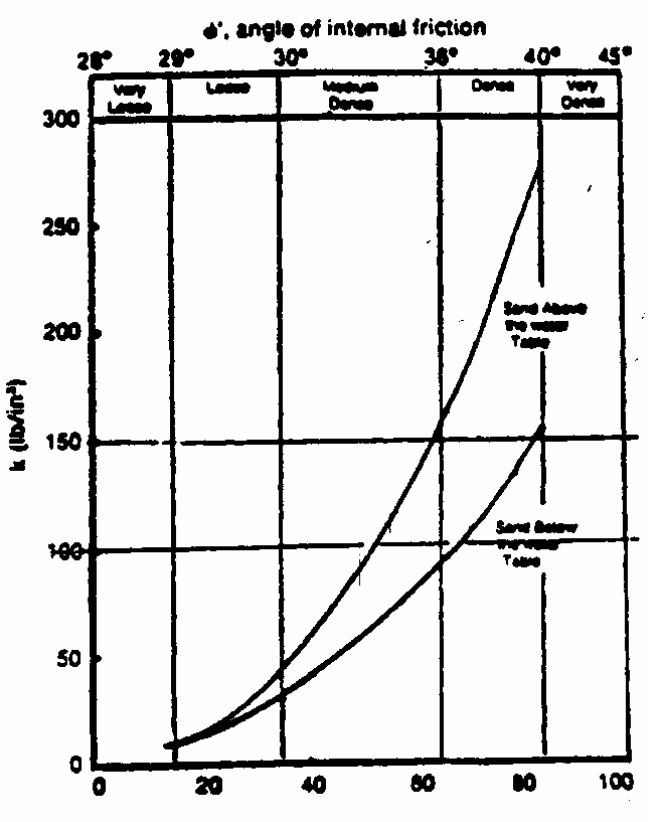

Figure 68. Initial Modulus of Subgrade Reaction (American Petroleum Institute)

A maximum deflection criteria of 3 inches with a factor of safety of 1.5 was used. Lateral analysis determined that lengths of 10 feet are inadequate to meet the deflection requirement at any diameter or horizontal spacing, as seen in Table 17 and Figure 69.

Table 17: LTBase Lateral Loading, Column Properties and Output

spacing (ℓ)	diameter	P*	M*	length	I	EI	FS	M_{cr}	M_{max}
(feet)	(feet)	(kips)	(kip-ft)	(feet)	(in^4)	(lbs - in^2)	3" deflection criteria	(kip-ft)	(kip-ft)
D	1	3.06	5.1	10	1017.876	3.17E+09	1.23	19.41	23.2
2D	1	6.12	10.2	10	1017.876	3.17E+09	0.83	19.41	26.2
3D	1	9.18	15.3	10	1017.876	3.17E+09	0.5	19.41	23.4
D	1	3.06	5.1	20	1017.876	3.17E+09	4.24	19.41	90.0
2D	1	6.12	10.2	20	1017.876	3.17E+09	2.11	19.41	87.9
3D	1	9.18	15.3	20	1017.876	3.17E+09	1.48	19.41	93.9
D	2	6.12	10.2	10	16286.02	5.073E+10	1.13	155.25	32.9
2D	2	12.24	20.4	10	16286.02	5.073E+10	0.63	155.25	37.2
3D	2	18.36	30.6	10	16286.02	5.073E+10	0.38	155.25	32.6
D	2	6.12	10.2	20	16286.02	5.073E+10	7.83	155.25	440.6
2D	2	12.24	20.4	20	16286.02	5.073E+10	5.97	155.25	447.3
3D	2	18.36	30.6	20	16286.02	5.073E+10	2.64	155.25	446.9
D	3	9.18	15.3	10	82447.96	2.568E+11	1.03	523.97	45.2
2D	3	1836	30.6	10	82447.96	2.568E+11	0.5	523.97	43.8
3D	3	27.54	45.9	10	82447.96	2.568E+11	0.38	523.97	50.7
D	3	9.18	15.3	20	82447.96	2.568E+11	7.18	523.97	607.1
2D	3	1836	30.6	20	82447.96	2.568E+11	3.71	523.97	633.3
3D	3	27.54	45.9	20	82447.96	2.568E+11	2.51	523.97	642.7
D	4	12.24	20.4	10	260576.3	8.116E+11	1.03	1242.01	62.0
2D	4	24.48	40.8	10	260576.3	8.116E+11	0.56	1242.01	70.3
3D	4	36.72	61.2	10	260576.3	8.116E+11	0.38	1242.01	70.2
D	4	12.24	20.4	20	260576.3	8.116E+11	6.51	1242.01	703.7
2D	4	24.48	40.8	20	260576.3	8.116E+11	3.3	1242.01	720.6
3D	4	36.72	61.2	20	260576.3	8.116E+11	2.24	1242.01	735.9

*Assumptions: h_p = 5 ft, unit weight = 120 pcf, c = 0, and ϕ = 20

Cracking moments for the PAV columns were assumed to be similar to concrete; therefore, the following equations were used.

$$f'_r = 7.5\sqrt{\sigma_c} \qquad \text{(Equation 7.5)}$$

$$M_{cr} = \frac{f'_r I}{r} \qquad \text{(Equation 7.6)}$$

Columns with diameters less than 4.0 feet exceed their cracking moments, as seen in Figure 69.

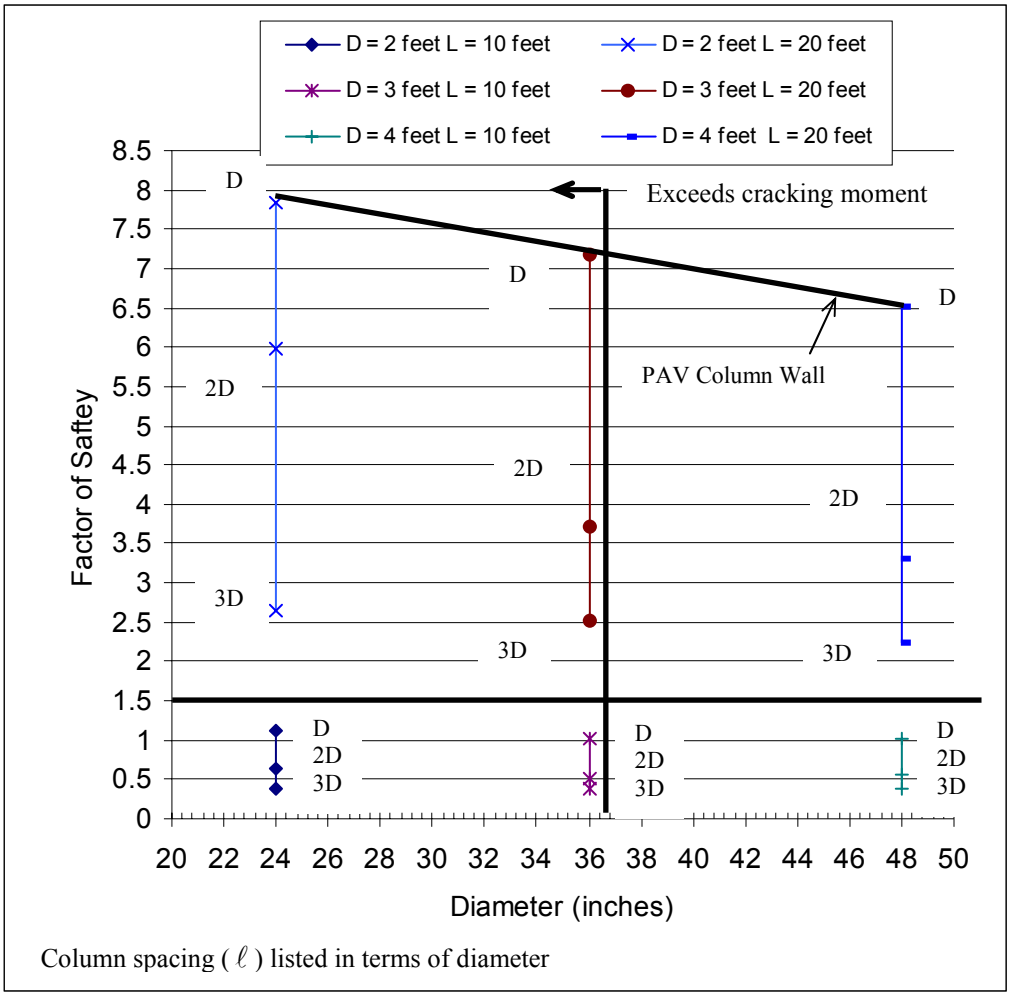

Figure 69. Lateral Results on Factor of Safety

A 4.0 foot diameter column placed 20 feet up the slope with an embedment length of 20 feet with a maximum horizontal spacing of 3D is the ideal placement.

Note that results apply only to the conditions at the US-1 slope site and should not be applied to other locations.

8.0 COST ANALYSIS

By examining the size and weight of PAV material, it is possible to calculate and compare the cost of producing igneous rock. If a rate of $0.05/kw-hr is assumed, then the 100-kw torch system averages $3.35 per hour while the 240-kw system reaches $8.75 per lab hour (Beaver and Mayne, 1995). PAV costs should include borehole installation, fuel-power, field mobilization, and maintenance and repair (Berkovitz, 1996). Other slope stability mitigation methods, such as geo-reinforced soil slopes (RSS), purchasing additional right-of-way to flatten slopes, removal and replacement with special fills, providing drainage, or a retaining structure could prove to be significantly less expensive than using PAV for slope stability purposes.

9.0 CONCLUSIONS AND RECOMMENDATIONS

Plasma arc technology is suitable to improve both weak in-situ materials and the stability of slopes. High strength columns can be created within the slope, intersecting planes of weakness, and transferring the load downwards.

Increased strength, equivalent to that of metamorphic and igneous rocks, can be achieved from vitrifying soil. Shear strength properties of the vitrified soil increased immensely. Uniaxial compressive strength of the vitrified rock was determined to be 33,649 psi. The modulus of elastic was determined to be 3,114,830 psi. The unit weight of the vitrified material was calculated to be 159.15 lb/ft^3. This represented a 46% increase in unit weight relative to the original soil.

Placement of the PAV columns within a slope will improve its resistance to movement. For the US-1 site, a length of 20 feet with a diameter of 1 foot at a horizontal spacing of 2 feet (2D), placed 20 feet up the slope was determined to be the ideal placement.

Based upon the results of our laboratory work and PAV modeling, we propose further research to focus on alternative fuel sources. In addition, studying burn rates would be useful (time burn vs. amount of improvement). Finding improvement within these areas would reduce the expense of conducting PAV burns. Currently, constructibility and high operation costs prove this method of slope stabilization to be prohibitive in practical application.

10.0 REFERENCES

AASHTO, (1989), *Standard Specifications for Highway Bridges*, Fourteenth Edition.

Abramson, G., Boyce, G., Lee, T., and Sharma, S., (1994), *Advanced Course of Soil Slope Stability*, U S Department of Transportation, Publication No. FHWA-SA-94-005.

Al-Homoud, A. S. and Tubeileh, T. K., (1998), *Analysis and remedies of landslides of cut slopes due to the presence of weak cohesive layers within stronger formations*, Environmental Geology Vol. 33 No. 4, pp. 299 – 311.

American Petroleum Institute, *Recommended Practice for Planning, Designing, and Constructing Fixed Offshore Platforms, API Recommended Practice 2A (RP 2A)*, Seventeenth Edition, April 1, 1987.

Anagnostopoulos, A. G. and Papadopoulos, B. P., (1995), *Restraint of an Active Landslide by Bored Piles*, Bengt B. Broms Symposium on Geotechnical Engineering, pp. 27 – 37.

Atkinson, J., (1993), *Introduction to the Mechanics of Soils and Foundations*, McGraw-Hill, Inc., NJ, pp. 256 – 274.

Bardet, J. P., (1997), *Experimental Soil Mechanics*, Prentice-Hall, Inc., Englewood Cliffs, NJ.

Beaver, J. R., Mayne, P. W., (1995), *Baseline Geoenvironmental Experiments for In-Situ Soil Transformation by Plasma Torch*, Proc. International Symp. on Environmental Technologies, , Georgia Institute of Technology and University of Bordeaux I, Atlanta, GA, pp. 617 – 630.

Beaver, J. R., Mayne, P. W., (1995), *Plasma Vitrification of Geomaterials*, Final Report, Georgia Institute of Technology, Atlanta, GA.

Beaver, J. R., Mayne, P. W., (1995), *Plasma Vitrification of Geomaterials*, Presented at the Southeastern Transportation Geotechnical Engineering Conference, Huntsville, AL.

Beles, A. A., Stanculescu, I. I., (1958), *Thermal Treatment as a Means of Improving the Stability of Earth Masses*, Geotechnique Vol. 8 No. 1, pp. 158 – 165.

Berkovitz, B. C., (1996), *Transportation Applications for Plasma Arc Technology*, Presented at the Southeastern Transportation Geotechnical Engineering Conference, Cocoa Beach, FL.

Bishop, A. W. and L. Bjerrum, "The Revelance of the Triaxial Test to the Solution of Stability Problems," *Research Conference on Shear Strength of Cohesive Soils*, Boulder, CO, ASCE, June, 1960.

Blundy, R. F., Zionkowski, P., Schumacher, R. F., and Herman, D. T. (1996). "Demonstration of plasma in-situ vitrification at the K-reactor seepage basin." *Rep. WSRC-TR-96-0390*, Westinghouse Savannah River Center, Aiken, S.C., 1-8.

Borden, R. H., Putrich, S. F., (1986), "Drained-Strength Parameters from Direct Shear Tests for Slope Stability Analyses in Overconsolidated Fissured Residual Soils," *Transportation Research Record*, No. 1089, pp. 102 – 113.

Bowles, J. E., (1996), *Foundation Analysis and Design*, McGraw-Hill Companies, Inc., New York City, NY.

Brand, E. W., (1977), *Some Thoughts on Rain-Induced Slope Failures*, 9th International Conference on SMFE, pp. 373 – 376.

Broms, B. B. "Lateral Resistance of Piles in Cohesive Soils," *Journal of the Soil Mechanics and Foundations Engineering Division*, American Society of Civil Engineers, Vol. 90, No. SM2, March, 1964a, pp. 27 – 63.

Broms, B. B. "Lateral Resistance of Piles in Cohesionless Soils," *Journal of the Soil Mechanics and Foundations Engineering Division*, American Society of Civil Engineers, Vol. 90, No. SM3, March, 1964b, pp. 123 – 156.

Broms, B. B. "Design of Laterally Loaded Piles," *Journal of the Soil Mechanics and Foundations Engineering Division*, American Society of Civil Engineers, Vol. 91, No. SM3, March, 1965, pp. 79 – 99.

Byers, M. G., FitzPatrick, V. F., and Holtz, R. D., (1991), "Site Remediation By In-Situ Vitrification," *Transportation Research Record*, 70th Annual Meeting, Transportation Research Board, Washington, D.C., Paper No. 910562.

Celes, J., (1999), *Transformation of Processed Kaolin by Plasma Magmavication,* MS thesis, Georgia Institute of Technology, Atlanta, GA.

Chandler, R. J., (1978), *Back Analysis Techniques for Slope Stabilization Works: A Case Record*, Geotechnique Vol. 27 No. 4, pp. 479 – 495.

Circeo, L. J., Mayne, P. W., (1993), *In-Situ Thermal Stabilization of Soils Using Plasma Arc Technology*, Final Report, Georgia Institute of Technology, Atlanta, GA.

Circeo, L. J., Mayne, P. W., Newsom, R. A., Elhakim, A., Mintz, E. A., Ingram, C. W., and Carney, C. L., (1999), *In-Situ Plasma Remediation of Contaminated Soils*, Semi-Annual Technology Progress Report, Georgia Institute of Technology, Atlanta, GA.

Circeo, L. J., Mayne, P. W., Newsom, R. A., Hendren, T., (1998), *In-Situ Stabilization of Geologic Materials by Vitrification Using Plasma Arc Technology*, Final Report, Georgia Institute of Technology, Atlanta, GA.

Circeo, L. J., Mayne, P. W., Newson, R. A., Mayer, K. A., (1996), *Demonstration of In-Situ Vitrification Technology for Savannah River Site Contaminated Soils*, Final Report, Georgia Institute of Technology, Atlanta, GA.

Coduto, D. P., (1994), *Foundation Design*, Prentice-Hall, Inc., Englewood Cliffs, NJ.

Duncan, J. M. and Stark, T. D., (1992), *Soil Strengths from Back Analysis of Slope Failures*, Stability and Performance of Slopes and Embankments II, ASCE Publication No. 31 Vol, 1, pp. 890 – 904.

FHWA, (1994), *Advanced Technology for Soil Stability*, Office of Technology Applications, Publication No. FHWA-SA-94-005, Vol. 1 Soil Stability Manual, Washington, DC.

Fujii, T., (1971), "The Practical Application of Thermal & Freezing Methods to Soil Stabilization," *Proceedings*, First Australian-New Zealand Conference in Geomechanics, 1971, 337 – 343.

Gabr, M. A. and Borden, R. H., (1987), *LTBASE: A Computer Program for Analysis of Laterally Loaded Piers Including Base and Slope Effects*, North Carolina State University, Raleigh, NC.

Hassan, K. H., and O'Neill, M. W., (1997), *Side Load-Transfer Mechanisms in Drilled Shafts in Soft Argillaceous Rock*, Journal of Geotechnical and Environmental Engineering Vol. 123 No. 2, pp. 145 – 152.

Hassiotis, S., Clameau, J. L., and Gunaratne, M., (1997), *Design Method for Stabilization of Slopes with Piles*, Journal of Geotechnical and Environmental Engineering Vol. 123 No. 4, pp. 314 – 323.

Hausmann, M. R., (1990), *Engineering Principles of Ground Modification*, McGraw-Hill Publishing Company, New York, pp. 382 – 400.

Hill, R. A., (1934), "Clay Stratum Dried Out to Prevent Landslips," *Civil Engineering*, Vol. 4, No. 8, 403 – 407.

Holtz, R. D. and Kovacs, W. D., (1981), *An Introduction to Geotechnical Engineering*, Prentice-Hall, Inc., Englewood Cliffs, NJ.

Irvine, L. R., (1930, 1934), "Road Making By Heat Treatment of Soils," *Transactions*, Institution of Engineers, Australia, Vol. XI, part 1, 405 – 416, and Vol, XIV, part 2, 113 – 120.

Jankiewicz, E. J., (1972), "Fusing Soils," *The Military Engineer*, No, 422, November – December, 1972, 422 – 423.

Kulhawy, F. H. and Mayne, P. W., (1990), *Manual on Estimating Soil Properties for Foundation Design*, Electric Power Research Institute, Design Manual EL-6800 Palo Alto, CA.

Lambe, P. C., (1990), *Determination of Shear Strength for Design on Cut Slopes in Partly Weathered Rock and Saprolite*, North Carolina State University, Raleigh, NC.

Lambe, T. W., and Whitman, R. V., (1969), *Soil Mechanics*, John Wiley & Sons, Inc., New York, NY.

Ledbetter, John F, (1968), North Carolina Department of Transportation Internal Publication.

Litinov, I. M., (1960), "Stabilization of Settling Weak Clayey Soils by Thermal Treatment," *Highway Research Board*, Special Report No. 60, 94 – 112.

Mayer, K. A., (1997), *Laboratory Chamber Experiments Simulating In-situ Plasmas Vitrification for Geoenvironmental Concerns,* MS thesis, Georgia Institute of Technology, Atlanta, GA.

Mayne, P. W., Burns, S. E., Circeo, L. J., (2000), *Plasma Magmavication of Soils by Nontransferred Arc*, Journal of Geotechnical and Geoenvironmental Engineering Vol. 126 No. 5, ASCE, pp. 387 – 396.

Mitchell, J. K., (1993), *Fundamentals of Soil Behavior*, John Wiley & Sons, Inc., New York, NY.

Moore, W., (1986), North Carolina Department of Transportation Internal Publication.

NAVFAC, (1982), *Soil Mechanics*, Naval Facilities Engineering Command, Design Manual DM-7.01, Alexandria, VA.

Pearlman, S. L., Camplbell, B. D., and Withiam, J. L., (1992), *Slope Stabilization Using In-Situ Earth Reinforcements*, Stability and Performance of Slopes and Embankments II, pp. 1333 – 1348.

Reh, B., (2002), Meteorologist for WLFL-TV, Telephone Interview April 23, 2002, Raleigh, NC.

Roberts, J., (1996), *Understanding Soil Mechanics*, Delmar Publishers, New York.

Schneider, J., Wagener, K., and Mayne, P. W., (1996). "Plasma vitrification of geomaterials from Savannah River site." *Rep. Prepared for Westinghouse/Bechtel*, Georgia Tech Research Corp., Atlanta.

Schuster, R. L., and Krizek, R. J., (1978), *Landslides: Analysis and Control*, Transportation Research Board Special Report 176, Washington, DC.

Sharma, S., (1994), *XSTABL: An Integrated Slope Stability Analysis Program for Personal Computers*, Interactive Software Designs, Inc., Moscow, ID.

Skempton, A. W. and J. N. J. Hutchinson, "Stability of Natural Slopes and Embankment Foundations," *Seventh International Conference on Soil Mechanics and Foundation Engineering*, Mexico City, State of the Art Volume, pp. 291 – 340, 1969.

Spangler, M. G. and Handy, R. L., (1982), *Soil Engineering*, Harper Collins Publishers, New York.

Terzaghi, K., Peck, R. B., and Mesri, G., (1996), *Soil Mechanics in Engineering Practice*, John Wiley & Sons, Inc., New York, NY.

Tice, J. A., Sams, C. E., (1974), *Experiences with Landlide Instrumentation in the Southeast*, Transportation Research Board Record 482, pp. 18 – 29.

Turner, A. K, and Schuster, R. L., (1996), *Landslides: Investigations and Mitigation*, Transportation Research Board Special Report 247, Washington, DC.

USDA, (1970), *Soil Survey: Wake County North Carolina*, Soil Conservation Service, Raleigh, NC.

Yurdanov, A.P., (1978), "Characteristics of Deep Roasting of Soils and Prospects of Its Improvement," *Osnov. Fund. Mech. Grunt.*, (20), 6, 14 – 16.

Wahls, H. E., (1999), *CE 741: Advanced Soil Mechanics Lecture Notes*, Department of Civil Engineering for North Carolina State University, Raleigh, NC.

Appendix A

Site Exploration

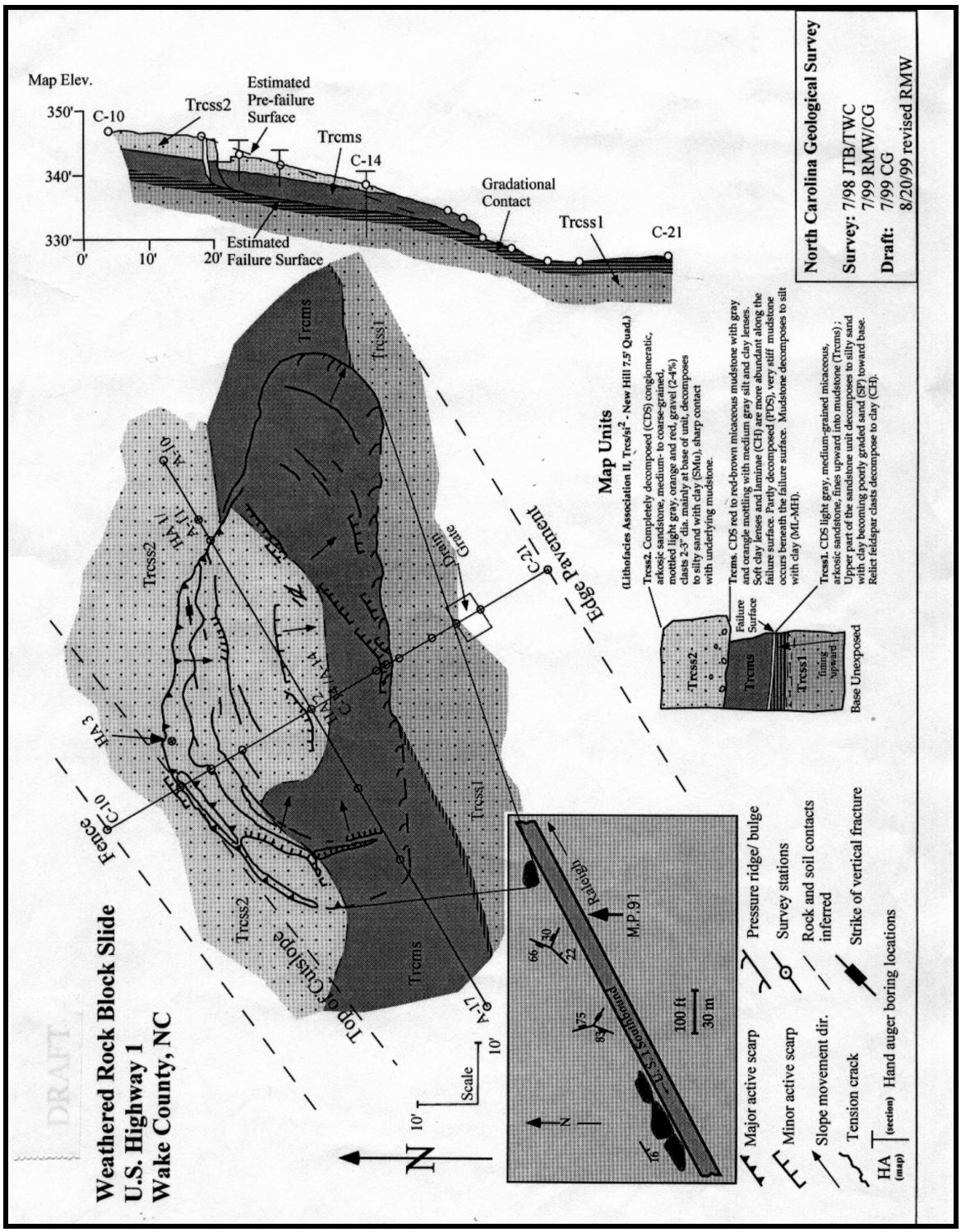

Figure A1: NCGS Field Survey Finding (NCGS)

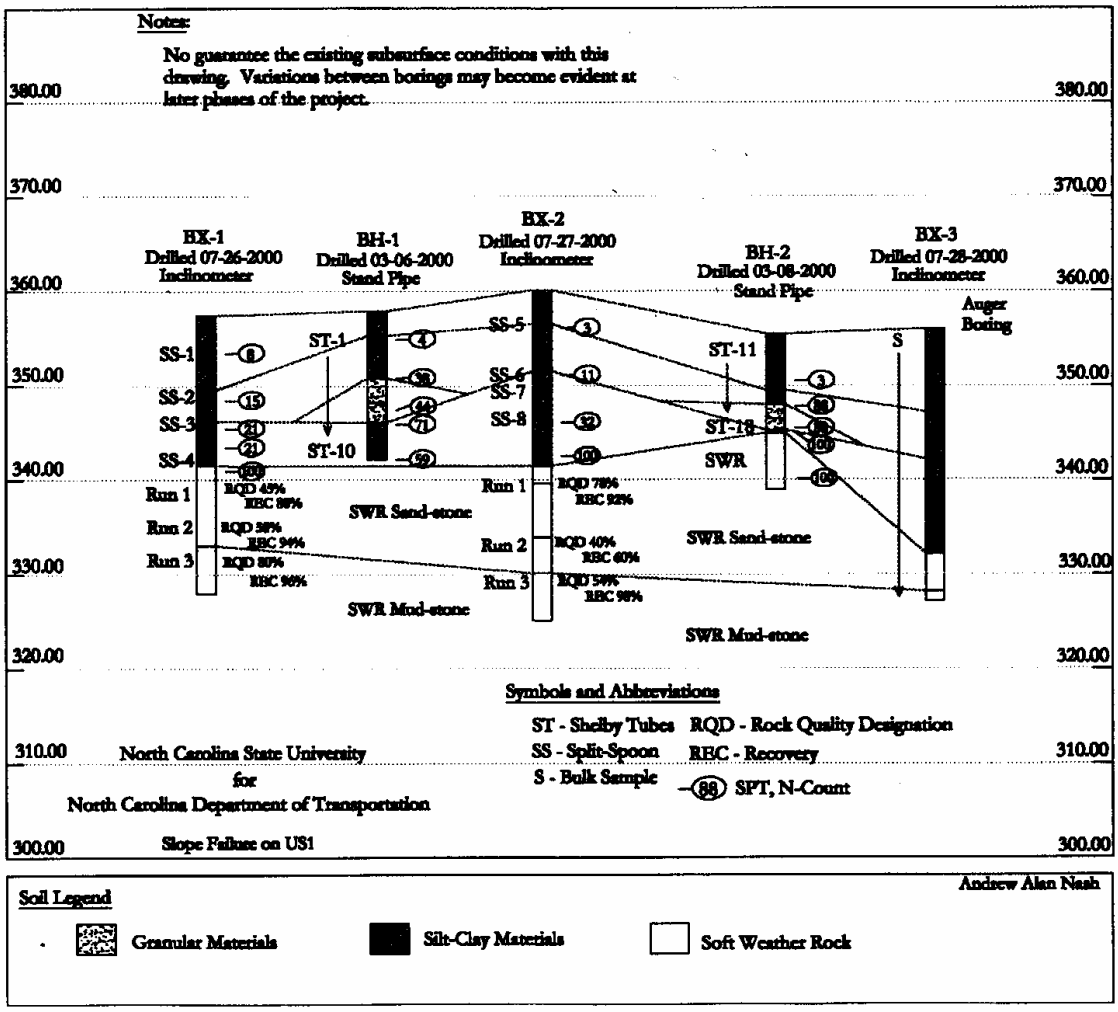

Figure A2: NCDOT Generalized Profile

Figure A3: NCDOT Drilling

Figure A4: NCDOT Breaking Split Spoon

Appendix B

Geophysical Testing

Appendix B. Geophysical Testing Program (Baseline)

A number of nondestructive tests were conducted aiming to characterize the US 1 slope site. The tests included:

- Magnetics
- Electromagnetic Conductivity (EM31)
- Earth Resistivity
- Downhole Test
- Ground Penetrating Radar- GPR[1].

These sets of tests were performed as a baseline to compare to the profile after vitrification. Figure B1 shows a site plan showing the extent of the EM31 and magnetics tests.

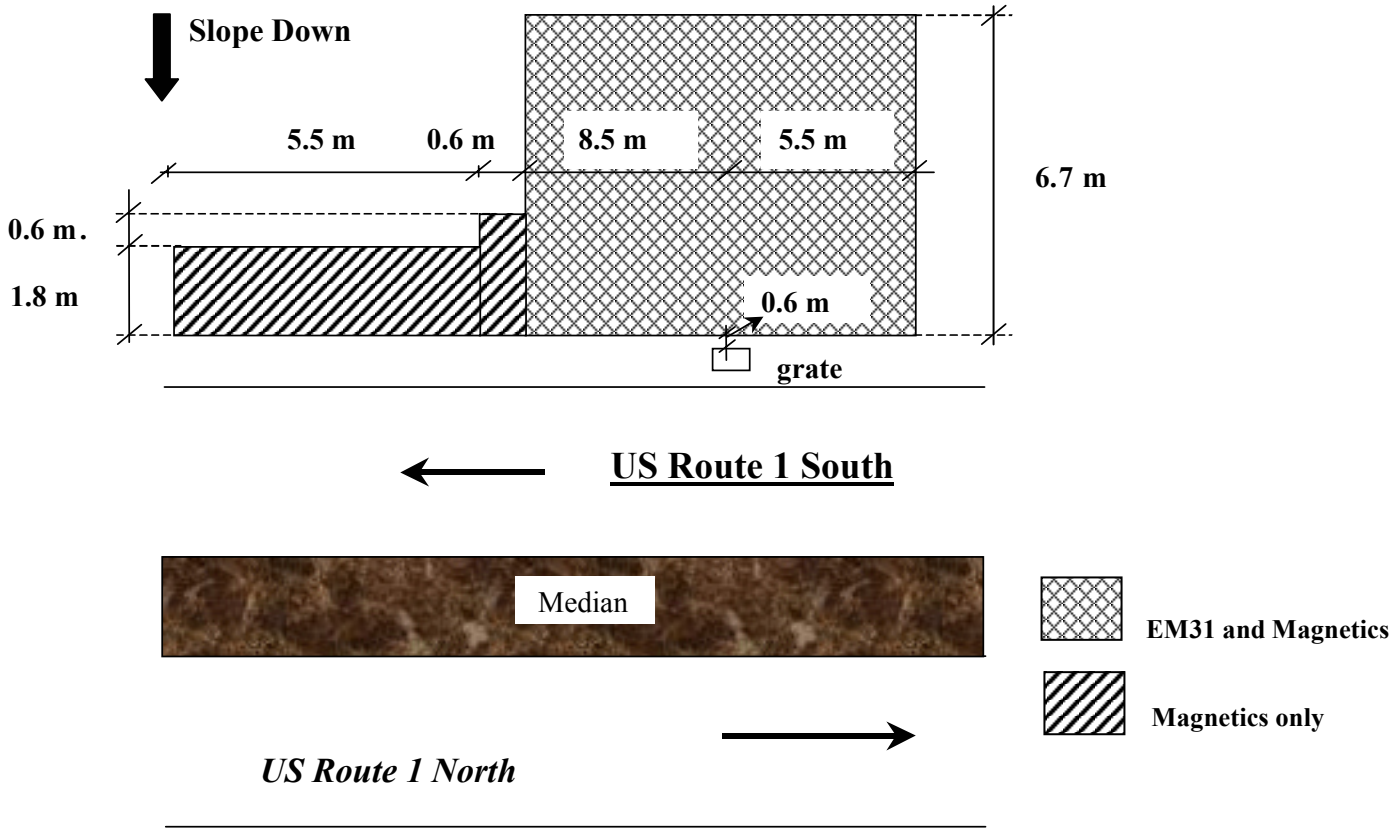

Figure B1. Area Covered by EM31 and Magnetics Tests, US 1, NC

[1] The GPR was conducted by NCDOT. Unfortunately, the testing results were skewed; thus, no accurate data can be reported.

Magnetics

Magnetometers measure the variation in the magnetic field of the Earth as well as local anomalies due to subsurface features. The magnetometer used for testing was a proton precession magnetometer (EG&G Geometrics model G-856AX). Magnetic metals cause distortions in the magnetometer data. Therefore, magnetometers are useful in detecting objects containing such minerals. A 0.6 m (2 ft) x 0.6 m (2 ft) grid was used for the pre-vitrification tests. Figure B2 shows the magnetometer test results.

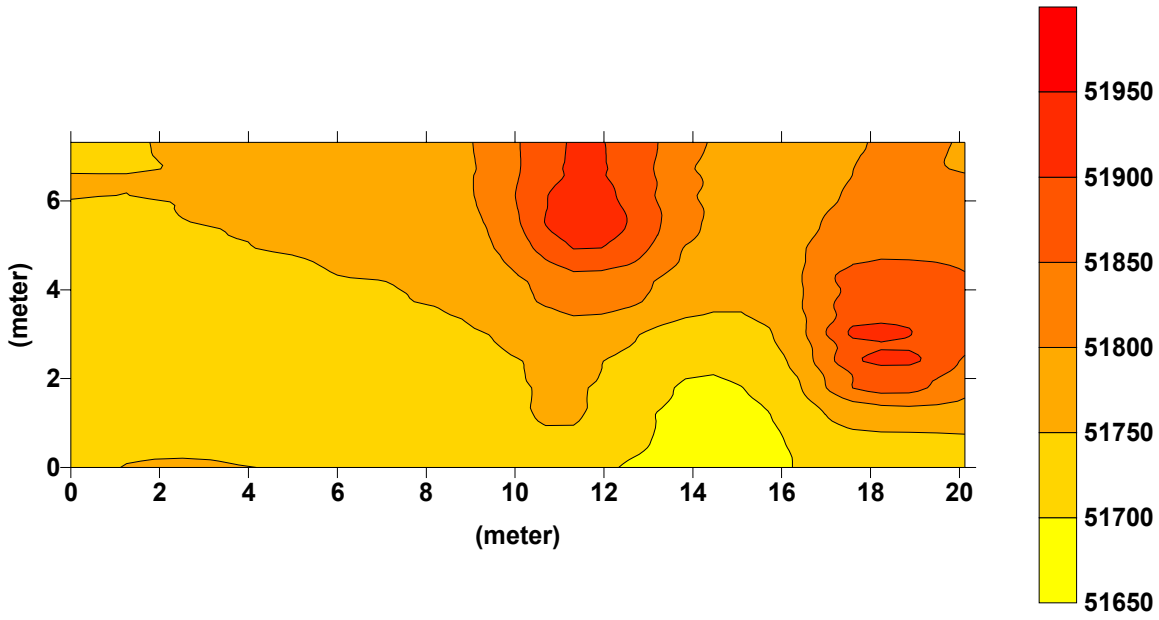

Figure B2. Magnetometer data – Initial Site Characterization

Electromagnetic Conductivity

The EM31 was utilized to measure the ground conductivity and relative variations locally. The EM31 produces an alternating current in the transmitter coil creating a magnetic field that induces electrical current fields in the ground. A second magnetic field is created by the current loops. Both these fields induce an alternating current in the EM31 receiver. The EM31 has the capability of detecting any changes in ground conductivity. The EM31 measures two phases of induced magnetic field: the quadrature phase and inphase components. The quadrature phase is a measurement of the ground conductivity, while the inphase is the ratio of the induced to primary magnetic field. The test could be conducted either in the horizontal or vertical modes. Typically, the EM31 could penetrate up to 6 m (20 ft) in the horizontal mode and 3 m (10 ft) in the vertical

mode. Readings were recorded at a 0.6 m (2 ft) x 0.6 m (2ft) grid. Figures B3 through B6 show the EM31 test results. The grate location is detected by the horizontal dipole inphase measurements.

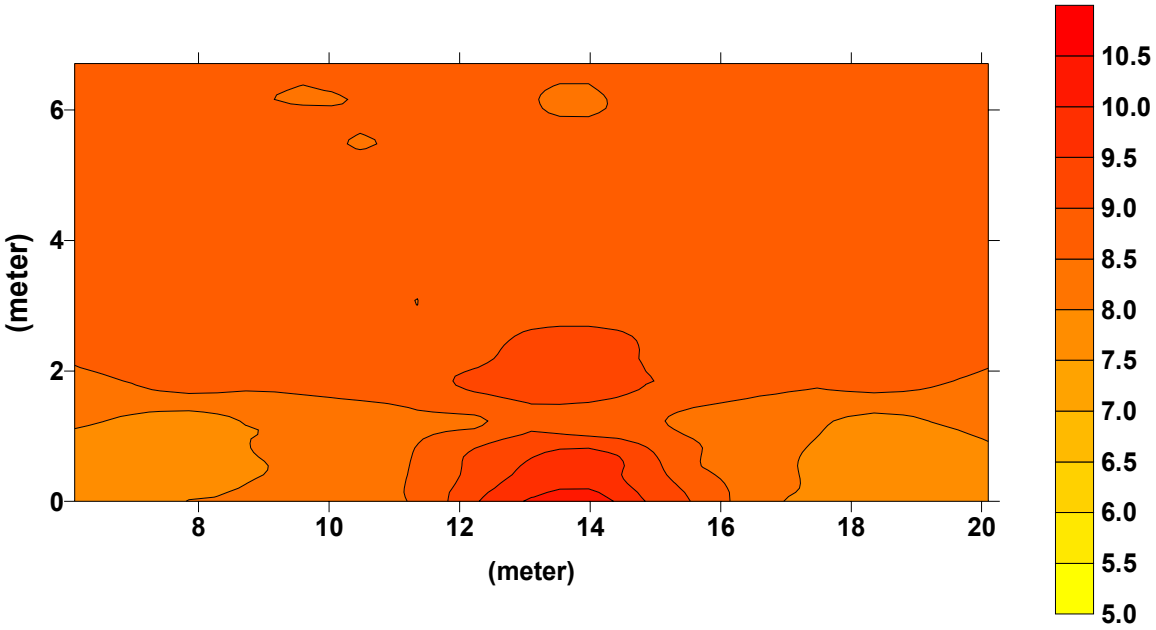

Figure B3. Electromagnetic Conductivity, Horizontal Dipole, Inphase-Initial Site Characterization

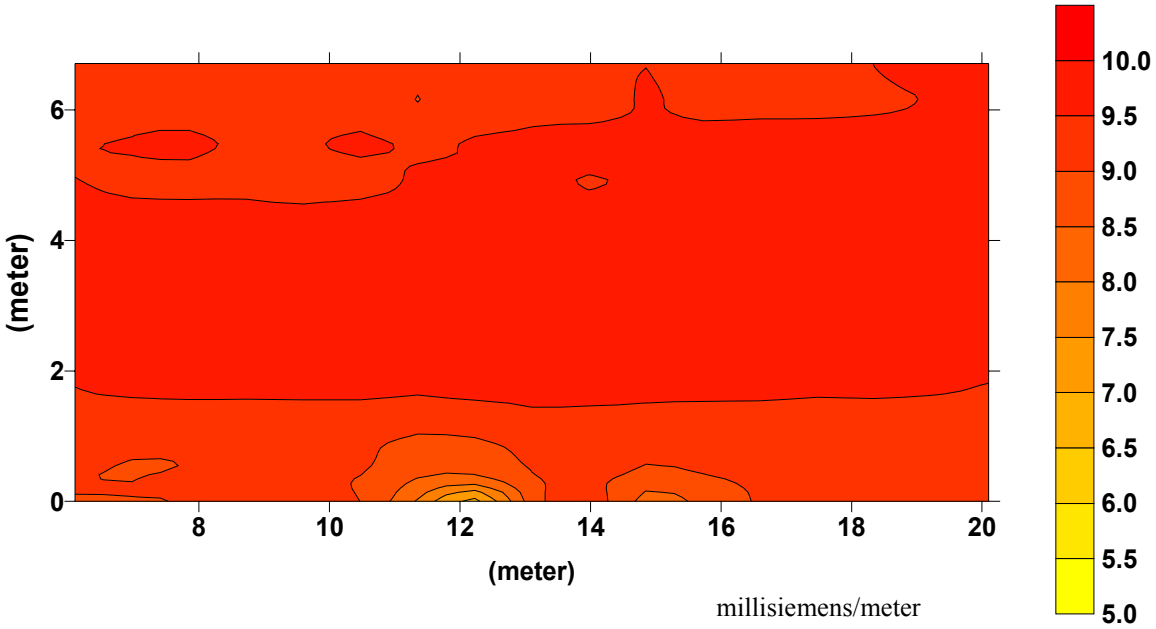

Figure B4. Electromagnetic Conductivity, Horizontal Dipole, Quadphase- Initial Site Characterization

40

36

32

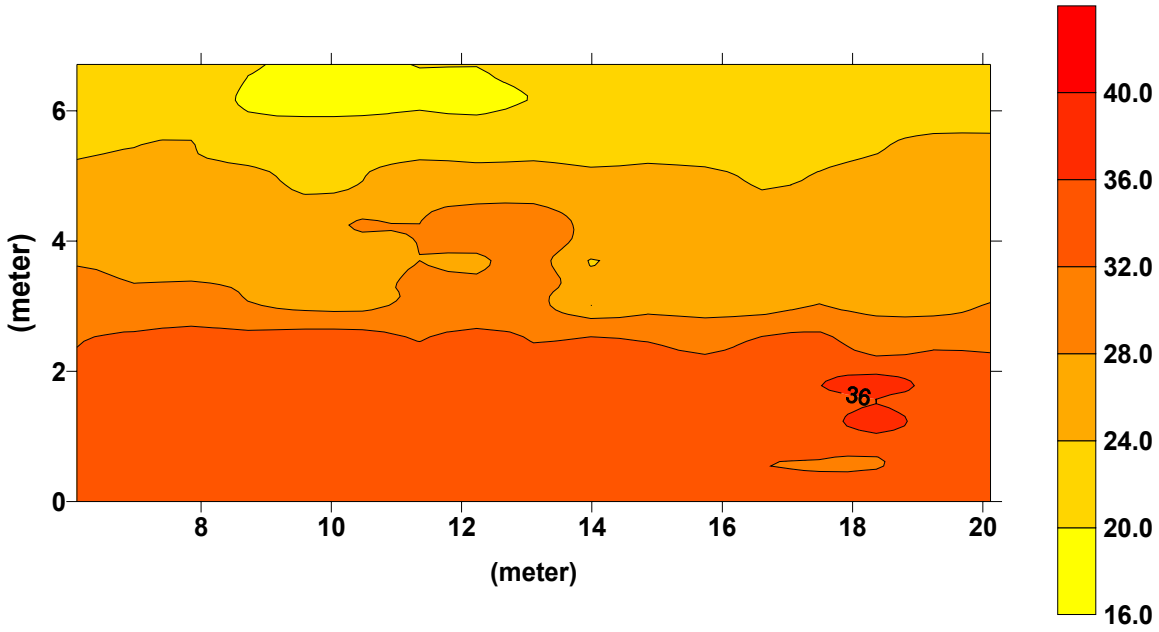

Figure B5. Electromagnetic Conductivity, Vertical Dipole, Inphase- Initial Site Characterization

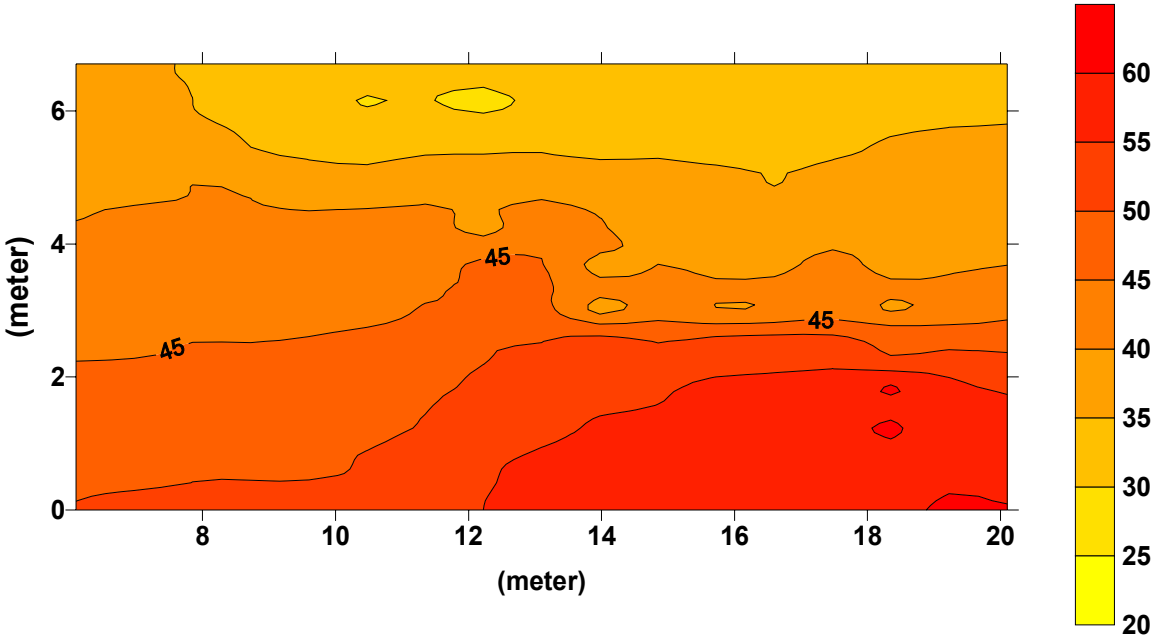

Figure B6. Electromagnetic Conductivity, Vertical Dipole, Quadphase- Initial Site Characterization

Earth Resistivity

In the earth resistivity method, a direct current or a low frequency alternating current is applied into the ground using pairs of electrodes connected to an electromagnetic force source. The induced potential distribution yields information about the electrical resistivity distribution. This process has been used in soil stratigraphy and searching for water bearing strata. Recently, it has been used in archaeology and observing in ground pollution (Parasnis, 1997).

Several electrode arrangements are possible. Examples of these arrays are Wenner, Schlumberger, and dipole-dipole arrays. For this site, a dipole-dipole array was selected. Figure B7 shows the dipole-dipole arrangement. A and B are the current electrodes, while M and N are the potential electrodes.

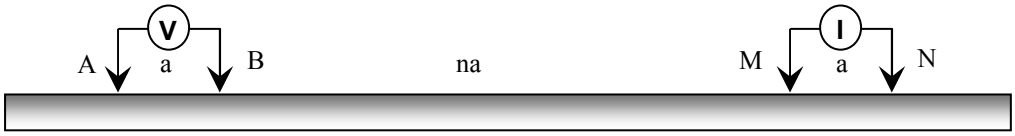

Figure B7. Dipole-Dipole Arrangement

The apparent resistivity is calculated using Equation B1.

$$\rho_a = \frac{\pi n(n+1)(n+2)aV_{MN}}{I} \qquad \text{(Equation B1)}$$

where:

ρ_a = apparent resistivity

V_{MN} = potential difference between M and N

I = current intensity

a = electrode spacing

na = distance between the two innermost electrodes (B and M)

A SYSCAL KID switch-24 resistivity meter was used to measure the apparent earth resistivity at the site. This compact multi-electrode resistivity meter has 24 electrodes

attached to it. A dipole-dipole arrangement, shown in Figure B7, was used. This meter automatically switches between the different electrodes trying all the different combinations. A spacing of 0.9 m (3 ft) was chosen between the electrodes. The test was repeated along eleven lines spaced 0.9 m (3 ft) apart, parallel to the slope. The results are shown in Figures B8 through B18. Most of the measurements were within 900 ohm.meter. Typically, clay and shale resistivities vary between 1 to 100 ohm meters and 20 to 2000 ohm.meter, respectively. Soil of higher resistance appeared near the surface of line 3.

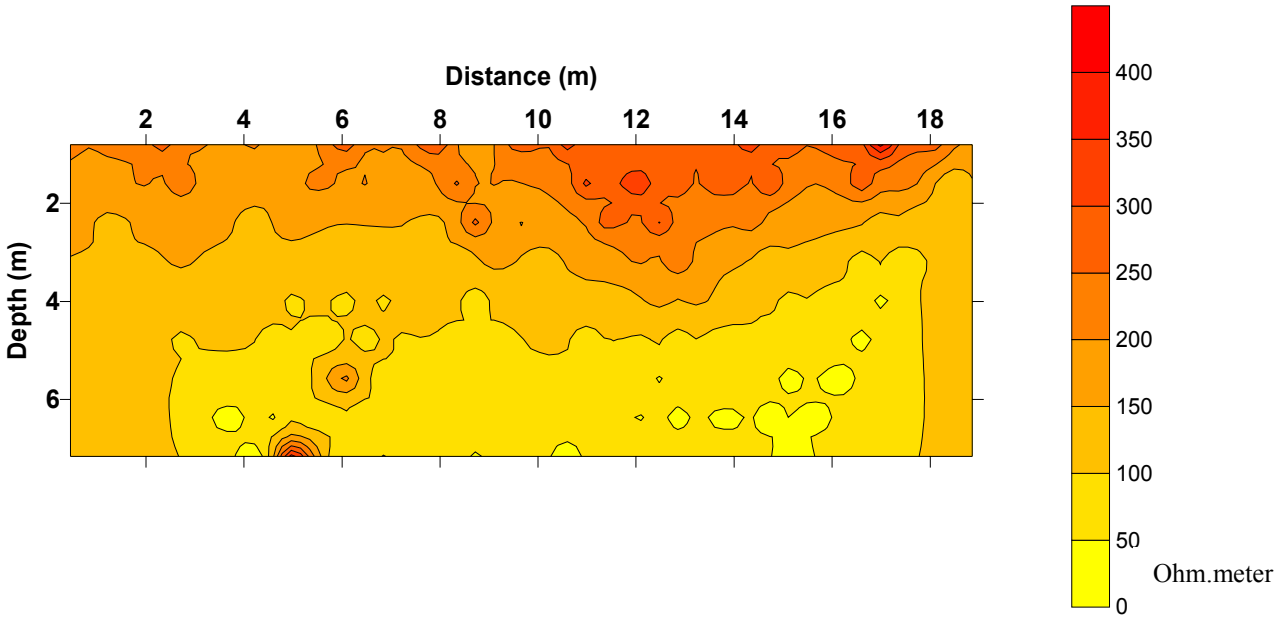

Figure B8. Soil Resistivity Profile along line 1 located 13.7 m (45 ft) up the slope from grate

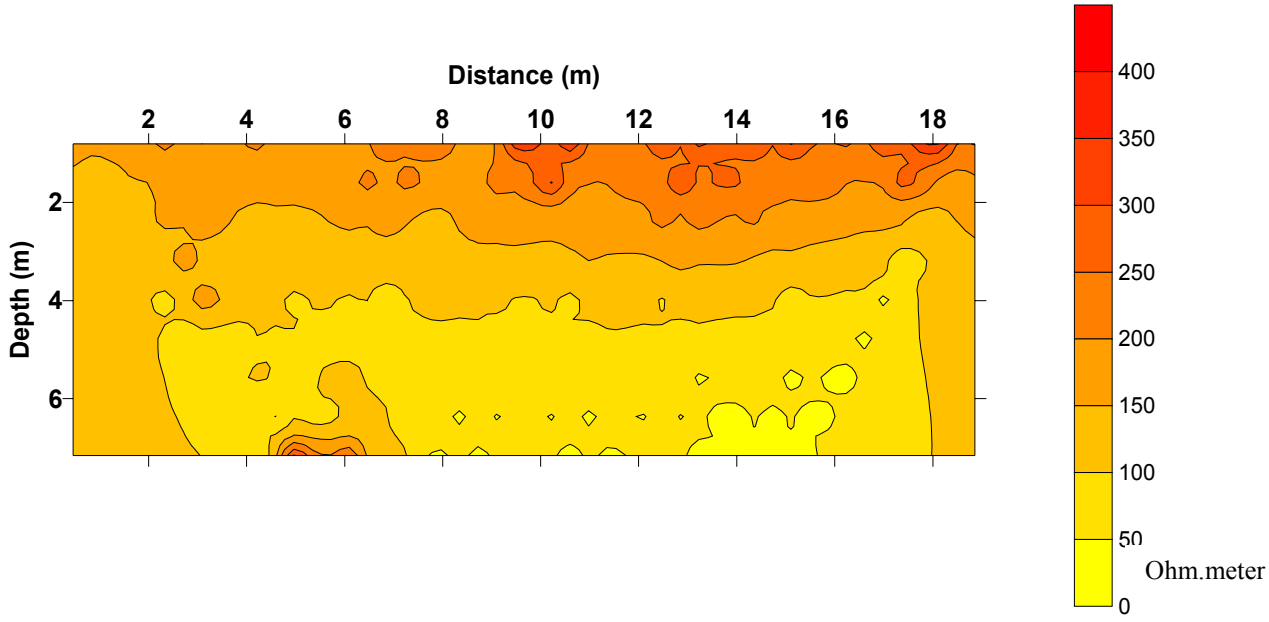

Figure B9. Soil Resistivity Profile along line 2 located 12.8 m (42 ft) up the slope from grate

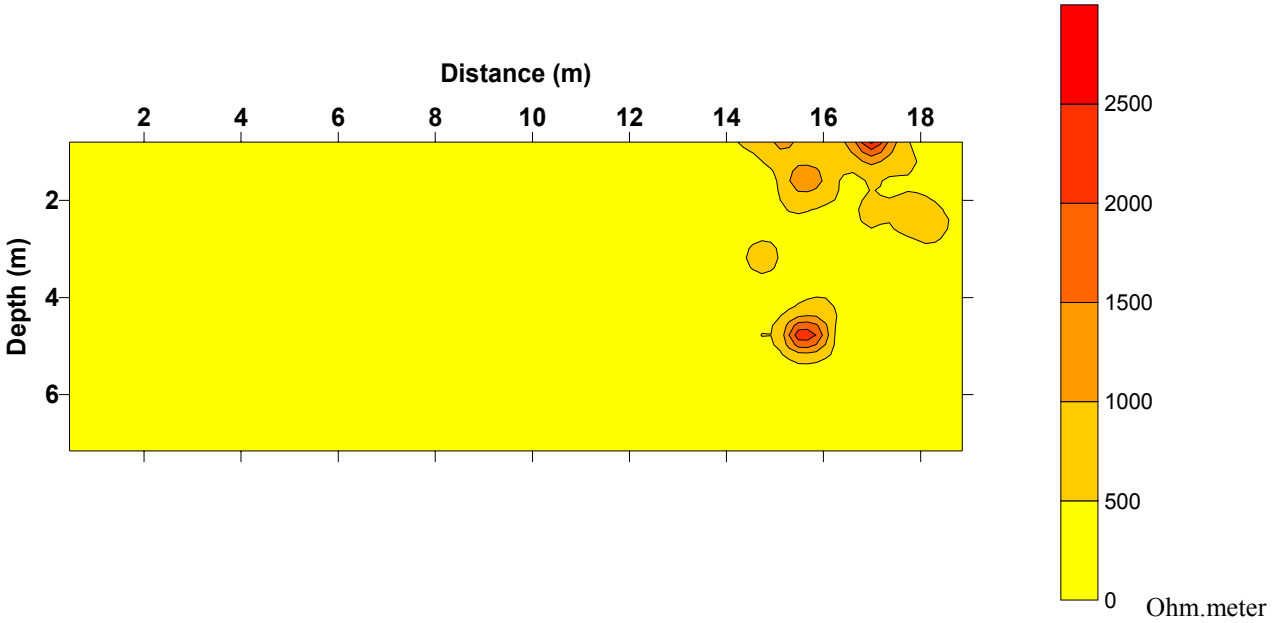

Figure B10. Soil Resistivity Profile along line 3 located 11.9 m (39 ft) up the slope from grate

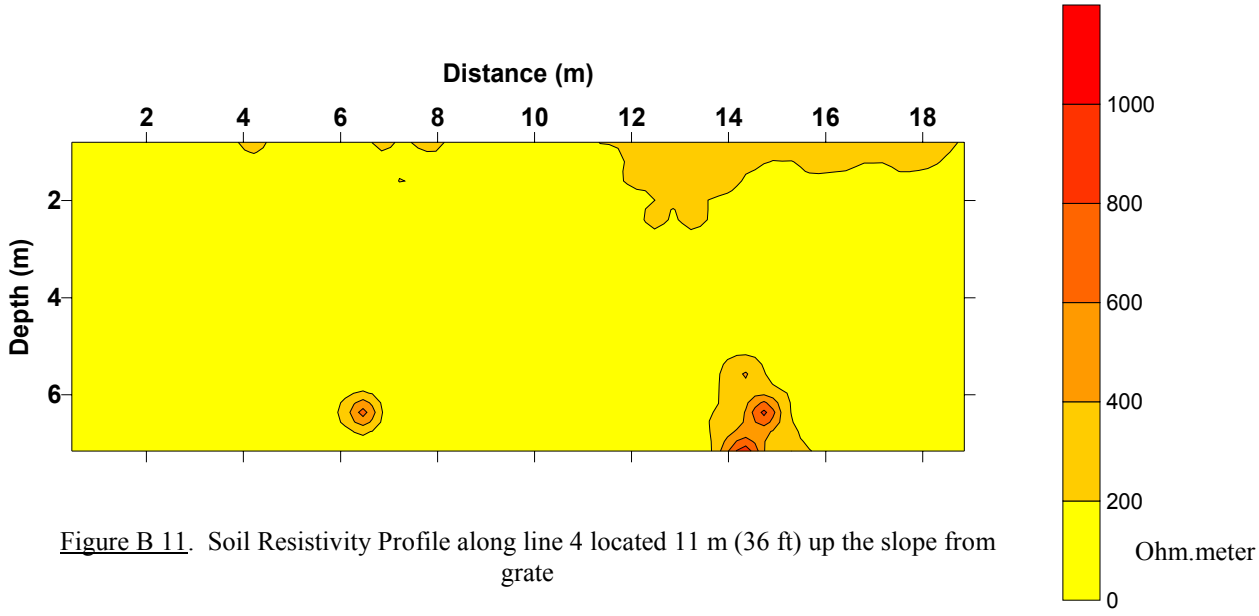

Figure B 11. Soil Resistivity Profile along line 4 located 11 m (36 ft) up the slope from grate

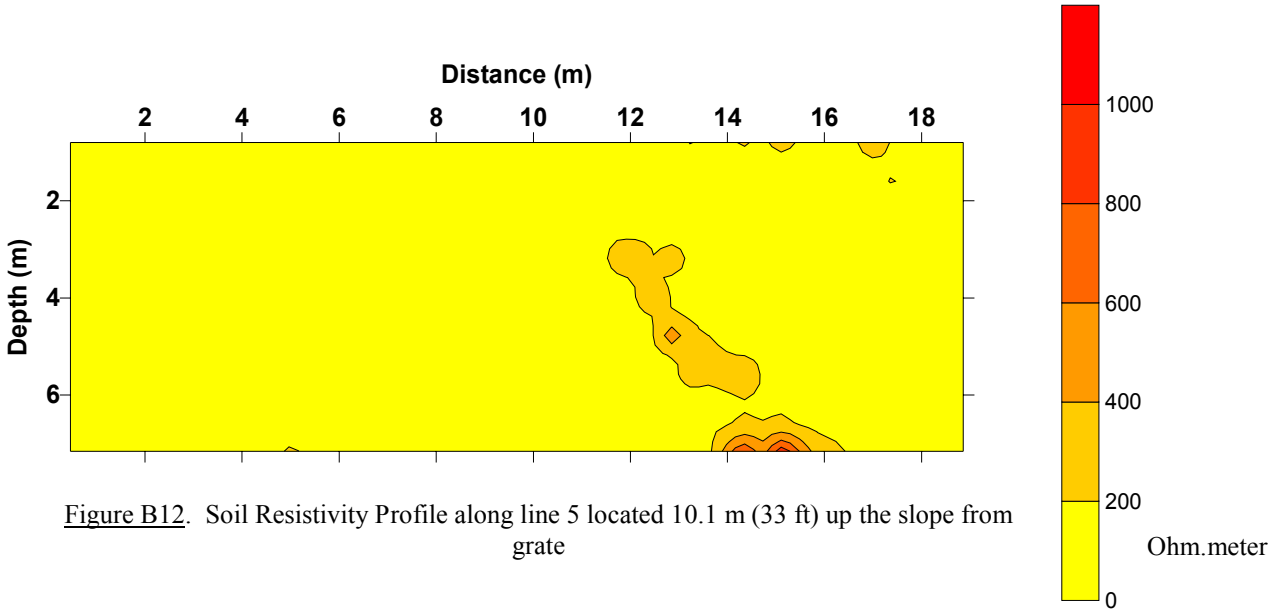

Figure B12. Soil Resistivity Profile along line 5 located 10.1 m (33 ft) up the slope from grate

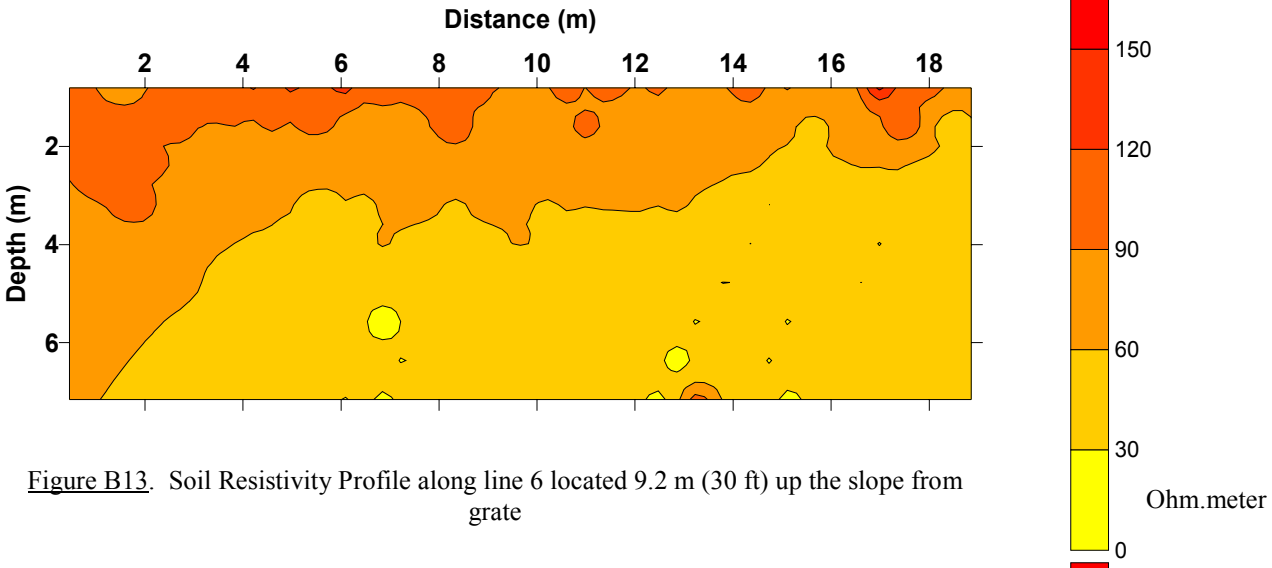

Figure B13. Soil Resistivity Profile along line 6 located 9.2 m (30 ft) up the slope from grate

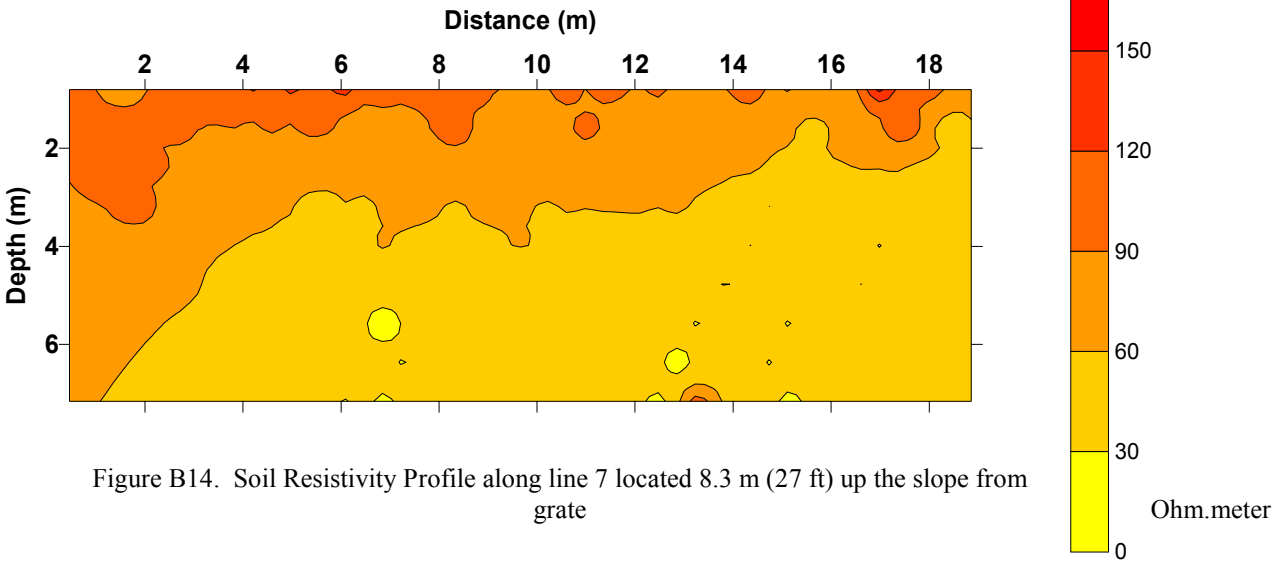

Figure B14. Soil Resistivity Profile along line 7 located 8.3 m (27 ft) up the slope from grate

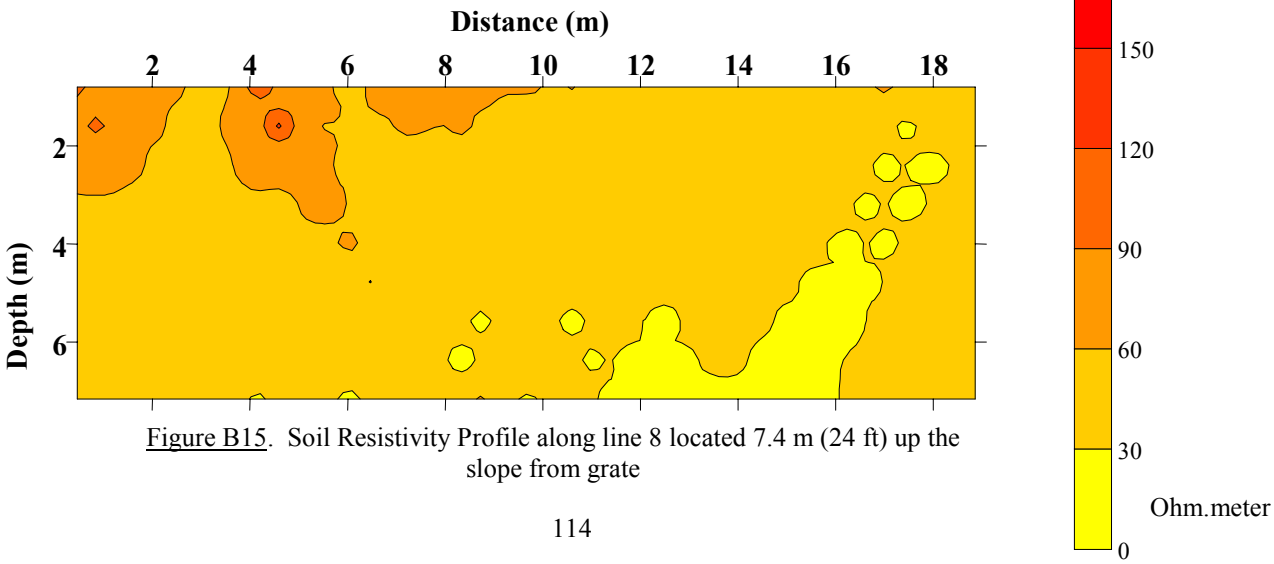

Figure B15. Soil Resistivity Profile along line 8 located 7.4 m (24 ft) up the slope from grate

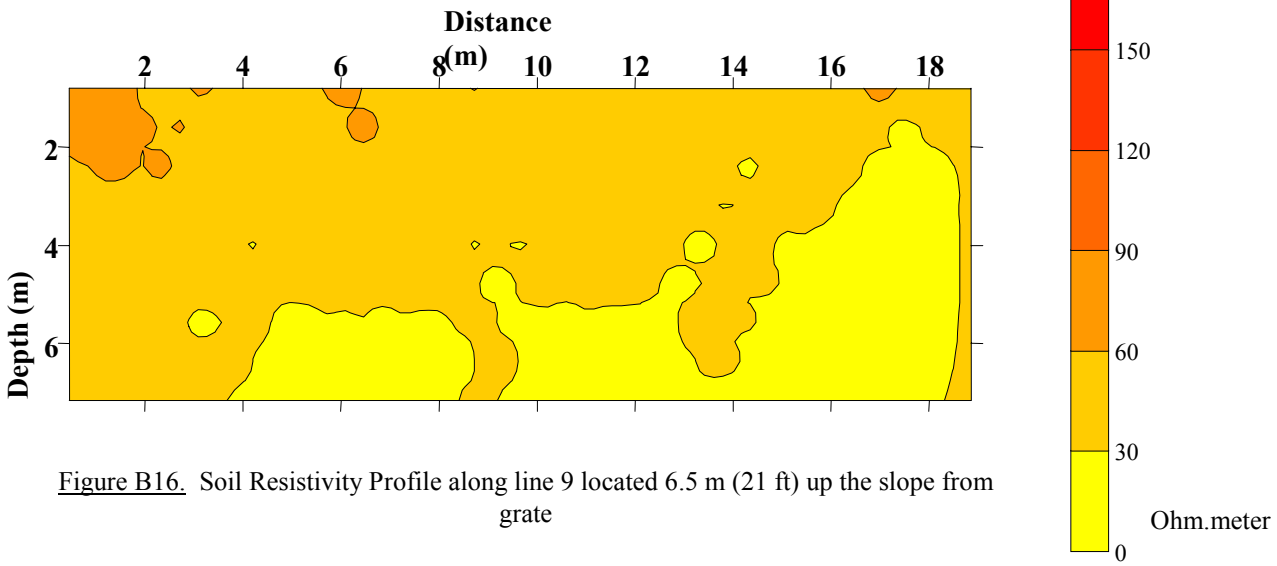

Figure B16. Soil Resistivity Profile along line 9 located 6.5 m (21 ft) up the slope from grate

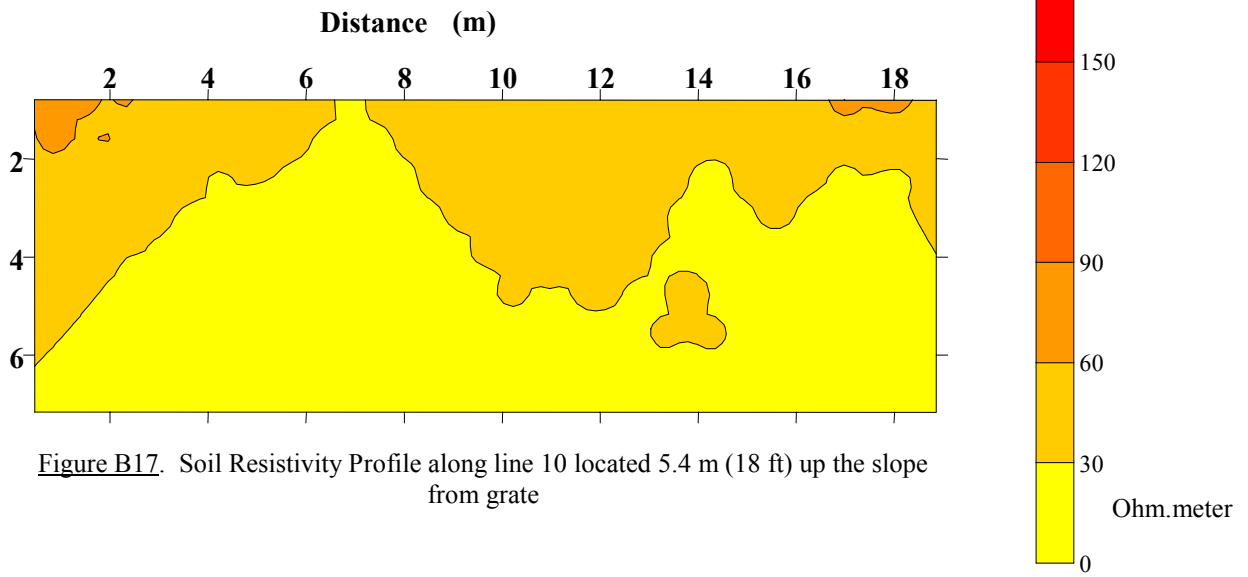

Figure B17. Soil Resistivity Profile along line 10 located 5.4 m (18 ft) up the slope from grate

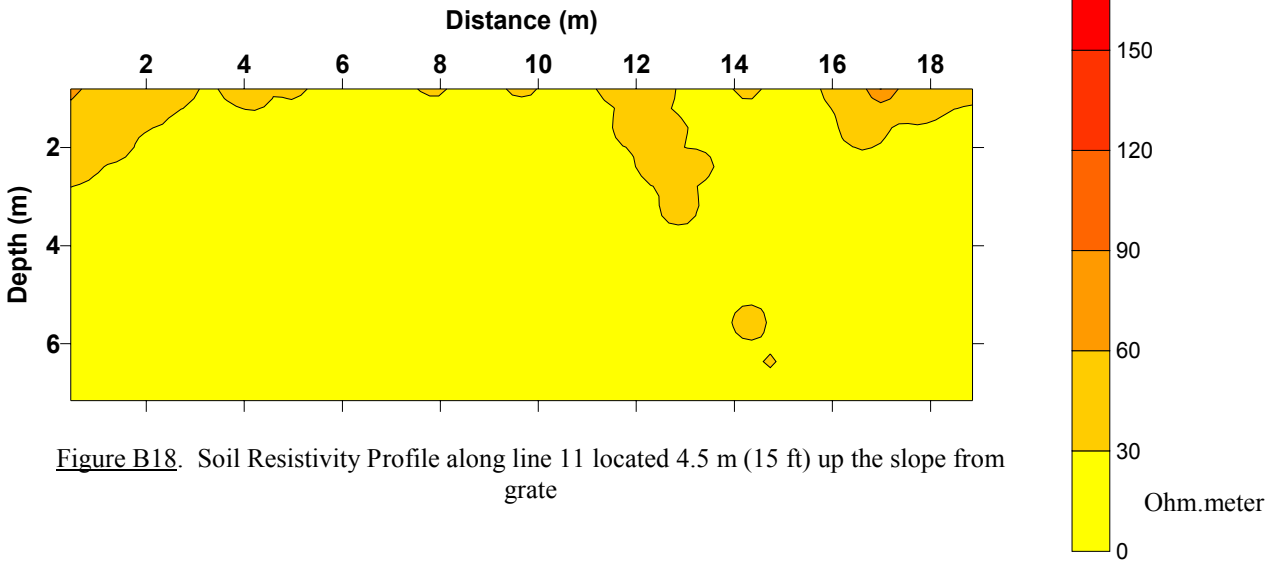

Figure B18. Soil Resistivity Profile along line 11 located 4.5 m (15 ft) up the slope from grate

Down-hole Tests

Down-hole geophysical tests were conducted to determine the variation of shear wave velocity with depth. The wave source was located on the ground surface next to the borehole where a receiver was lowered. The receiver geophone was connected to an oscilloscope that is used to measure the wave travel time from the source to the receiver. Test setup is shown in Figure B19. The shear wave velocity is directly related to the low-strain shear modulus (G_o) and soil density using Equation B2, shown below:

$$G_o = \rho V_s^2 \qquad \text{(Equation B2)}$$

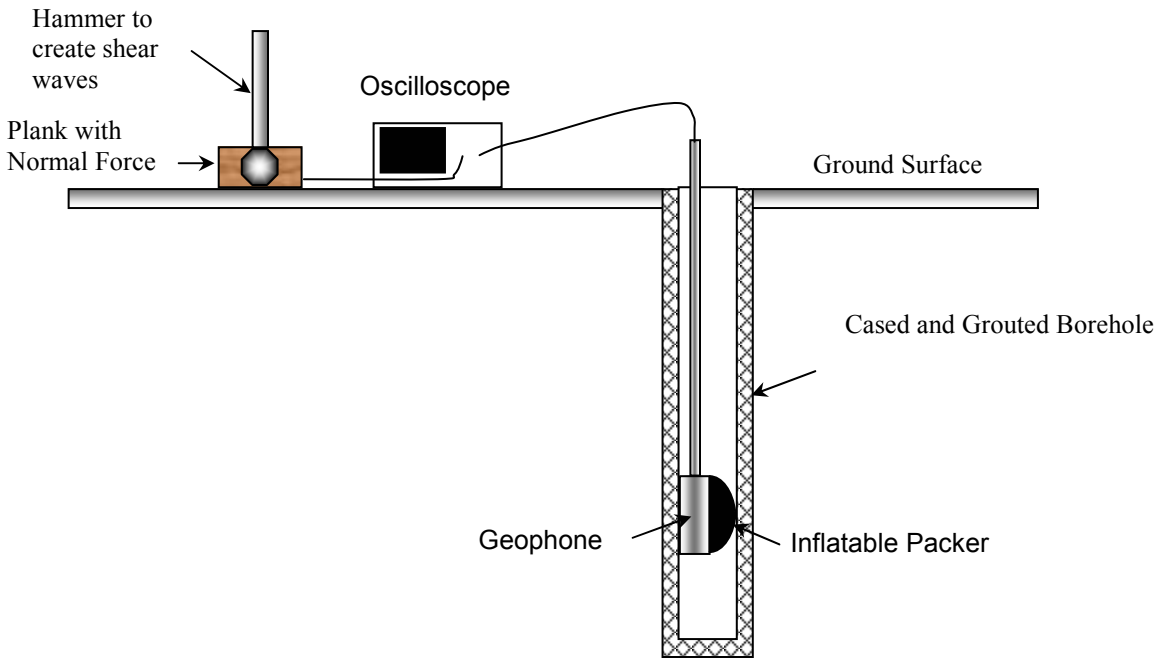

Figure B19. Setup Downhole Seismic Testing Setup

A plot of the travel time versus depth was generated to calculate the travel velocity. The slope of the travel-time plot at each depth is the wave velocity at this depth. Test results and their interpretation are shown in Figures B20 and B21, respectively.

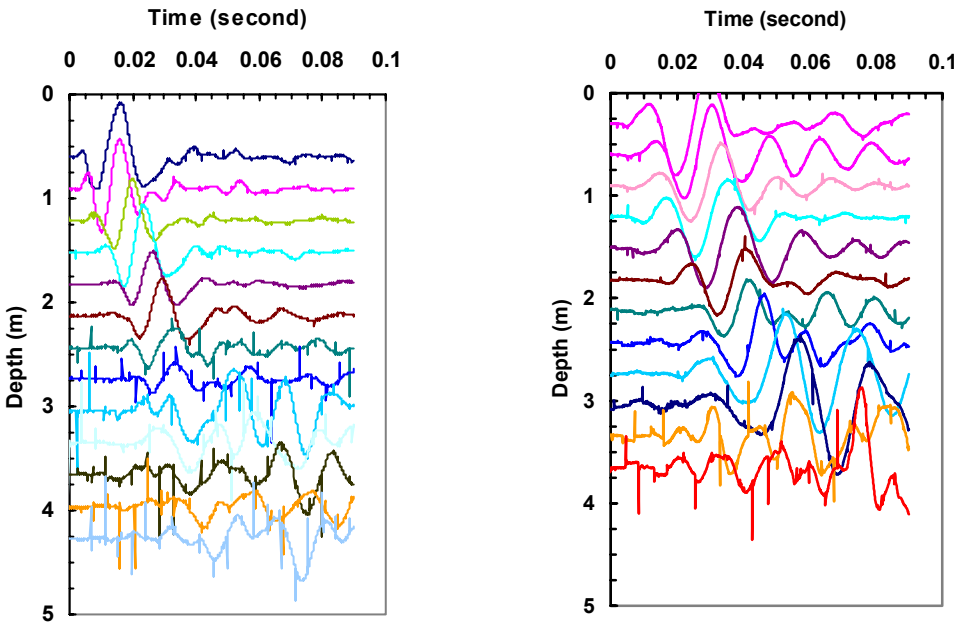

Figure B20. Down-hole Shear Wave Test Results

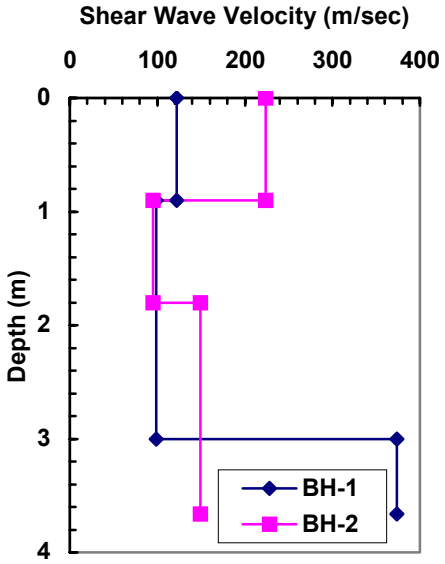

Figure B21. Soil Shear Wave Velocities at US 1 Slope Site

Several attempts were conducted with the surface waves technique. However, the data analysis was not quite successful because this test is suitable for a sequence of infinitely extending horizontal layers. This condition is not satisfied in our case due to the fact that we were dealing with a slope.

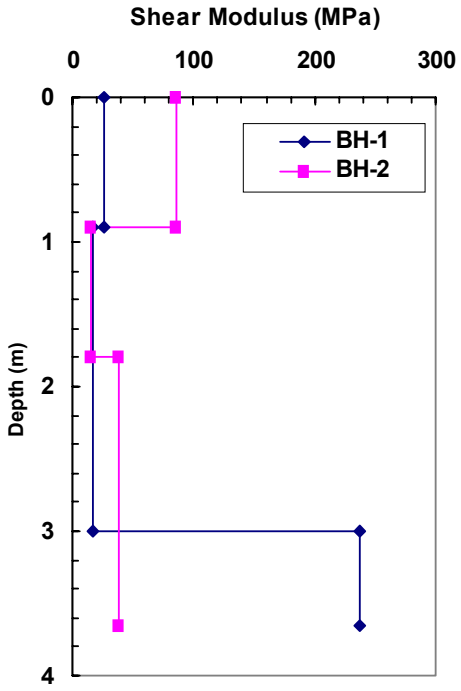

Figure B22. Shear Modulus Profile Based on Downhole Velocity Measurements

Appendix C

Inclinometer

Appendix C. Inclinometer

North Carolina Department of Transportation (NCDOT) conducted tilt measurements with depth, starting from the bottom of the borehole upwards, at discrete time intervals. Two measurements were made: normal to the slope (A-axis) and parallel to the slope (B-axis). The first measurements are considered as a baseline for comparison. Typically, the slope motion would appear from the measurement parallel to the slope. Based on these measurements, the actual failure plane as well as the slippage rate could be determined

Figure C1**:** Inclinometer Probe

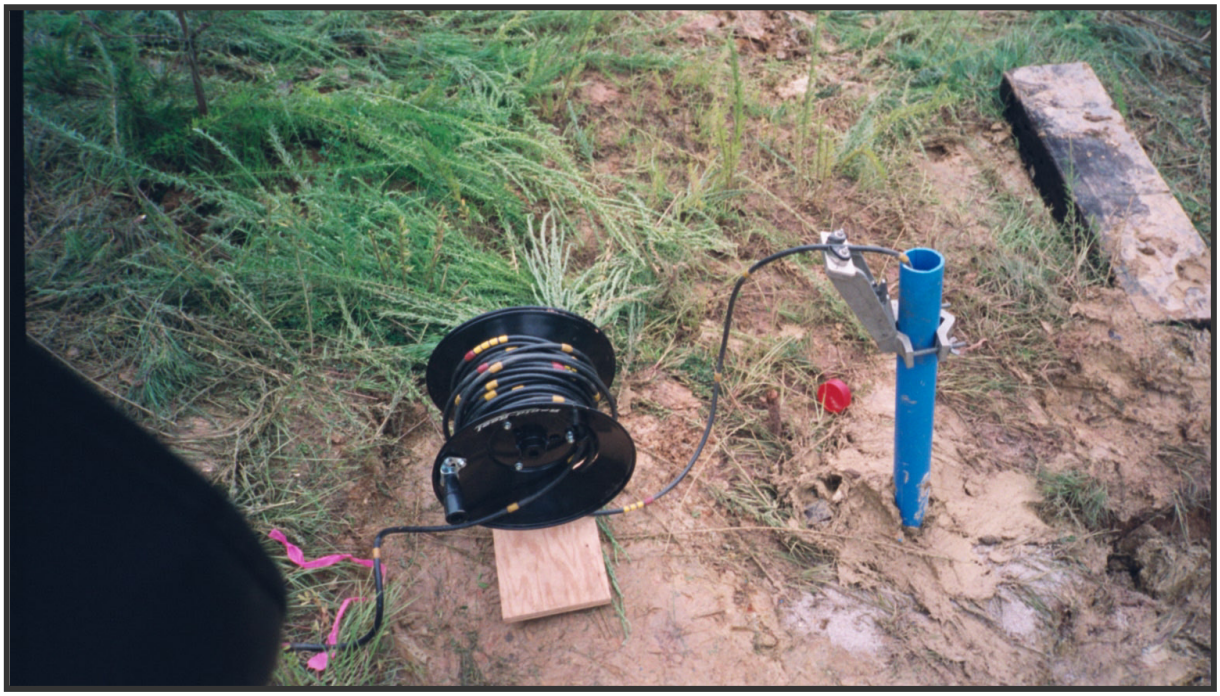

Figure C2**:** Inclinometer Testing from borehole BX-1

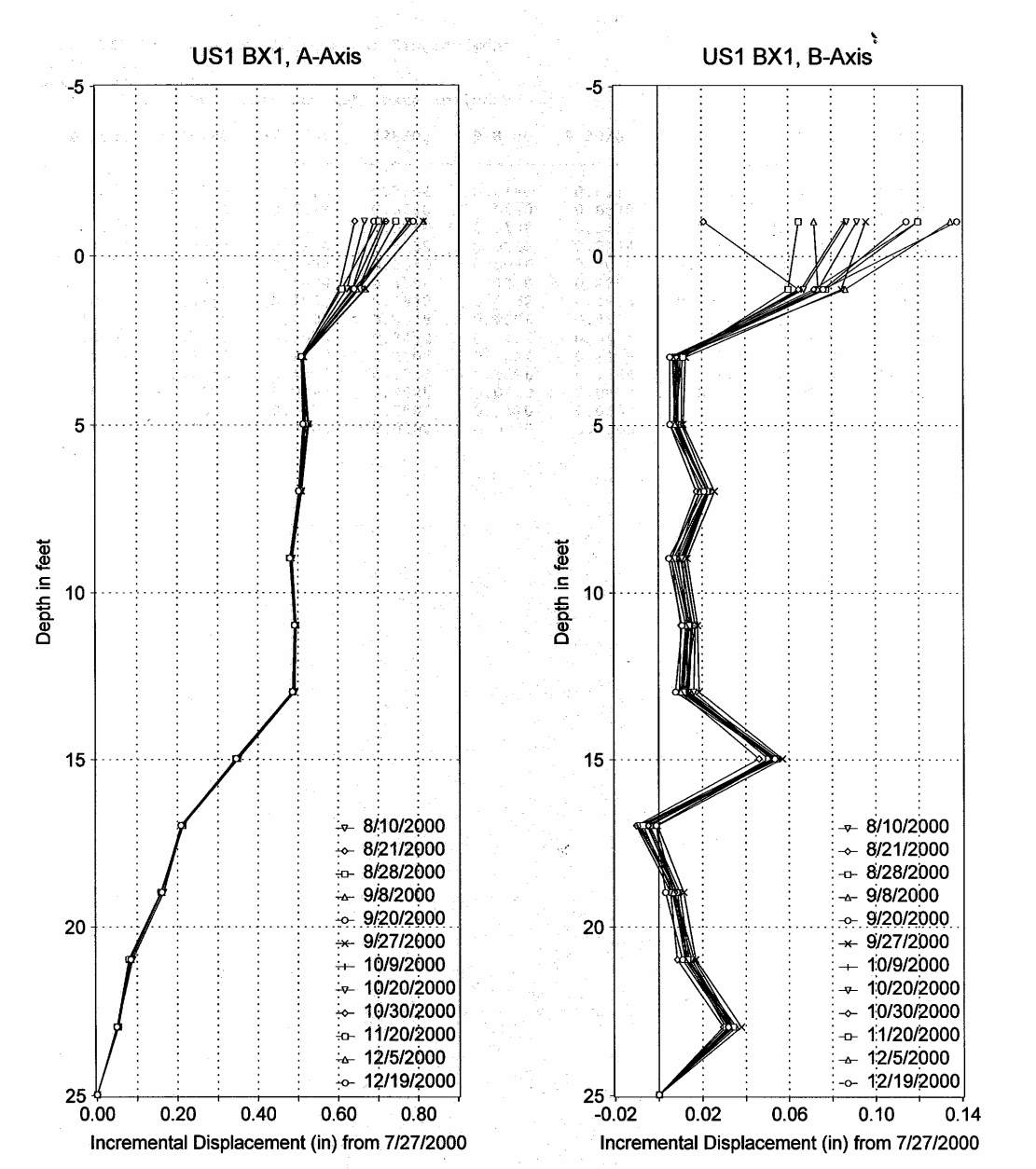

Figure C3**:** Inclinometer Measurements from borehole BX-1

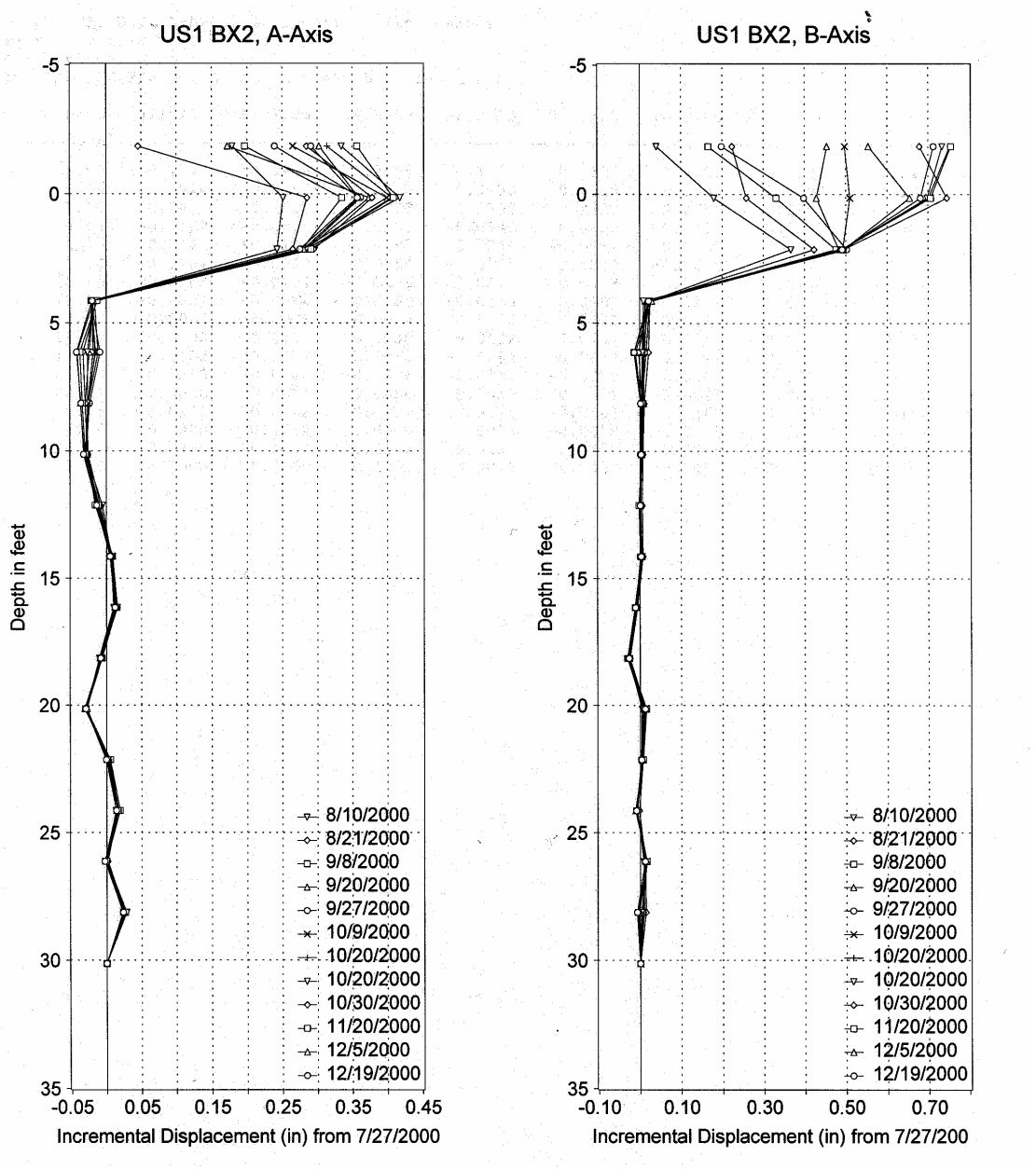

Figure C4**:** Inclinometer Measurements from borehole BX-2

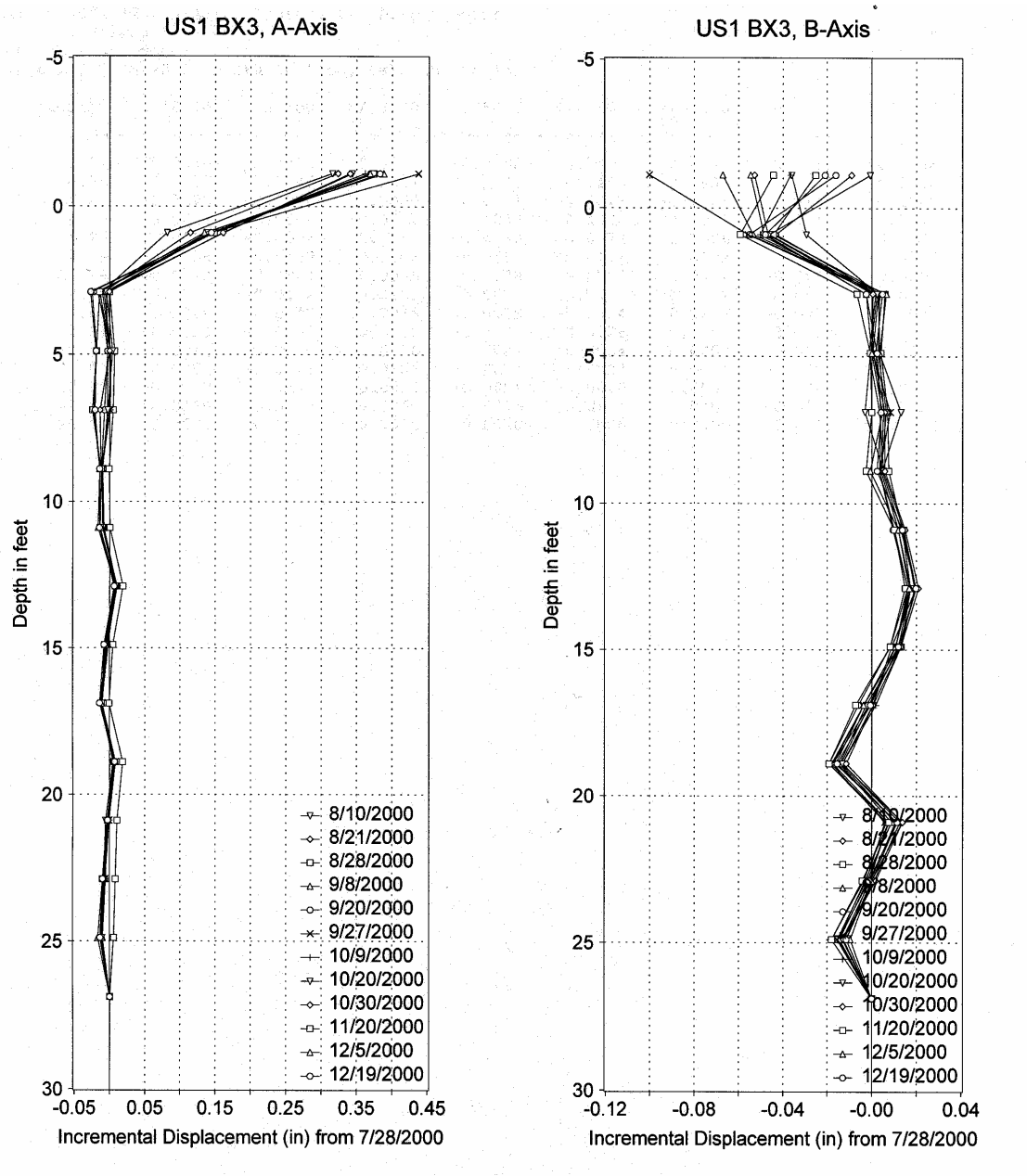

Figure C5**:** Inclinometer Measurements from borehole BX-3

Appendix D

Additional Plasma Arc Laboratory Photographs

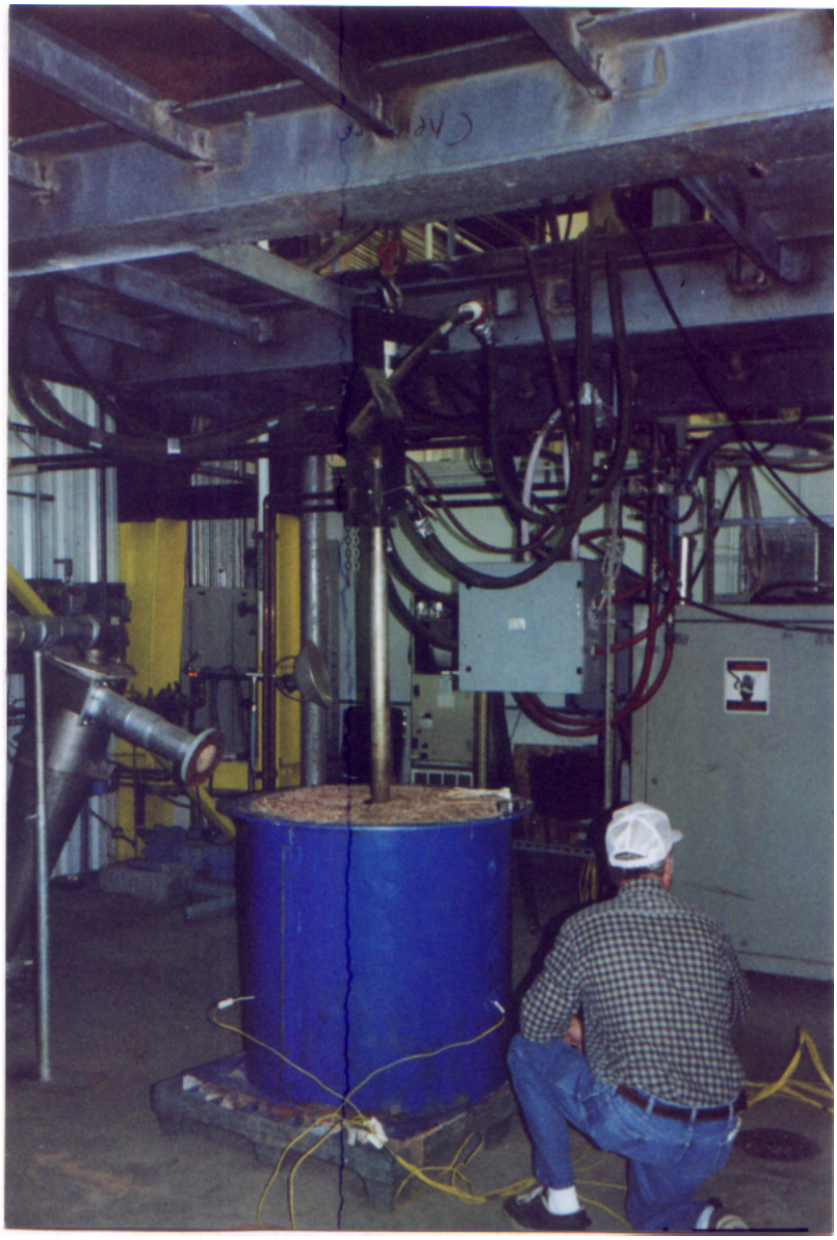

Figure D1. Laboratory Vitrification Setup

Figure D2. Chamber Set-up

Figure D3. Setting the thermocouples

Figure D4. Starting the torch

Figure D5. Plasma torch in progress

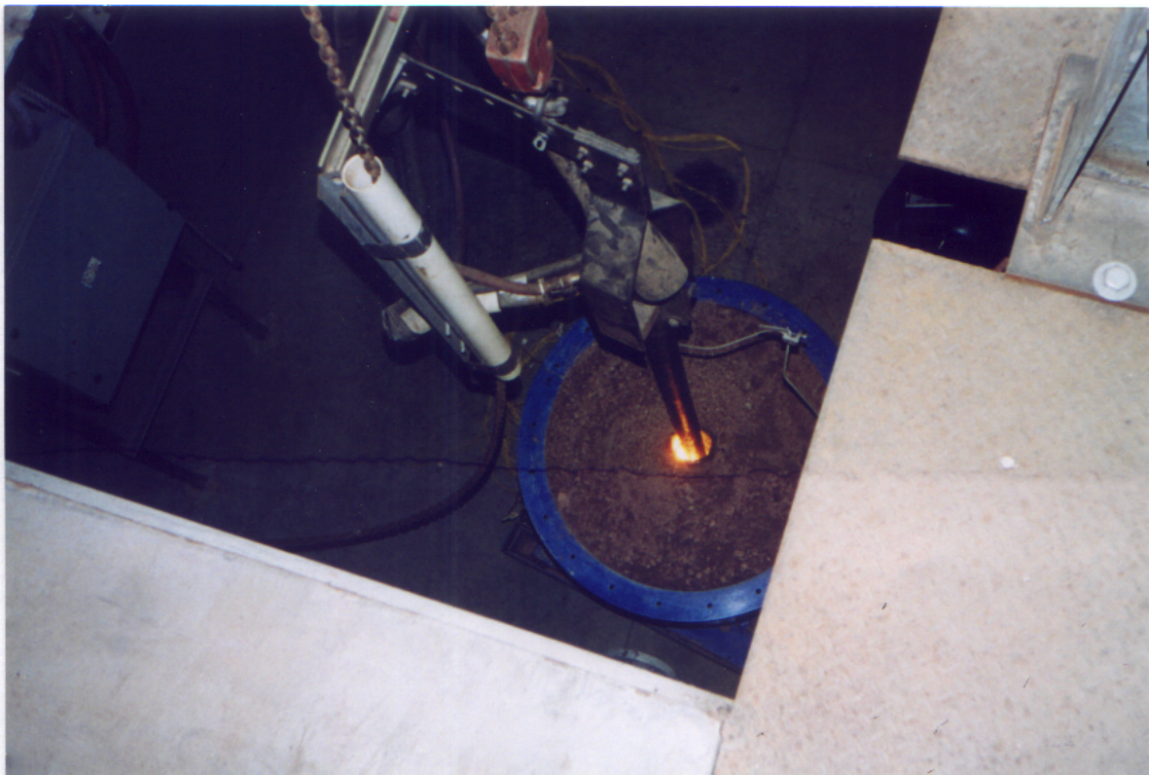

Figure D6. Overhead view of plasma torch in progress

Figure D7. Torch vitrification in progress

Figure D8. Vitrified material

Appendix E

Sample Slope Models and Input Data

Sample Input Data

```
PROFIL                                          FILE: PAV5420
Distance 5 Diameter 4 Length 20
  36     8
```

```
      .0        47.5        50.0        47.5    2
```
Ground Surface
```
     50.0        47.5        55.0        46.3    2
     55.0        46.3        65.0        48.3    2
     65.0        48.3        69.0        50.0    7
     69.0        50.0        82.5        55.3    2
     82.5        55.3       110.0        66.3    1
    110.0        66.3       125.0        66.3    1
    125.0        66.3       160.0        66.3    2
```

```
     82.5        55.3       125.0        66.3    2
```
Subsurface
```
      .0        41.0        40.0        41.0    3
     40.0        41.0        64.8        47.6    3
     69.1        48.6       125.0        63.5    3
    125.0        63.5       160.0        63.5    3
      .0        37.5        40.0        37.5    4
     40.0        37.5        64.7        44.3    4
     69.2        45.3       125.0        60.0    4
    125.0        60.0       160.0        60.0    4
      .0        32.5        40.0        32.5    5
     40.0        32.5        64.6        39.0    5
     69.3        39.8       125.0        53.5    5
    125.0        53.5       160.0        53.5    5
      .0        25.0        40.0        25.0    6
     40.0        25.0        64.5        29.0    6
     69.4        29.5       125.0        38.5    6
    125.0        38.5       160.0        38.5    6
```

```
     64.5        29.0        64.6        39.0    7
     64.6        39.0        64.7        44.3    7
     64.7        44.3        64.8        47.6    7
```

(top boundary)

← Top of PAV Column

←

PAV Column intersection are shaded

PAV Column

```
     64.8        47.6        64.9        48.0   7
     64.9        48.0        65.0        48.3   7
     69.0        50.0        69.1        48.6   2
     69.1        48.6        69.2        45.3   3
     69.2        45.3        69.3        39.8   4
     69.3        39.8        69.4        29.5   5
     69.4        29.5        69.5        29.0   6
```

```
     64.5        29.0        69.5        29.0   6
```

PAV Column Bottom

```
SOIL
  7
  100.0    100.0         .0    15.00      .000          .0    1
  110.0    110.0         .0    15.00      .000          .0    1
  115.0    115.0         .0    25.00      .000          .0    1
  130.0    125.0         .0    25.00      .000          .0    1
  140.0    130.0         .0    37.00      .000          .0    1
  140.0    140.0         .0    30.00      .000          .0    1
  160.0    160.0  360000.0    45.00      .000          .0
1
```

← PAV Column

```
WATER
  1       62.40
   7
        60.0         46.3
        70.0         48.8
        80.0         51.4
        90.0         53.9
       100.0         56.5
       110.0         59.0
      160.0       59.0
```

```
CIRCL2
  20    20
       .0       55.0       110.0       160.0
                .0         3.0          .0          .0
```

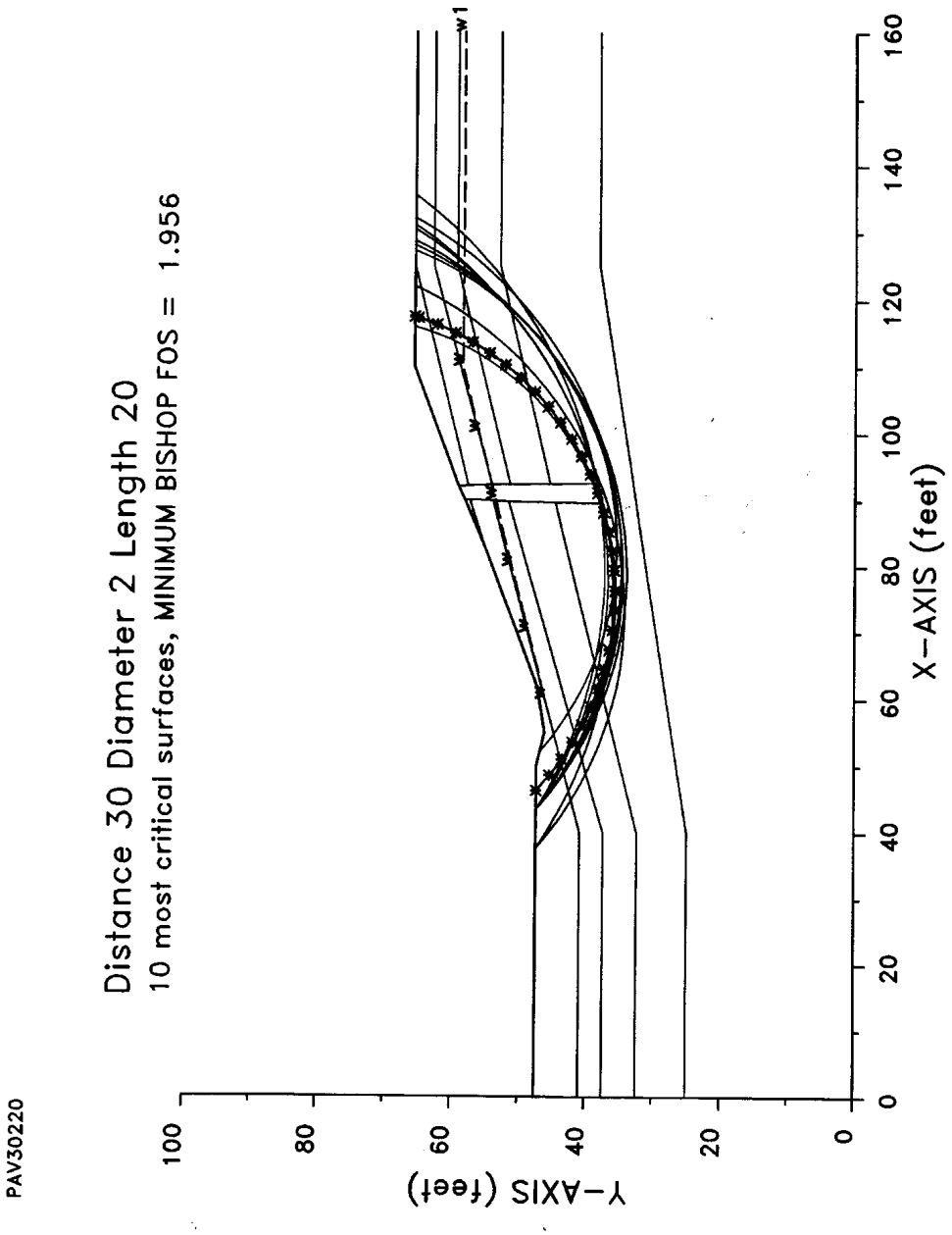

Figure E1. Deep Slip Surface Model Output Plo

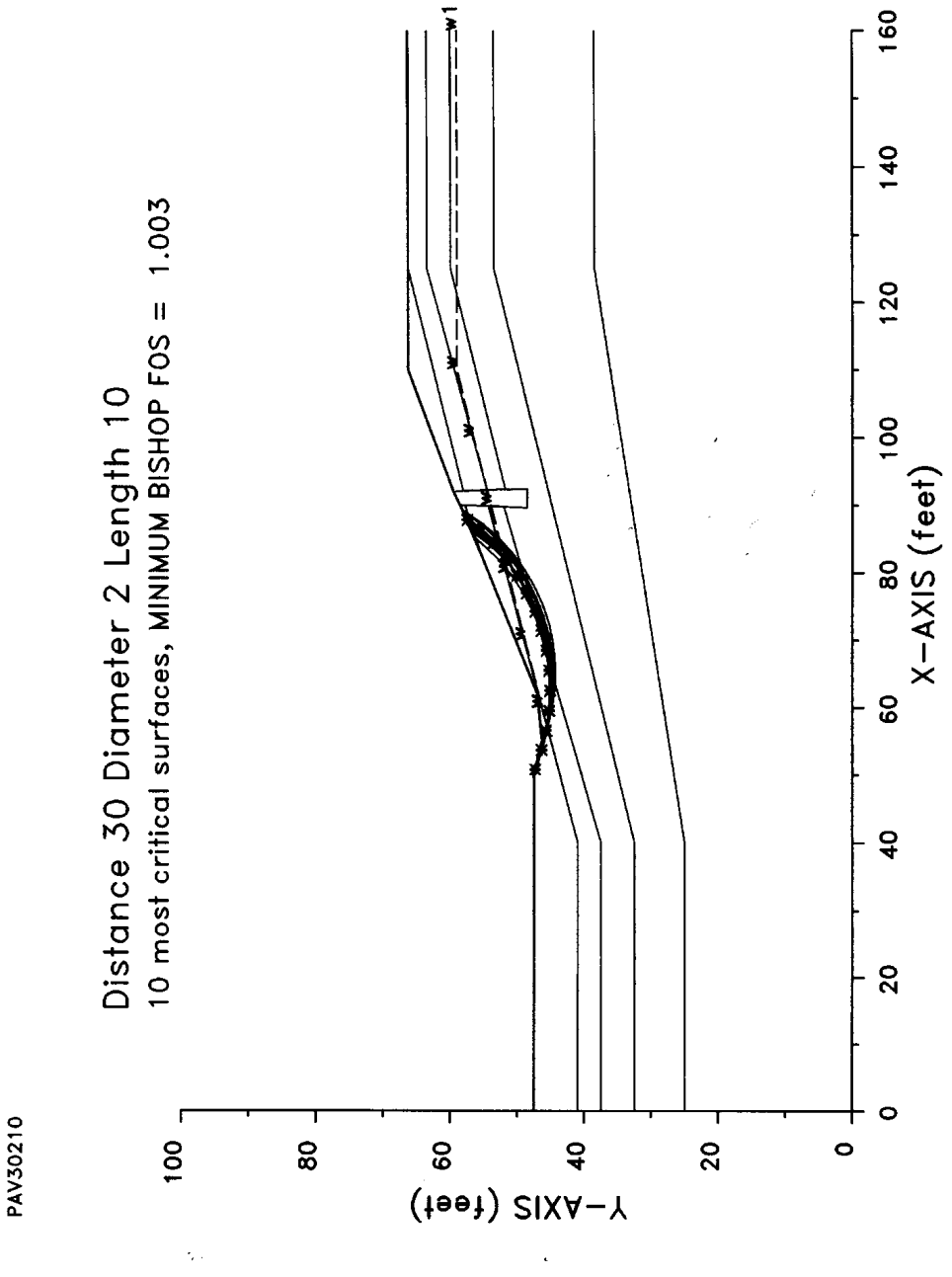

Figure E2. Frontal Slip Surface Model Output Plot

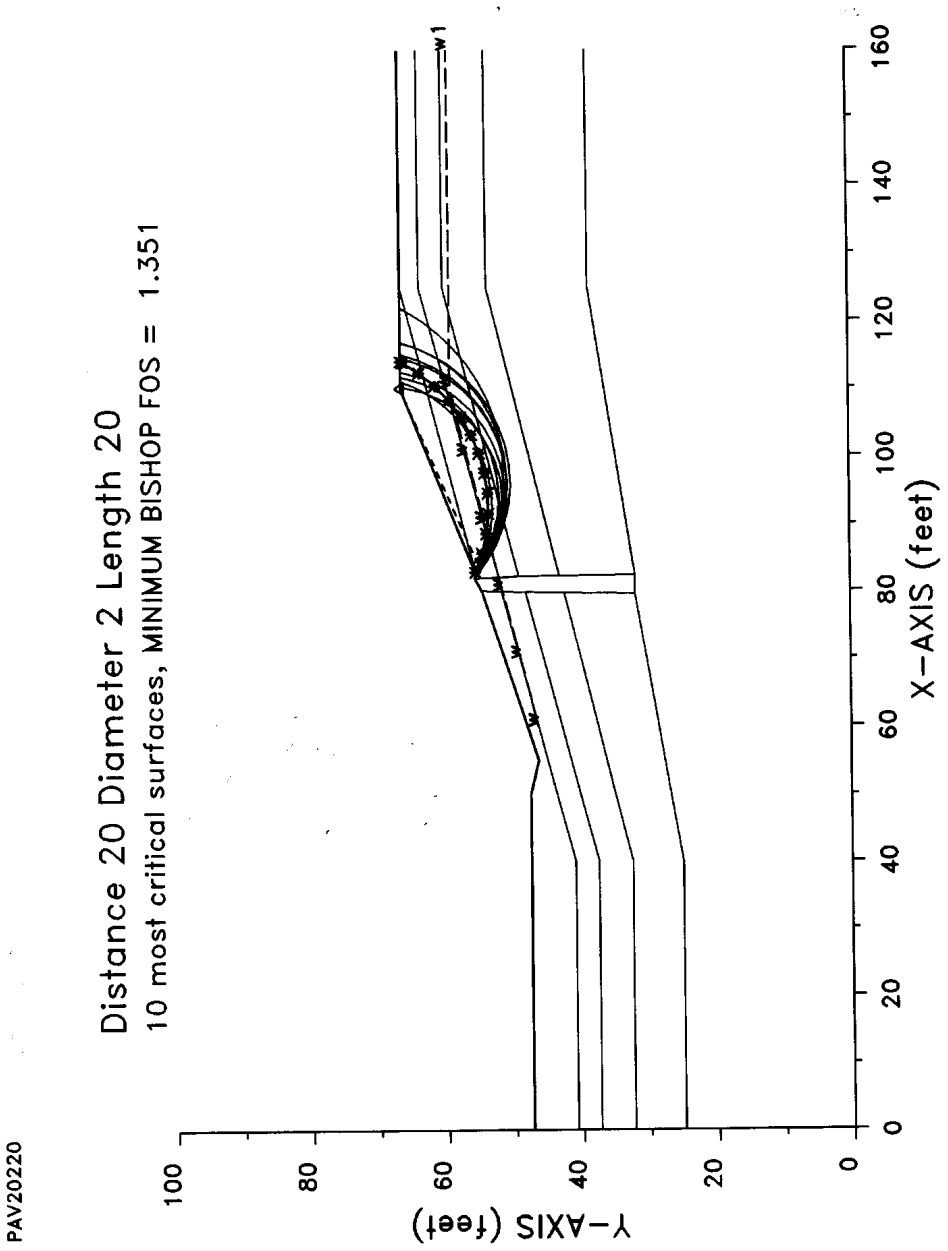

Figure E3. Rear Slip Surface Model Output Plot